SCIENCES AND TECHNOLOGIES FACULTY

Doctoral School **ED SMRE**

Unity of Catalysis and Solid State Chemistry
(UCCS-UMR 8181)

THESIS

Defended by

Natalia Stefania MEDINA MOLANO

In order to become

Doctor of the University Lille
Speciality: Chemistry of Materials

Contribution of radioactivity to catalytic performance in heterogeneous media

---

Thesis defended the 10th May 2023 before the Committee Members:

Dr HDR. Mohamed GHAZZAL	Université Paris-Saclay	Reviewer
Pr. Ludovic PINARD	Université de Caen	Reviewer
Pr. Valérie KELLER	Université de Strasbourg	Examiner
Pr. Olivier TOUGAIT	Université de Lille	President
Dr. Isabelle HABLOT	Orano	Invited
Dr. Laurent VENAULT	CEA	Invited
Pr. Benjamin KATRYNIOK	Ecole Centrale de Lille	Director
Dr. Jean-Sebastien GIRARDON	Université de Lille	Co-Director

FACULTÉ DES SCIENCES ET TECHNOLOGIES

École doctorale **ED SMRE**

Unité de recherche Unité de Catalyse et Chimie du Solide
(UCCS-UMR 8181)

THÈSE

Présentée par

Natalia Stefania MEDINA MOLANO

En vue de l'obtention du grade de

Docteur de l'Université de Lille
Spécialité Chimie des Matériaux

Contribution de la radioactivité sur les performances catalytiques en milieu hétérogène

---

Thèse soutenue le 10 Mai 2023 devant le jury composé de :

Dr HDR. Mohamed GHAZZAL	Université Paris-Saclay	Rapporteur
Pr. Ludovic PINARD	Université de Caen	Rapporteur
Pr. Valérie KELLER	Université de Strasbourg	Examinatrice
Pr. Olivier TOUGAIT	Université de Lille	Président
Dr. Isabelle HABLOT	Orano	Invité
Dr. Laurent VENAULT	CEA	Invité
Pr. Benjamin KATRYNIOK	Ecole Centrale de Lille	Directeur
Dr. Jean-Sebastien GIRARDON	Université de Lille	Co-Encadrant

ACKNOWLEDGEMENTS

I would like to express my sincere gratitude to my director, Pr Benjamin KATRYNIOK, it would not have been possible without his constant guidance, knowledge and support throughout this time. Also, for making every moment a great memory. To my co-supervisor Jean Sebastien GIRARDON and my ORANO supervisor Isabelle HABLOT, thank you for all the valuable discussions, motivations and encouragement throughout these 3 years.

I express my deep gratitude to Dr. Mohamed GHAZZAL and Pr. Ludovic PINARD who accepted to judge my work and to be the reviewers. I would also like to thank Pr. Valérie KELLER, Pr. Olivier TOUGAIT, who honoured me by accepting to participate in the jury.

I thank the UCCS laboratory, the University of Lille, ORANO and its joint laboratory LR4CU for their support and funding of this research project.

I would like to give special thanks to the CEA and all the members of the ATALANTE L18 laboratory, in particular Philippe GUILBAUT, Laurent VENAULT, Emilie BROUSSARD, Myriam DUNAND and Claude BERTHON, for their welcome and their unconditional support in the development of each of my missions.

To my colleagues and technical staff at the UCCS, especially Svetlana HEYTE, Olivier GARDOLL and Johann JEZEQUEL, for their help in my work.

I would like to thank all my friends, especially Sebastian ROA, Carmen CIOTONEA, Pardis SIMON, Juliana CARDENAS, Marcia ARAQUE, Karen SILVA, Nisrine HAMMI and Paola PONTON who were close to me during these years, giving me all their support, help and endless unforgettable moments.

Finally, I would like to thank all my dear family, especially my parents Ramon and Yolanda and my brother Jan, for supporting me and being by my side in all the moments of my life.

ABSTRACT

This thesis aimed to identify applications of noble metals recovered from spent nuclear fuels such as platinoids. To study the effect of the radiation three different applications were selected: heterogeneous catalysis, with the hydrogenation of cinnamaldehyde (CNA) as model reaction; photocatalysis, with the decolorization of methyl orange (MO) as model reaction; and the regeneration of catalysts, deactivated with the synthesis of hydroxymethyl furfural. Protocols were developed for the synthesis of the catalysts and the performance testing in restricted nuclear environment, namely in glove box and for the implementation of the reactions in glove box, fume hood and extractor column as appropriate.

Regarding the results it was found that β-radiation did not show any effect on the hydrogenation of CNA independent of the applied reaction conditions. On the other hand, the decolorization of MO was successfully activated by the β-radiation of the catalyst. A decrease in absorbance (at the isosbestic point) was observed and was correlated to the amount of the catalyst employed, evidencing the effect of the irradiation doses. Finally, the regeneration of the Pd-based catalyst showed promising results after γ-irradiation, notably with a partial recovery of the initial catalytic performance after γ-irradiation. Meanwhile, the Ru-based catalyst, although generally not performing well, showed increased activity compared to the fresh catalyst upon γ-irradiation.

Keywords: Catalysis; Radioactive element; Catalyst regeneration

RESUME

Afin d'établir des voies possibles d'utilisation de métaux nobles récupérés du combustible nucléaire tels que les platinoïdes, la présente thèse vise à étudier l'effet du rayonnement dans trois applications différentes : la catalyse hétérogène, avec – comme réaction modèle – l'hydrogénation du cinnamaldéhyde (CNA) ; la photocatalyse, avec – comme réaction modèle – la décoloration du méthyl orange (MO) et la régénération des catalyseurs, désactivés lors de la synthèse de l'hydroxyméthyl furfural. Des protocoles ont été élaborés pour répondre aux exigences de sécurité nucléaire : applicable en boîte à gant et sorbonne, selon le cas.

Le rayonnement β émis par le ^{107}Pd n'a montré aucun effet lors de l'hydrogénation du CNA, indépendamment des conditions de réaction. En revanche, la décoloration a été initiée par la présence de la radiation β sur le catalyseur en substituant de la lumière visible. Une diminution de l'absorbance (au point isosbéstique) a été observée. Ce dernier corrélait avec la quantité de catalyseur radioactif, mettant en évidence l'activation par le rayonnement β. Enfin, la régénération du catalyseur à base de Pd non radioactif a donné des résultats prometteurs après l'irradiation γ, montrant notamment une augmentation de la performance catalytique après irradiation du catalyseur désactivé. Par ailleurs, le catalyseur à base de Ru, bien que généralement peu performant, a montré une activité plus élevée que l'activité du catalyseur frais après irradiation par rayonnement γ.

Mots clés : Catalyse ; Elément radioactif ; Régénération de catalyseurs

SYMBOLS, ACRONYMS AND ABBREVIATIONS

*	Radioactive element
5-HMF	5-Hydroxymethylfurfural
A	Absorbance
Al_2O_3	Alumina
BE	Binding energy
BET	Brunauer-Emmett-Teller
C	Concentration
CB	Conduction band
CEA	Commissariat à l'Énergie Atomique et aux Énergies Alternatives
CNA	Cinnamaldehyde
CNOL	cinnamyl alcohol
Deact.	Deactivated
D_p	Pore size
Ea	Absolute error
FID	Flame ionization detector
GC	Gas chromatography
HCNA	Hydrocinnamaldehyde
HCNOL	Hydrocinnamyl alcohol
IR	Irradiated
IUPAC	International Union of Pure and Applied Chemistry

LR4CU	Laboratoire de Recherche Commun « Cycle du Combustible et Chimie de l'Uranium »
M	Molarity
MB	Methylene blue
MIBK	4-methyl-2-pentanone
MO	Methyl Orange
NMR	Nuclear magnetic resonance
P	Pressure
P_0	Saturation pressure
Pd	Palladium
PdH_x	Palladium hydride
PdO	Palladium oxide
P_{H_2}	Hydrogen pressure
pH_{pzc}	pH point of zero charge
R	Rate
REP	Repetition
Rh	Rhodium
RhB	Rhodamine B
Ru	Ruthenium
S	Selectivity
S_{BET}	Specific surface area determined by BET
SiO_2	Silica

STP	Standard temperature and pressure
T	Temperature
t	Time
t_f	Final time
TGA	Thermogravimetric analysis
t_i	Initial time
TiO_2	Titanium oxide
TPR	Temperature-programmed reduction
Tri	Trimetallic
UCCS	Unité de catalyse et de chimie du solide
UV-vis	Ultraviolet–visible spectroscopy
VB	Valence band
V_p	Pore volume
X	Conversion
XPS	X-ray Photoelectron Spectroscopy
XPS	X-ray Photoelectron Spectroscopy
XRD	X-ray Diffraction
β	Beta
γ	Gamma

SUMMARY

LIST OF FIGURES

LIST OF TABLES

Chapter 1

Bibliographical introduction and objectives

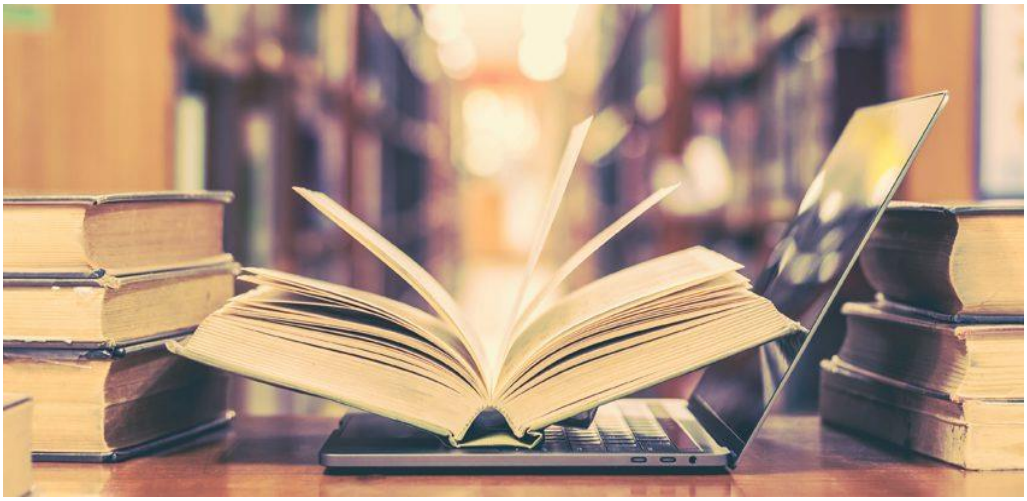

1.1. General context of the study

In the 1940s, the first research in the field of nuclear energy focused on the development and production of the atomic bomb. Later, this research was extended to the production of electricity. Today, 30 countries in the world have nuclear power plants for electricity production. In addition, some countries such as Denmark and Italy, which do not have nuclear facilities, use about 10% of the nuclear electricity imported from other countries [1]. France is the most nuclear-friendly country in the European Union: more than 73% of its electricity is origin from nuclear power, with 58 nuclear reactors in operation with a combined net capacity of 63.1 Gwe of electricity [2].

Electrical energy can be obtained in two ways: nuclear fusion, in which energy is released when the nuclei of atoms combine or fuse to form a larger nucleus, and nuclear fission, used by nuclear power plants, in which nuclei split to form smaller nuclei, releasing energy [3]. The production of this type of energy is more environmentally friendly, as it avoids the emission of greenhouse gases and the use of fossil fuels [4]. However, one of the disadvantages is the generation of radioactive waste from nuclear fuel. Today, companies such as Orano have reprocessing plants to recycle the spent nuclear fuel.

During the recycling process of nuclear fuels, which aims at recovering valuable materials such as uranium and plutonium, various solid particles are produced in the dissolution process. The latter consist of a mixture of noble metals and particles from the fission process, which due to their radioactive nature are currently confined [5]. These particles contain potentially interesting elements for catalysis, such as Ru, Pd and Rh. For this reason, Orano, a world leader in nuclear fuel recycling [6], is studying the possibilities of valorizing these recovered platinoid-type elements in electrochemistry and heterogeneous catalysis.

Catalysts based on Pd, Ru and Rh, are for example commonly used in hydrogenation reactions such as the hydrogenation of unsaturated aldehydes. This reaction is very attractive for research in the field of catalysis due to its industrial importance, since hydrogenated products are used in the pharmaceutical, perfumery and food industries, among others [7,8]. Oxidation reactions have also shown good performance with the use of catalysts based on these metals. On the one hand, the oxidation of benzyl alcohol for example, showed a good yield, and even a high selectivity towards aldehydes using Ru-based catalysts [9]. On the other hand, oxidation of glycerol, reported significant activity with Pd-based catalysts, which was highly dependent on the nature of the support [10].

One of the aforementioned potential routes of valorisation is the use of these metals in heterogeneous catalysis applied to model reactions such as those mentioned above. However, promising results have been reported on the effects of radiation in photocatalytic reactions [11,12]. In photocatalysis, one of the approaches that has gained more importance in recent years are the reactions that aim at the decontamination of wastewater, as is the case of the decolorization of azo dyes, compounds generally used in the textile industry. The main objective of this reaction is the removal of azo compounds from industrial effluents, which has become an environmental problem. For this purpose, TiO_2-based photocatalysts are most widely used [13–16].

The present study is one of the research lines of the joint laboratory LR4CU (Laboratoire de Recherche Commun «Cycle du Combustible et Chimie de l'Uranium») created between the University of Lille, Orano, CNRS and Centrale Lille Institute. The main objective is to evaluate the influence of radioactive isotopes in catalysts, on the hydrogenation of cinnamaldehyde and the decolorization of Azo-dyes respectively. In this sense, a simple catalyst preparation and reaction protocol will be created and optimized with non-radioactive metals, in order to be implemented in the ATALANTE laboratory facilities at CEA-Marcoule with radioactive metals

from the nuclear fuel recovery process. Finally, the results of the non-radioactive and radioactive tests will be analyzed and compared. In parallel, the effect of γ irradiation on deliberately deactivated catalysts with the deposition of carbon molecules (humins) will also be evaluated.

1.2. Bibliography

1.2.1. Recoverable fines from nuclear fission

Figure 1-1 below summarises, in a very simplified way, the recycling of nuclear fuels as carried out on the Orano La Hague site. During recycling, solid particles are produced along the dissolution operation. These particles are made up of a mixture of non-soluble noble metals (palladium, rhodium and ruthenium) and particles from the fission process. The conditioning of these radioactive insolubles, which are mainly in metallic form, is carried out by vitrification in stable matrices, adapted to the activity and life cycle of the waste, in view to its final disposal [5].

However, Orano and CEA are currently developing and optimising different processes that aim to recover and purify these metals.

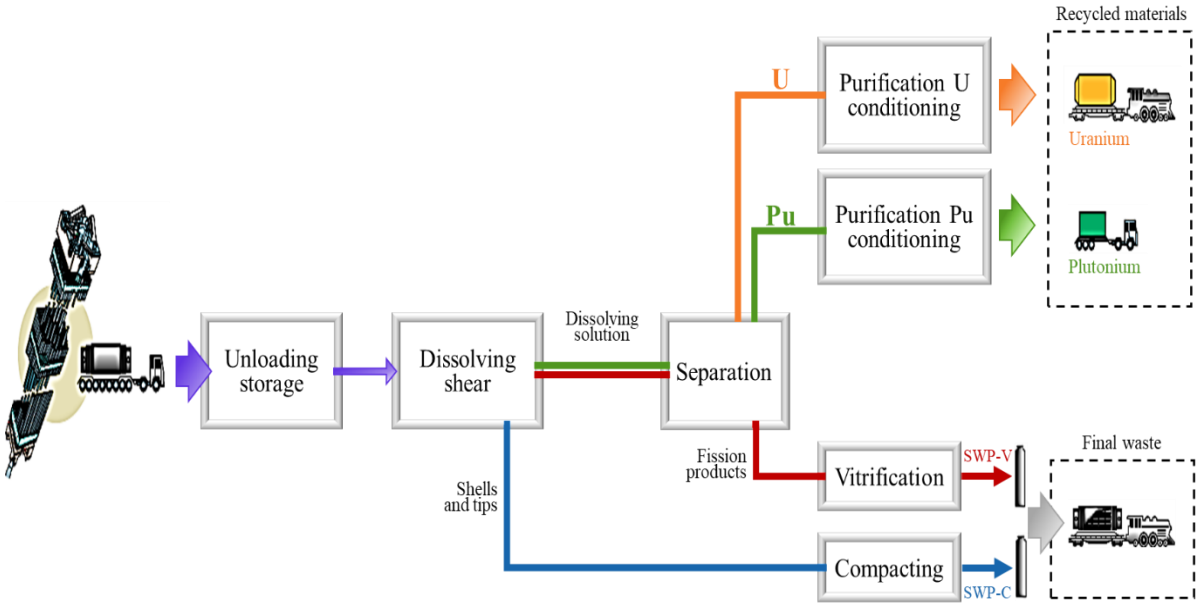

Figure 1-1:*Simplified scheme of the treatment of spent fuel [5].*

One of the possibilities to use these metals is in the field of heterogeneous catalysis. Indeed, the use of these radioactive metals in heterogeneous catalysts could have several advantages, in particular in the expected "additional" contribution of radioactivity compared to non-radioactive metals via the formation of radicals or the limitation of deactivation by reducing the

deposit of coke. Moreover, the orientation of the valorisation of radioactive metals via heterogeneous catalysis proves to be a safe alternative because the totality of the noble metal(s) would be isolated at the end of the reaction thus avoiding any risk of contamination.

1.2.1.1. Recoverable metals

- *Palladium*

Palladium is a chemical element with atomic number 46 and symbol Pd, considered as a rare metal. It exists in six stable isotopes (^{102}Pd, ^{104}Pd, ^{105}Pd, ^{106}Pd, ^{108}Pd and ^{110}Pd) and 20 radioisotopes, the most stable of which are ^{107}Pd with a half-life of 6.5 million years, ^{103}Pd with a half-life of 17 days and ^{100}Pd with a half-life of 3.63 days. The main mode of decay is β^- emission, however for some isotopes such as ^{103}Pd and ^{100}Pd it is electron capture [17–19]. Of all the radioactive isotopes, the only one likely to be detected in the environment due to its long physical half-life is ^{107}Pd, whose reported mass activity is 1.90E+07 $Bq \cdot g^{-1}$ and a maximum beta energy of 30 keV [20].

In catalysis, Pd is used in the automotive and chemical industry for hydrogenation and dehydrogenation reactions, or, for example, for the oxidation of primary alcohols in alkaline media [21].

Pd-based catalysts are commonly synthesized by impregnation techniques – using i.e. Palladium nitrate as precursor – followed by heat treatments, in order to achieve loading between 0.5 and 12 wt.% [22,23] on Al_2O_3, SiO_2 or even TiO_2. Some hydrogenation reactions [24–26], with monometallic Pd catalysts supported on alumina showing high activity and stability that make them, according to some authors [27], a better option in different hydrogenation reactions, such as hydrodechlorination, which is a promising technology for the treatment of wastewater containing polluting chlorinated organic compounds, and hydrogenolysis [24].

- *Ruthenium*

Ruthenium (Ru), atomic number 44, is used as an alloy to strengthen palladium and platinum in electrodes. The Ru has 7 naturally occurring isotopes ranging from ^{96}Ru to ^{104}Ru, the most abundant being ^{102}Ru (31.6%) and 34 radioactive isotopes. The most stable radioisotopes are ^{106}Ru, ^{103}Ru, ^{97}Ru with half-lives of 373.59, 39.26, 2.9 days, respectively. The primary decay mode before the most abundant isotope, ^{102}Ru, is electron capture and the primary mode after is β^- emission [18,28,29]. The reported mass activity for ^{103}Ru and ^{106}Ru is 1.90E+14 and 1.22E+14 $Bq \cdot g^{-1}$ respectively [30].

In organic chemistry, the Ru has been used for the reduction of the carbonyl bond and the metathesis reaction [31,32]. In heterogeneous catalysis, it has been used in the conversion of stearic acids to diesel-cut alkanes [33], in the hydrogenolysis of sorbitol to glycols [34] or in hydrogenation reactions such as hydrogenation of levulinic acid to ɣ-valerolactone [35] or furfural to furfuryl alcohol [36].

Ruthenium catalysts are also commonly supported on alumina, silica or titanium dioxide and prepared using impregnation techniques followed by heat treatments. Metal loadings vary from 1 to 5 wt.% for liquid phase reactions [34,35] and can reach 10 wt.% for gas phase reactions [37].

1.2.2. Catalyst and radioactivity

So far, there is little literature that accurately relates the effect of radioactivity on the catalytic activity of heterogeneous catalysts. In 1958, Balandin et al. [38] reported that the introduction of radioactive sulphur (^{35}S) significantly increased the catalytic activity of a mixture of $MgSO_4$ + Na_2SO_4 catalysts during the dehydration of cyclohexanol to cyclohexene (Figure 1-2).

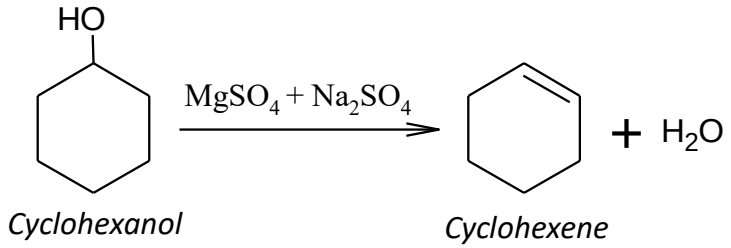

Figure 1-2: *Dehydration of cyclohexanol.*

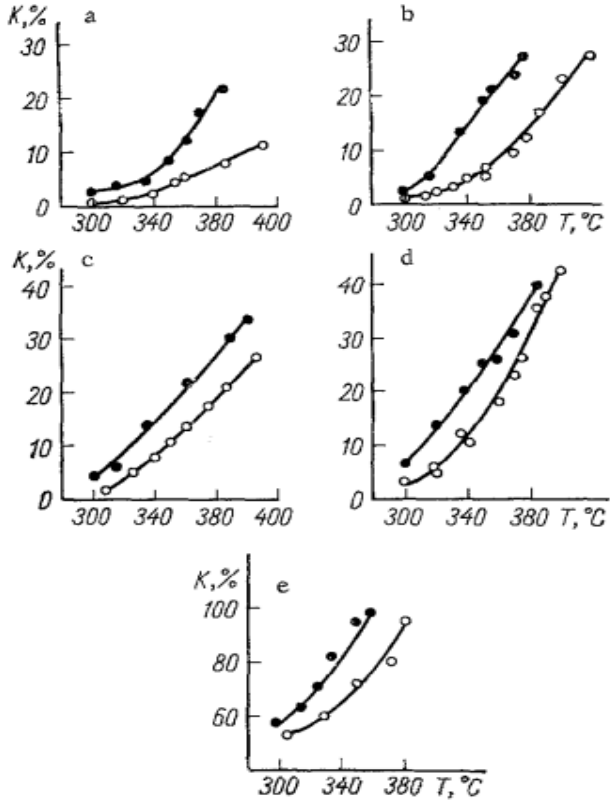

Figure 1-3: *Degree of conversion of alcohol K, plotted vs. temperature over radioactive $MgSO_4$. a) n-Amyl alcohol; b) n-hexyl alcohol; c) n-decyl alcohol; d) n-dodecyl alcohol; e) cyclohexanol; ○) non-radioactive; ●) radioactive $MgSO_4$, activity 103-105 $mCi \cdot g^{-1}$ [39].*

Later in 1961, the same authors analyzed the catalytic activity of magnesium sulphate catalysts with the radioactive isotopes ^{35}S and ^{45}Ca in the same reaction (Figure 1-2) and found that this type of isotope contributed to an increase in catalytic activity: the reaction rate increased proportional to the logarithm of the amount of ^{35}S [40]. In contrast, Spitsyn et al. [41] did not obtain the same results with the ^{231}Pa isotope, which did not alter the performance of the catalyst. These authors postulate that the radioactive isotope must be a constituent of the catalyst

and interpret that the increase in catalytic activity (Figure 1-3) is due to the continuous radiation from its nucleus to the active centers of the catalyst, which transfers energy to the cyclohexanol molecules, thereby decreasing the activation energy of the reaction [39,40].

Other radioactive isotopes such as ^{144}Ce and ^{137}Cs were used on alumina catalysts by Spitsyn et al. [42]. These authors observed an increase in catalytic activity in the dehydration reaction of n-decyl alcohol. However, in other types of reactions, for example the cracking of cumene, no favourable effect of radioactive calcium phosphate catalysts with ^{45}Ca and ^{32}P isotopes was observed compared to the non-radioactive catalyst [43]. In this sense, the influence of radioactivity on the catalytic activity depends on the nature of the catalyst and the reaction studied [44].

Concerning heterogeneous photocatalysis, Jones et al. studied the transformation of CO_2 into other components, using UV light or radioactive radiation to activate the catalyst (Figure 1-4). For this, yttrium-90 (^{90}Y) was selected as a source of β particles together with a strontium titanate ($SrTiO_3$) catalyst. They showed that the conversion of CO_2 to methanol and formic acid was enabled by the β emission (Table 1-1) [45].

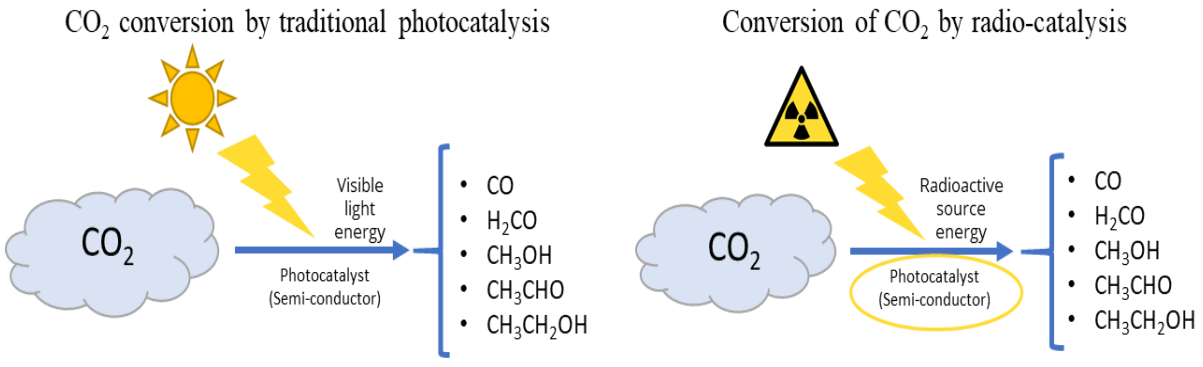

Figure 1-4: *General scheme of CO_2 transformation by photocatalysis and radio-catalysis.*

Table 1-1:*Organic products identified [45].*

Treatments	***Products Identified***			
	Methanol ($mg \cdot L^{-1}$)	Ethanol ($\mu g \cdot L^{-1}$)	Propanol ($\mu g \cdot L^{-1}$)	Formic Acid ($\mu g \cdot L^{-1}$)
0,5M $NaHCO_3$	-	-	-	487
0,5M $NaHCO_3$+$SrTiO_3$	-	-	-	418
0,5M $NaHCO_3$+$SrTiO_3$+^{90}Y	2.4	-	-	785

1.2.3. Model reaction

Although there is currently a great industrial potential related to the use of radioactive catalysts, the synthesis and reactivity measurements involve specific conditions and areas that are in line with the regulations for the management of radioactive substances. Hence, the choice of the reaction to be studied is an important stage in the development of this study, since its protocol, including the analysis of the samples, must comply with the current requirements of the ATALANTE nuclear facility (Marcoule, CEA Research Centre, France), which allow its implementation under radioactive conditions in a glove box. Specifically, the requirements that governed the search for and choice of the model reactions are described below:

- Protocol allowing easy handling in glove box.
- Low total pressures and temperatures, 10 bar and 100°C maximum.
- Preferably not requiring the use of gases such as H_2 at high pressures.
- Sample analysis possible with NMR or UV-Vis spectroscopy, as these are the only two techniques available in the ATALANTE laboratory for the analysis of radioactive matter.
- Catalytic performance with low concentrations of noble metals specially Pd. with the aim of not exceeding the maximum limit of radioactive activity allowed in a glove box.
- Avoid use of highly flammable chemicals products.

1.2.3.1. Hydrogenation and oxidation reactions

Following the literature research on hydrogenation reactions catalysed by heterogeneous catalysis, a compilation of the different model reactions and their parameters is presented in Table 1-2. These reactions were selected based on the possibility of implementing a simple protocol, which in turn meets the requirements of: pressure, temperature, solvent, analysis technique, catalyst mass, type of metal and percentage of metal present in the catalyst which were described in the previous section.

Table 1-2: *Compilation of parameters for different model reactions for heterogenous catalysis.*

Model reaction	***NMR***	***Catalyst***		***Conditions***			
		Metal	***Quantity [wt.%]***	***T [°C]***	***P [bar]***	***Solvent***	***$m_{catalyst}$ [mg]***
Hydrogenation of benzene [46–49]	🟢	Pd Rh Pd-Rh Ru	6-8	120-170	10-40	Aqueous $ZnSO_4$ solution	2.5-20
Hydrogenation of cinnamaldehyde [50–56]	🟢	Pd Rh Ru	0.5-7	25-150	1-45	Toluene Cyclohexane Dioxane 2-propanol Ethanol p-xylene	1-400
Oxidation of glycerol [57–59]	🔴	Pd Rh Ru	1-2	40-100	3-10	Water	50-700
Oxidation of benzyl alcohol [60–63]	🟠	Pd Ru	0.3-5	27-140	1-2	CH_3CN Cyclohexane	20-200
Reduction of 4-nitrophenol [64–66]	🟠	Pd Ru	1-3	Room T	Atm.	$NaBH_4$	0,2-10

In green are shown the parameters that fulfil the requirements established for the choice of the model reaction and in red those that do not. For example, the hydrogenation of benzene: although it is possible to analyse the reaction products by NMR, it was discarded due to high pressure and metal load of the catalyst exceed the acceptable limits for the development of this study. On the other hand, the oxidation of benzyl alcohol works at low pressures and low amounts of catalyst with low metal content, however, the characterization with NMR is complex, due to the superposition of the characteristic signals of each of the products, which is why it is not the most suitable reaction for the present study. This is also the case for the reduction of 4-nitrophenol and the oxidation of glycerol.

Finally, to measure the impact of radioactivity applied to heterogeneous catalysis, the hydrogenation of cinnamaldehyde has been selected as a model reaction since it handles mild reaction conditions (atmospheric temperature and pressure and low amounts of catalyst with low metallic loadings), besides, it allows the identification of reaction products with NMR, which agrees with the selection criteria. More details on this reaction will be discussed in the next section. The reaction mechanism of the hydrogenation of cinnamaldehyde is presented in Figure 1-5 [67].

Initially, the C=C and C=O bonds are hydrogenated, with the C=C bond being the most thermodynamically favoured. Under very severe conditions over-hydrogenation can occur, giving rise to β-methylstyrene, 1-propylbenzene or 3-cyclohexylpropane. Finally, the formation of acetals is directly linked to the polarity of the solvent. It is well known that the reaction of cinnamaldehyde (CNA) and hydrocinnamaldehyde (HCNA) with polar solvents induces C=O bond hydrogenation [68–72]. However, it was observed that acetalization could be reversible with methanol over a Pd/Al_2O_3 catalyst [73].

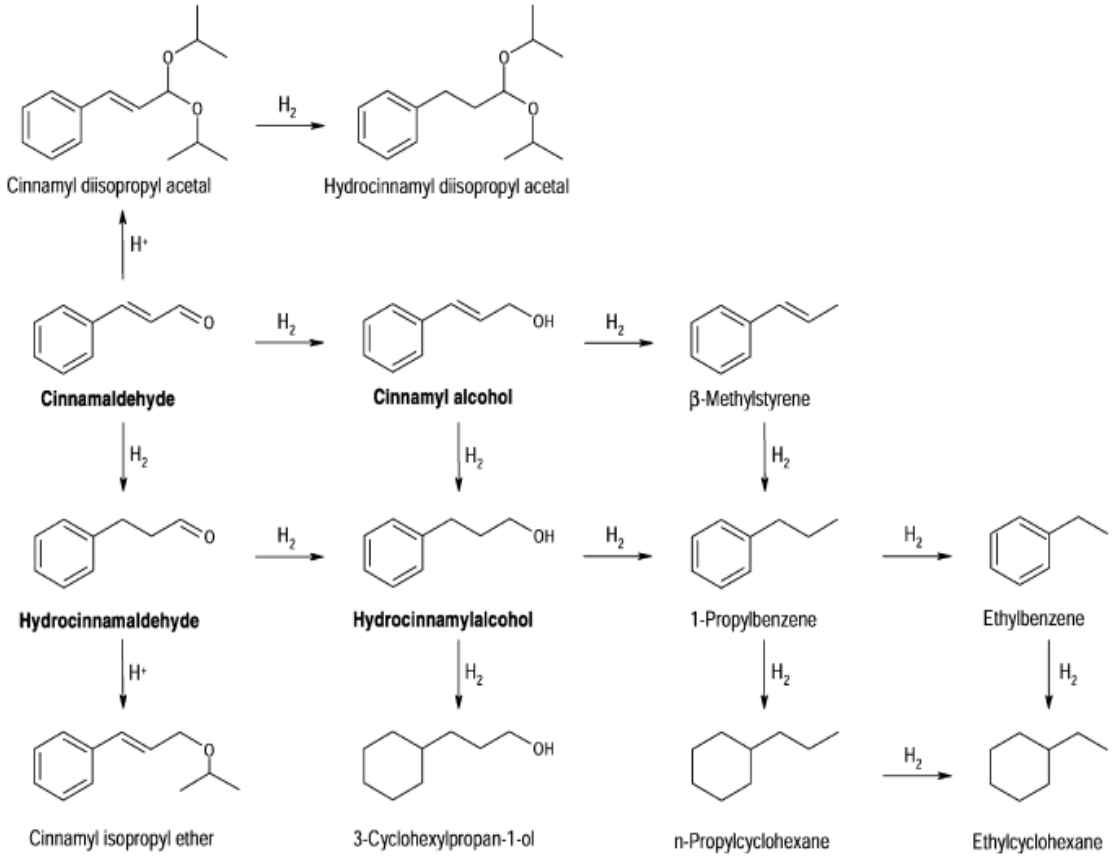

Figure 1-5: *Reaction network of cinnamaldehyde hydrogenation [67].*

1.2.3.1. Photocatalytic reactions

In order to choose the model reaction for the heterogeneous photocatalysis, it was equally important to fulfil the selection criteria so that it could be easily implemented in the ATALANTE installation. Therefore, after the literature search, the decolorization of azo-dyes, which is a reaction of great industrial interest, was directly considered. According to the literature, these reactions are carried out in liquid phase, at atmospheric pressure at low temperatures, and the energy source can be either artificial light or solar energy [74,75]. Moreover, monitoring and analysis of the reaction solutions is possible with UV-Vis spectroscopy, which is available in the facility [76]. Table 1-3 shows the parameters for some examples of decolorization of different azo-dyes.

Table 1-3: *Azo-dyes decolorization reaction parameters.*

Type of azo-dye	*Energy source*	*T [°C]*	*Catalyst*	*Analysis technique*
Dye reactive blue 4 [74]	Solar	Ambient	TiO_2*	Spectrometry UV-VIS
Eriochrome black T (EB) dye [77]	Solar	25-50	$CoO–NiFe_2O$*	Spectrometry UV-VIS
MB and RhB dye [76]	Solar	Ambient	Cu/nano-zeolite X*	Spectrometry UV-VIS
Methyl orange (MO) [78–80]	Artificial	25	TiO_2*, γ-Al_2O_3, Pd/γ-Al_2O_3	Spectrometry UV-VIS
Azure B dye [81]	Artificial	Ambient	Co(II), Cu(II)	Spectrometry UV-VIS
Acid brown 14 [82]	Solar	25-30	ZnO* and TiO_2*	Spectrometry UV-VIS

*Semicondiuctor

Methyl orange was selected as the azo-dye molecule for the photocatalytic model reaction, since the literature search showed good performance with the use of photocatalysts such as TiO_2, Al_2O_3 and even supported photocatalysts such as Pd/γ-Al_2O_3.

Figure 1-6 shows the degradation mechanism of methyl orange.

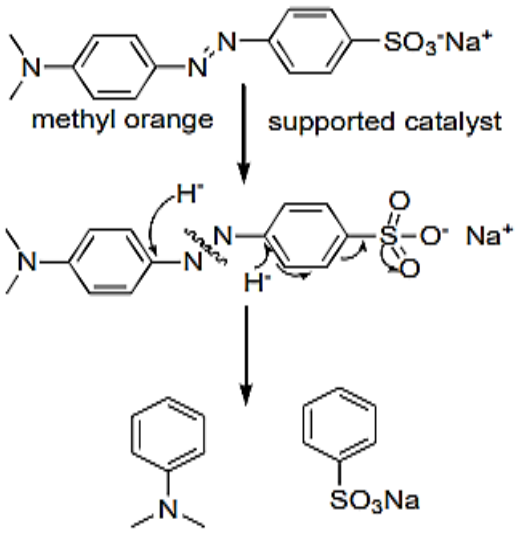

Figure 1-6: *General reaction network of degradation of MO [83].*

1.2.3.2. Deactivation / Regeneration studies

With respect to the finiteness of fossil resources and growing concern for environmental protection, carbohydrates such as cellulose and starch have become indispensable raw materials for the chemical industry, as they are renewable and abundant biomass resources [84]. 5-Hydroxymethylfurfural (5-HMF) is a promising chemical building block derived from biomass to obtain chemical products, among which, there are some that are nowadays produced from petroleum derivatives. Among the main derivatives of 5-HMF are some monomers for the formation of polymers (furandicarboxylic, caprolactam), fine chemicals (for pharmaceuticals and agribusiness, among others) and biofuels [85]. 5-HMF is synthesized by dehydration of fructose, using ideally high concentration of the reactant in order to avoid huge reactors and excessive energy consumption during work-up. However, in turn, the use of highly concentrated sugar solutions accelerates intermolecular side reactions to form dark brown insoluble by-products known as humins (Figure 1-7), which compete with the desired products, restrict catalyst activity and hinder recycling [86,87].

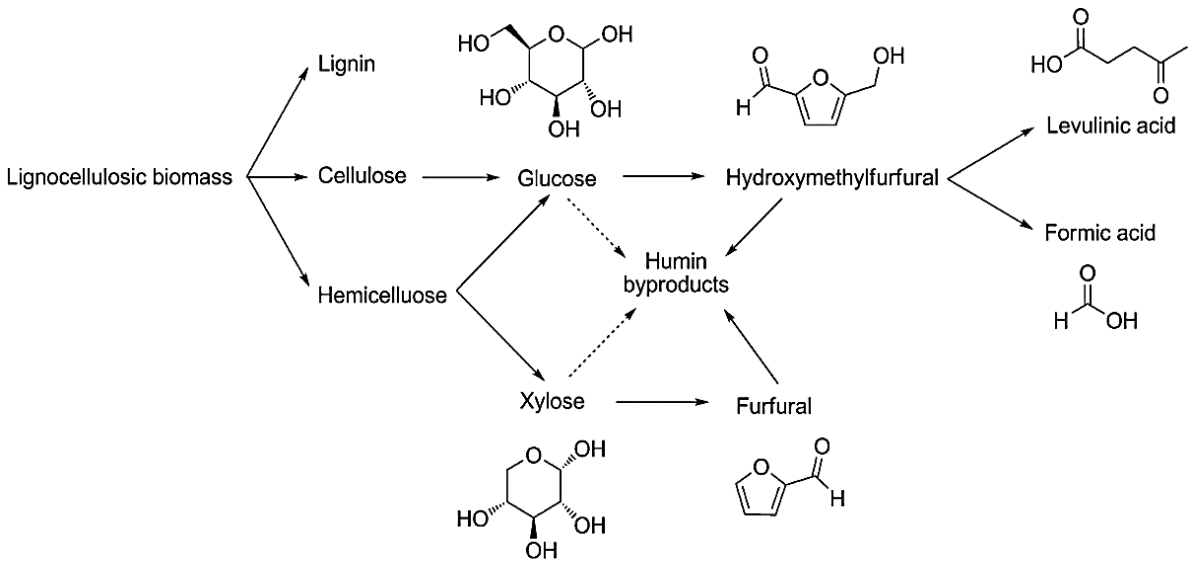

Figure 1-7: *Production of chemicals from lignocellulosic biomass and the related formation of humin byproducts by polymerization of sugars and their derivatives [87].*

In this sense, the synthesis of 5-HMF from concentrated aqueous fructose solutions was chosen as an arbitrary reaction for the deactivation of a catalyst. The deactivated catalysts were subjected to gamma irradiation to study the potential use of irradiation for catalyst regeneration.

1.3. Objectives and approach of this work

To study of the influence of radioactivity on the catalytic performance two model reactions were selected:

1.3.1. Heterogeneous catalysis

The first one aims to evaluate the impact of radioactivity on the model reaction of cinnamaldehyde hydrogenation, using potentially radioactive catalysts. For this purpose, the methodology proposed in general consists of:

- Synthesise monometallic, bimetallic and trimetallic catalysts based on non-radioactive Pd, Ru and Rh, with a metal loading of 5 wt.% and supported on Al_2O_3, by developing a simple and reproducible protocol for use in the ATALANTE facility.
- Establish and optimise a simple reaction protocol for the hydrogenation of cinnamaldehyde that meets the requirements.
- To evaluate the catalytic activity of the catalysts mentioned above, in order to screen the best formulations.
- Replicate the synthesis of the best catalyst formulation with radioactive metal and evaluate them in the model reaction at the ATALANTE facility.
- Finally, to analyse and compare the results obtained in the tests with radioactive and non-radioactive catalysts.

1.3.2. Decomposition of Methyl orange

The second one is aimed at evaluating the use of radioactivity as an energy source in the photocatalytic reaction by replacing the irradiation source by a radioactive metal catalyst supported on TiO_2. For this purpose, the methodology proposed in a general way is as follows:

- Synthesise a monometallic catalyst based on non-radioactive Pd, with a 5% metal loading supported on TiO_2 by developing a simple and reproducible protocol for use in the ATALANTE facility.
- To create and optimise a simple reaction protocol for the decolorization of methyl orange that meets the requirements.
- To evaluate the catalytic activity of the non-radioactive catalyst, in order to have a comparative reference with the radioactive catalyst.
- Replicate the synthesis of the catalyst with radioactive Pd and evaluate in absence of light in the ATALANTE facility.
- Finally, to analyse and compare the results obtained in the tests with radioactive and non-radioactive catalysts.

In addition, in order to get an idea of whether radioactive radiation impacts on catalyst regeneration, Pd and Ru-based catalysts were deliberately deactivated by deposition of humins using the synthesis of 5-hydroxymethylfurfural (5-HMF) as an arbitrary reaction, and then irradiated with γ-irradiation at 600 kGy for 2 months. Finally, the fresh, deactivated and deactivated-irradiated catalysts were evaluated on the hydrogenation of cinnamaldehyde.

The manuscript was divided as follows, 7 chapters starting with the state of the art and ending with a general conclusion.

Chapter 1 - **Bibliographical introduction and objectives** contained the general context of the study, a brief state of the art of the use of radioactivity in heterogeneous catalysis as well as the search and selection of the model reactions to be studied, according to the technical limitations also presented in this chapter. Finally, the objectives of our research were presented.

The catalyst synthesis method, the characterization techniques implemented and the different reaction protocols, with which the catalytic performance was evaluated, are described in chapter 2 - **Experimental and analytical methods**.

Chapter 3 - **Catalyst characterization** dedicated to present the results of the preliminary analysis of the different catalysts used in the course of the whole study.

Chapter 4 - **Impact of radioactivity on the hydrogenation of cinnamaldehyde** is focused on evaluating the effect of radioactivity on the hydrogenation of CNA with the use of radioactive catalyst.

Chapter 5 - **Impact of radioactivity on the decolorization of azo-dyes** is devoted to the results obtained in the study of the effect of radioactivity on the methyl orange decolorization model reaction, comparing the radioactive and non-radioactive catalyst.

Chapter 6 - **Catalyst regeneration by gamma irradiation** presents the study of the effect of gamma radiation on the regeneration of catalysts, which were evaluated in the hydrogenation of CNA.

Finally, in chapter 7 - **General conclusion**, the aim is to make a balance of the study taking into account the different approaches used to evaluate the effect of radioactivity in order to finally propose new perspectives to continue with the studied topic.

1.4. References

[1] P. Oriol, "Énergie nucléaire," Situation de l'énergie nucléaire dans le monde, 2018, https://energie-nucleaire.net/applications/energie-nucleaire-monde.

[2] Foro nuclear, Energía nuclear en el mundo, https://www.foronuclear.org/descubre-la-energia-nuclear/energia-nuclear-en-el-mundo/.

[3] N. Mayer, "Futura sciences," Fission nucléaire et fusion nucléaire : quelle différence ?, 2002, https://www.futura-sciences.com/sciences/dossiers/physique-energie-nucleaire-a-z-126/page/5/.

[4] I. Juste, "Ecología verde," Ventajas y desventajas de la energía nuclear, 2018, https://www.ecologiaverde.com/ventajas-y-desventajas-de-la-energia-nuclear-1114.html.

[5] Orano Cycle, Traitement des combustibles usés provenant de l'étranger dans les installations d'Orano la Hague, France, 2017.

[6] Fabien Burgaud, leader du recyclage des combustibles nucléaires usés va créer cinq emplois à Vendeuvre-sur-Barse, 2020.

[7] H.G. Manyar, B. Yang, H. Daly, H. Moor, S. McMonagle, Y. Tao, G.D. Yadav, A. Goguet, P. Hu, C. Hardacre, Selective Hydrogenation of α,β-Unsaturated Aldehydes and Ketones using Novel Manganese Oxide and Platinum Supported on Manganese Oxide Octahedral Molecular Sieves as Catalysts, ChemCatChem 5 (2013) 506–512. https://doi.org/10.1002/cctc.201200447.

[8] T. Szumełda, A. Drelinkiewicz, R. Kosydar, J. Gurgul, Hydrogenation of cinnamaldehyde in the presence of PdAu/C catalysts prepared by the reverse "water-in-oil" microemulsion method, Applied Catalysis A: General 487 (2014) 1–15. https://doi.org/10.1016/j.apcata.2014.08.036.

[9] A. Köckritz, M. Sebek, A. Dittmar, J. Radnika,A. Brückner, U. Bentrup, M.-M. Pohl, H. Huglb,W.Mägerlein, Ru-catalyzed oxidation of primary alcohols, Journal ofMolecular Catalysis A: Chemical (2006) 85–99.

[10] A. Namdeo, S.M. Mahajani and A.K Suresh, Palladium catalysed oxidation of glycerol −Effect of catalyst support, Journal ofMolecular Catalysis A: Chemical (2016) 45–56.

[11] M.A. Rauf, S. Salman Ashraf, Radiation induced degradation of dyes—An overview, Journal of Hazardous Materials (2009) 6–16.

[12] Y. Ling, G. Wang, T. Chen, X. Fei, S. Hu, Q. Shan, D. Hei, H. Feng, W. Jia, Irradiation-catalysed degradation of methyl orange using BaF_2–TiO_2 nanocomposite catalysts prepared by a sol–gel method, Royal Society Open Science (2019).

[13] Lung-Chuan Chen∗, Fu-Ren Tsai, Chao-Ming Huang, Photocatalytic decolorization of methyl orange in aqueous medium of TiO_2 and Ag–TiO_2 immobilized on □-Al2O3, Journal of Photochemistry and Photobiology A: Chemistry (2005) 7–14.

[14] L. Castro-Peña, J.E. Durán-Herrera, Degradación y decoloración de agua contaminada con colorantes textiles mediante procesos de oxidación avanzada, TM 27 (2014) 40. https://doi.org/10.18845/tm.v27i2.1807.

[15] C. Baiocchi, M.C. Brussino, E. Pramauro, A.B. Prevot, L. Palmisano, G. Marcì, Characterization of methyl orange and its photocatalytic degradation products by HPLC/UV–VIS diode array and atmospheric pressure ionization quadrupole ion trap mass spectrometry, International Journal of Mass Spectrometry 214 (2002) 247–256. https://doi.org/10.1016/S1387-3806(01)00590-5.

[16] S. Al-Qaradawi, S.R. Salman, Photocatalytic degradation of methyl orange as a model compound, Journal of Photochemistry and Photobiology A: Chemistry 148 (2002) 161–168. https://doi.org/10.1016/S1010-6030(02)00086-2.

[17] Commission on Atomic Weights and Isotopic Abundances report for the International Union of Pure and Applied Chemistry in Isotopic Compositions of the Elements 1989, Naturally occurring isotope abundances, 1998.

[18] G. Audi, O. Bersillon, J. Blachot, A.H. Wapstra, The Nubase evaluation of nuclear and decay properties, Nuclear Physics A 729 (2003) 3–128. https://doi.org/10.1016/j.nuclphysa.2003.11.001.

[19] B.J.W. Arblaster, The Discoverers of the Palladium Isotopes, platin met rev 50 (2006) 97–103. https://doi.org/10.1595/147106706X110817.

[20] J. C. Gariel, Fiche radionucléide palladium 107 et environnement, 2002, https://www.irsn.fr/FR/Larecherche/publications-documentation/fiches-radionucleides/Documents/environnement/Palladium_Pd107_v1.pdf.

[21] C. Liu, S. Tang, A. Lei, Oxidant controlled Pd-catalysed selective oxidation of primary alcohols, Chemical communications (Cambridge, England) 49 (2013) 1324–1326. https://doi.org/10.1039/c2cc38086b.

[22] E. Diaz, A.F. Mohedano, J.A. Casas, C. Shalaby, S. Eser, J.J. Rodriguez, On the performance of Pd and Rh catalysts over different supports in the hydrodechlorination of the MCPA herbicide, Applied Catalysis B: Environmental 186 (2016) 151–156. https://doi.org/10.1016/j.apcatb.2015.12.054.

[23] S. Wu, H. Ma, X. Jia, Y. Zhong, Z. Lei, Biopolymer-metal complex wool–Pd as a highly active heterogeneous catalyst for Heck reaction in aqueous media, Tetrahedron 67 (2011) 250–256. https://doi.org/10.1016/j.tet.2010.10.062.

[24] M. Munoz, Z.M. de Pedro, J.A. Casas, J.J. Rodriguez, Improved γ-alumina-supported Pd and Rh catalysts for hydrodechlorination of chlorophenols, Applied Catalysis A: General 488 (2014) 78–85. https://doi.org/10.1016/j.apcata.2014.09.035.

[25] J.H. Kang, E.W. Shin, W.J. Kim, J.D. Park, S.H. Moon, Selective Hydrogenation of Acetylene on TiO2-Added Pd Catalysts, Journal of Catalysis 208 (2002) 310–320. https://doi.org/10.1006/jcat.2002.3583.

[26] M.J. Tenorio, C. Pando, J. Renuncio, J.G. Stevens, R.A. Bourne, M. Poliakoff, A. Cabañas, Adsorption of Pd(hfac)2 on mesoporous silica SBA-15 using supercritical CO2 and its role in the performance of Pd–SiO2 catalyst, The Journal of Supercritical Fluids 69 (2012) 21–28. https://doi.org/10.1016/j.supflu.2012.05.003.

[27] G. Yuan, M.A. Keane, Aqueous-Phase Hydrodechlorination of 2,4-Dichlorophenol over Pd/Al 2 O 3 Reaction under Controlled pH, Ind. Eng. Chem. Res. 46 (2007) 705–715. https://doi.org/10.1021/ie060802o.

[28] D.R. Lide (Ed.), CRC handbook of chemistry and physics: A ready-reference book of chemical and physical data: 2004-2005, 85th ed., CRC Press, Boca Raton [etc], op. 2004.

[29] C. Ronneau, J. Cara, A. Rimski-Korsakov, Oxidation-enhanced emission of ruthenium from nuclear fuel, Journal of Environmental Radioactivity 26 (1995) 63–70. https://doi.org/10.1016/0265-931X(95)91633-F.

[30] Chem Europe, Ruthenium, https://www.chemeurope.com/en/encyclopedia/Ruthenium.html#Isotopes.

[31] H. Nagao, T. Mizukawa, K. Tanaka, Carbon-Carbon Bond Formation in the Electrochemical Reduction of Carbon Dioxide Catalyzed by a Ruthenium Complex, Inorg. Chem. 33 (1994) 3415–3420. https://doi.org/10.1021/ic00093a033.

[32] M. Mori, A. Kinoshita, Total Synthesis of (-)-Stemoamide Using Ruthenium-catalyzed Enyne Metathesis Reaction, HETEROCYCLES 46 (1997) 287. https://doi.org/10.3987/COM-97-S14.

[33] L. Di, S. Yao, S. Song, G. Wu, W. Dai, N. Guan, L. Li, Robust ruthenium catalysts for the selective conversion of stearic acid to diesel-range alkanes, Applied Catalysis B: Environmental 201 (2017) 137–149. https://doi.org/10.1016/j.apcatb.2016.08.023.

[34] I.M. Leo, M.L. Granados, J.L.G. Fierro, R. Mariscal, Sorbitol hydrogenolysis to glycols by supported ruthenium catalysts, Chinese Journal of Catalysis 35 (2014) 614–621. https://doi.org/10.1016/S1872-2067(14)60086-3.

[35] C. LI, X. NI, X. DI, C. LIANG, Aqueous phase hydrogenation of levulinic acid to γ-valerolactone on supported Ru catalysts prepared by microwave-assisted thermolytic method, Journal of Fuel Chemistry and Technology 46 (2018) 161–170. https://doi.org/10.1016/S1872-5813(18)30008-2.

[36] C. Ramirez-Barria, M. Isaacs, K. Wilson, A. Guerrero-Ruiz, I. Rodríguez-Ramos, Optimization of ruthenium based catalysts for the aqueous phase hydrogenation of furfural to furfuryl alcohol, Applied Catalysis A: General 563 (2018) 177–184. https://doi.org/10.1016/j.apcata.2018.07.010.

[37] L.F. Bobadilla, A. Muñoz-Murillo, O.H. Laguna, M.A. Centeno, J.A. Odriozola, Does shaping catalysts modify active phase sites? A comprehensive in situ FTIR spectroscopic study on the performance of a model Ru/Al2O3 catalyst for the CO methanation, Chemical Engineering Journal 357 (2019) 248–257. https://doi.org/10.1016/j.cej.2018.09.166.

[38] Vikt, I. Spitsyn, A. A. Balandin, N. P. Dobrosel'skaya and I. E. Mikhailenko, Dokl. AN SSSR 121, Institute of Physical Chemistry, Academy of Sciences of the USSR (1958).

[39] Vikt. I. Spitsyn and N. E. Mikhailenko, Use of radioactive catalysts for dehydrating alcohols 21 (1966) 277–281.

[40] A.A. Balandin, V.I. Spitsyn, N.P. Dobrosel'skaya, I.E. Mikhailenko, I.V. Veteshchinskii, P.Y. Glazunov, On the influence of the radioactive radiation of a solid body on its catalytic properties, Russ Chem Bull (1961) 521–525. https://doi.org/10.1007/BF00909112.

[41] Vikt. I. Spitsyn, A. A. Baladin, N. P. Dobrosel'skaya and R. A. D'yaehkova, Catalytic dehydration of cyclohexanol on magnesium sulfate-protactinium-231, Institute of Physical Chemistry, Academy of Sciences, USSR (1964) 564–565.

[42] Vikt. I. Spitsyn, G. N. Pirogova, and I. E. Mikhailenko, The effect of ionizing radiation on the catalytic dehydration of N-dodecyl alcohol, The Institute of Physical Chemistry, Acad. Sci., USSR 9 (1962) 1515–1520.

[43] A. A. Balandin, Vikt. Spitsyn and N. P. Dobrosel'skaya, Cracking of cumene on a radioactive tricalcium phosphate catalyst, Institute of Physical Chemistry, Academy of Sciences of the USSR 12 (1965) 2095–2100.

[44] A. A. Balandin, Vict. I. Spitsyn, N. P. Dobrosel. Skaya, and I. E. Mikhailenko, On the Problem of Radioactive Radiation of Sulfur-35 Influencing the Catalytic Dehydration of Cyclohexanol, Institute of Physical Chemistry 86 (1964) 299–300.

[45] B. Jones, J. F. Kelly, Methods and products for converting carbon dioxide to one or more small organic compounds., WO 2020/124169 A1 (2020).

[46] B. Yoon, H.-B. Pan, C.M. Wai, Relative Catalytic Activities of Carbon Nanotube-Supported Metallic Nanoparticles for Room-Temperature Hydrogenation of Benzene, J. Phys. Chem. C 113 (2009) 1520–1525. https://doi.org/10.1021/jp809366w.

[47] J. Wang, Y. Wang, S. Xie, M. Qiao, H. Li, K. Fan, Partial hydrogenation of benzene to cyclohexene on a Ru–Zn/m-ZrO2 nanocomposite catalyst, Applied Catalysis A: General 272 (2004) 29–36. https://doi.org/10.1016/j.apcata.2004.04.038.

[48] KENNETH M. SANCIER, Hydrogen Migration on Alumina/Palladium catalyst for Benzene Hydrogenation*, Journal of Catalysis 20 (1971) 106–109.

[49] W. Wang, H. Liu, T. Wu, P. Zhang, G. Ding, S. Liang, T. Jiang, B. Han, Ru catalyst supported on bentonite for partial hydrogenation of benzene to cyclohexene, Journal of Molecular Catalysis A: Chemical 355 (2012) 174–179. https://doi.org/10.1016/j.molcata.2011.12.013.

[50] R. Li, W. Yao, Y. Jin, W. Jia, X. Chen, J. Chen, J. Zheng, Y. Hu, D. Han, J. Zhao, Selective hydrogenation of the C=C bond in cinnamaldehyde over an ultra-small Pd-Ag alloy catalyst, Chemical Engineering Journal 351 (2018) 995–1005. https://doi.org/10.1016/j.cej.2018.06.146.

[51] G. Roberto, S. Philippe, K. * Philippe, K. Yolande, S. Joachim, M. Christiane, D. and Jean-Luc, Preparation of Rhodium Catalysts Supported on Carbon Nanotubes by a Surface Mediated Organometallic Reaction, Eur. J. Inorg. Chem. https://doi.org/10.5194/tc-2016-52-RC4.

[52] B. Coq, P.S. Kumbhar, C. Moreau, P. Moreau, F. Figueras, Zirconia-Supported Monometallic Ru and Bimetallic Ru-Sn, Ru-Fe Catalysts: Role of Metal Support Interaction in the Hydrogenation of Cinnamaldehyde, J. Phys. Chem. 98 (1994) 10180–10188. https://doi.org/10.1021/j100091a038.

[53] Rh_bnz nmr Mizoroki 1977.

[54] A. Giroir-Fendler, D. Richard, P. Gallezot, Selectivity in Cinnamaldehyde Hydrogenation of Group-VIII Metals Supported on Graphite and Carbon, in: Heterogeneous Catalysis and Fine Chemicals, Proceedings of an International Symposium, Elsevier, 1988, pp. 171–178.

[55] M. Lashdaf, A. Krause, M. Lindblad, M. Tiitta, T. Venäläinen, Behaviour of palladium and ruthenium catalysts on alumina and silica prepared by gas and liquid phase deposition in cinnamaldehyde hydrogenation, Applied Catalysis A: General 241 (2003) 65–75. https://doi.org/10.1016/S0926-860X(02)00423-4.

[56] Y. Zhang, S. Liao, Y. Xu, D. Yu, Catalytic selective hydrogenation of cinnamaldehyde to hydrocinnamaldehyde, Applied Catalysis A: General 192 (2000) 247–251. https://doi.org/10.1016/S0926-860X(99)00400-7.

[57] S. Hirasawa, H. Watanabe, T. Kizuka, Y. Nakagawa, K. Tomishige, Performance, structure and mechanism of Pd–Ag alloy catalyst for selective oxidation of glycerol to dihydroxyacetone, Journal of Catalysis 300 (2013) 205–216. https://doi.org/10.1016/j.jcat.2013.01.014.

[58] E.G. Rodrigues, S.A.C. Carabineiro, X. Chen, J.J. Delgado, J.L. Figueiredo, M.F.R. Pereira, J.J.M. Órfão, Selective Oxidation of Glycerol Catalyzed by Rh/Activated Carbon: Importance of Support Surface Chemistry, Catal Lett 141 (2011) 420–431. https://doi.org/10.1007/s10562-010-0515-9.

[59] L.E. Chinchilla, C.M. Olmos, A. Villa, A. Carlsson, L. Prati, X. Chen, G. Blanco, J.J. Calvino, A.B. Hungría, Ru-modified Au catalysts supported on ceria–zirconia for the selective oxidation of glycerol, Catalysis Today 253 (2015) 178–189. https://doi.org/10.1016/j.cattod.2015.02.030.

[60] Y. Chen, H. Lim, Q. Tang, Y. Gao, T. Sun, Q. Yan, Y. Yang, Solvent-free aerobic oxidation of benzyl alcohol over Pd monometallic and Au–Pd bimetallic catalysts supported on SBA-16 mesoporous molecular sieves, Applied Catalysis A: General 380 (2010) 55–65. https://doi.org/10.1016/j.apcata.2010.03.026.

[61] A. Köckritz, M. Sebek, A. Dittmar, J. Radnik, A. Brückner, U. Bentrup, M.-M. Pohl, H. Hugl, W. Mägerlein, Ru-catalyzed oxidation of primary alcohols, Journal of Molecular Catalysis A: Chemical 246 (2006) 85–99. https://doi.org/10.1016/j.molcata.2005.10.020.

[62] T. Sato, T. Komanoya, Selective oxidation of alcohols with molecular oxygen catalyzed by Ru/MnO /CeO2 under mild conditions, Catalysis Communications 10 (2009) 1095–1098. https://doi.org/10.1016/j.catcom.2009.01.004.

[63] T. Tang, C. Yin, N. Xiao, M. Guo, F.-S. Xiao, High Activity in Catalytic Oxidation of Benzyl Alcohol with Molecular Oxygen over Carboxylic-Functionalized Carbon Nanofiber-Supported Ruthenium Catalysts, Catal Lett 127 (2009) 400–405. https://doi.org/10.1007/s10562-008-9708-x.

[64] M.V. Morales, M. Rocha, C. Freire, E. Asedegbega-Nieto, E. Gallegos-Suarez, I. Rodríguez-Ramos, A. Guerrero-Ruiz, Development of highly efficient Cu versus Pd catalysts supported on graphitic carbon materials for the reduction of 4-nitrophenol to 4-aminophenol at room temperature, Carbon 111 (2017) 150–161. https://doi.org/10.1016/j.carbon.2016.09.079.

[65] M. Gopiraman, S. Saravanamoorthy, I.-M. Chung, Highly active human-hair-supported noble metal (Ag or Ru) nanocomposites for rapid and selective reduction of p-nitrophenol to p-aminophenol, Res Chem Intermed 43 (2017) 5601–5614. https://doi.org/10.1007/s11164-017-2950-3.

[66] H. Park, D.A. Reddy, Y. Kim, S. Lee, R. Ma, M. Lim, T.K. Kim, Hydrogenation of 4-nitrophenol to 4-aminophenol at room temperature: Boosting palladium nanocrystals efficiency by coupling with copper via liquid phase pulsed laser ablation, Applied Surface Science 401 (2017) 314–322. https://doi.org/10.1016/j.apsusc.2017.01.045.

[67] HAJEK, J. N. Kumara, P. Mäki-Arvela, T. Salmi, D.Yu. Murzin, I. Paseka, T. Heikkilä, E. Laine P. Laukkanend, J. Väyrynen, Ruthenium-modified MCM-41 mesoporous molecular sieve and Y zeolite catalysts for selective hydrogenation of cinnamaldehyde, Applied Catalysis A: General 251 (2003) 385–396. https://doi.org/10.1016/S0926-860X(03)00345-4.

[68] T. Shimizu, M. Ota, Y. Sato, H. Inomata, Effect of pore structure on catalytic properties of mesoporous silica supported rhodium catalysts for the hydrogenation of cinnamaldehyde, Chemical Engineering Research and Design 104 (2015) 174–179. https://doi.org/10.1016/j.cherd.2015.08.004.

[69] S. Bhogeswararao, D. Srinivas, Chemoselective Hydrogenation of Cinnamaldehyde over Pd/CeO2–ZrO2 Catalysts, Catal Lett 140 (2010) 55–64. https://doi.org/10.1007/s10562-010-0423-z.

[70] F. Jiang, J. Cai, B. Liu, Y. Xu, X. Liu, Particle size effects in the selective hydrogenation of cinnamaldehyde over supported palladium catalysts, RSC Adv. 6 (2016) 75541–75551. https://doi.org/10.1039/C6RA17000E.

[71] Zhang, Winterbottom, Boyes, Raymahasay, Studies on the hydrogenation of cinnamaldehyde over Pd/C catalysts, J. Chem. Technol. Biotechnol 72 (1998) 264–272.

[72] F. Zhao, Y. Ikushima, M. Chatterjee, M. Shirai, M. Arai, An effective and recyclable catalyst for hydrogenation of α,β-unsaturated aldehydes into saturated aldehydes in supercritical carbon dioxide, Green Chem 5 (2003) 76–79. https://doi.org/10.1039/B209252M.

[73] V.G. W.S. Millman (Ed.), Proceedings of the 6th Meeting on Catal. Org. Synth., 1977.

[74] B. Neppolian, H.C. Choi, S. Sakthivel, B. Arabindoo, V. Murugesan, Solar light induced and TiO2 assisted degradation of textile dye reactive blue 4, Chemosphere 46 (2002) 1173–1181. https://doi.org/10.1016/S0045-6535(01)00284-3.

[75] G.A. Cerrón-Calle, A.J. Aranda-Aguirre, C. Luyo, S. Garcia-Segura, H. Alarcón, Photoelectrocatalytic decolorization of azo dyes with nano-composite oxide layers of ZnO nanorods decorated with Ag nanoparticles, Chemosphere 219 (2019) 296–304. https://doi.org/10.1016/j.chemosphere.2018.12.003.

[76] A. Nezamzadeh-Ejhieh, M. Karimi-Shamsabadi, Decolorization of a binary azo dyes mixture using CuO incorporated nanozeolite-X as a heterogeneous catalyst and solar irradiation, Chemical Engineering Journal 228 (2013) 631–641. https://doi.org/10.1016/j.cej.2013.05.035.

[77] A.A. Oladipo, A.O. Ifebajo, M. Gazi, Magnetic LDH-based CoO–NiFe2O4 catalyst with enhanced performance and recyclability for efficient decolorization of azo dye via Fenton-like reactions, Applied Catalysis B: Environmental 243 (2019) 243–252. https://doi.org/10.1016/j.apcatb.2018.10.050.

[78] N. Guettaı, H. Ait Amar, Photocatalytic oxidation of methyl orange in presence of titanium dioxide in aqueous suspension. Part I: Parametric study, Desalination (2005) 427–437.

[79] L.-C. Chen, F.-R. Tsai, C.-M. Huang, Photocatalytic decolorization of methyl orange in aqueous medium of TiO_2 and Ag–TiO_2 immobilized on γ-Al_2O_3, Journal of Photochemistry and Photobiology A: Chemistry 170 (2005) 7–14. https://doi.org/10.1016/j.jphotochem.2004.07.012.

[80] K. Avvaru Praveen, B. Dinesh, T. Aschalew, Photocatalytic degradation of organic dyes: Pd-g-Al_2O_3 and PdO-g-Al_2O_3 as potential photocatalysts, Royal Society of Chemistry (2021) 6396–6406.

[81] P. Verma, P. Baldrian, F. Nerud, Decolorization of structurally different synthetic dyes using cobalt(II)/ascorbic acid/hydrogen peroxide system, Chemosphere 50 (2003) 975–979. https://doi.org/10.1016/S0045-6535(02)00705-1.

[82] S. Sakthivel, B. Neppolian, M.V. Shankar, B. Arabindoo, M. Palanichamy, V. Murugesan, Solar photocatalytic degradation of azo dye: comparison of photocatalytic efficiency of ZnO and TiO_2, Solar Energy Materials and Solar Cells 77 (2003) 65–82. https://doi.org/10.1016/S0927-0248(02)00255-6.

[83] H. Salavati, A. Teimouria, S. Kazemib, Synthesis and Characterization of Novel Composite-Based Phthalocyanine Used as Efficient Photocatalyst for the Degradation of Methyl Orange, Chemical Methodologies (2017) 15–31.

[84] Y. Nishimura, M. Suda, M. Kuroha, H. Kobayashi, K. Nakajima, A. Fukuoka, Synthesis of 5-hydroxymethylfurfural from highly concentrated aqueous fructose solutions using activated carbon, Carbohydrate Research 107826.

[85] N. Villanueva Martinez, Obtención de 5-hidroxmetilfurfural a partir de glucosa proveniente de licores de corteza de pino y eucalipto, utilizando catalizadores sólidos en medio acuoso, Concepción, Chile, 2017.

[86] H. Shen, H. Shan, L. Liu, Evolution Process and Controlled Synthesis of Humins with 5-Hydroxymethylfurfural (HMF) as Model Molecule, ChemSusChem (2020) 513–519.

[87] I. van Zandvoort, Y. Wang, C.B. Rasrendra, E.R.H. van Eck, P.C.A. Bruijnincx, H.J. Heeres, B.M. Weckhuysen, Formation, Molecular Structure, and Morphology of Humins in Biomass Conversion: Influence of Feedstock and Processing Conditions, ChemSusChem (2013) 1745–1758.

Chapter 2

Experimental and analytical methods

2.1. Introduction

The experimental protocols, especially the catalyst preparation and reaction protocols, are of great value due to the technical constraints and difficulties involved in operating under radioactive conditions. This is why the manner in which each step was carried out was selected in such a way that it would be simple to implement and above all, reproducible.

This chapter describes how the experiments were carried out in the course of the study. Thus, the first part shows the different unitary steps of the synthesis of the non-radioactive and radioactive catalysts, from the preparation of the support to the calcination by heat treatment, as well as the characterization techniques used. Finally, the second part presents the catalytic test tools used to study the activity of the different catalysts.

2.2. Catalyst preparation

2.2.1. Synthesis protocol

The different steps in the synthesis of the catalysts, from conditioning of the support to calcination, are shown in Figure 2-1.

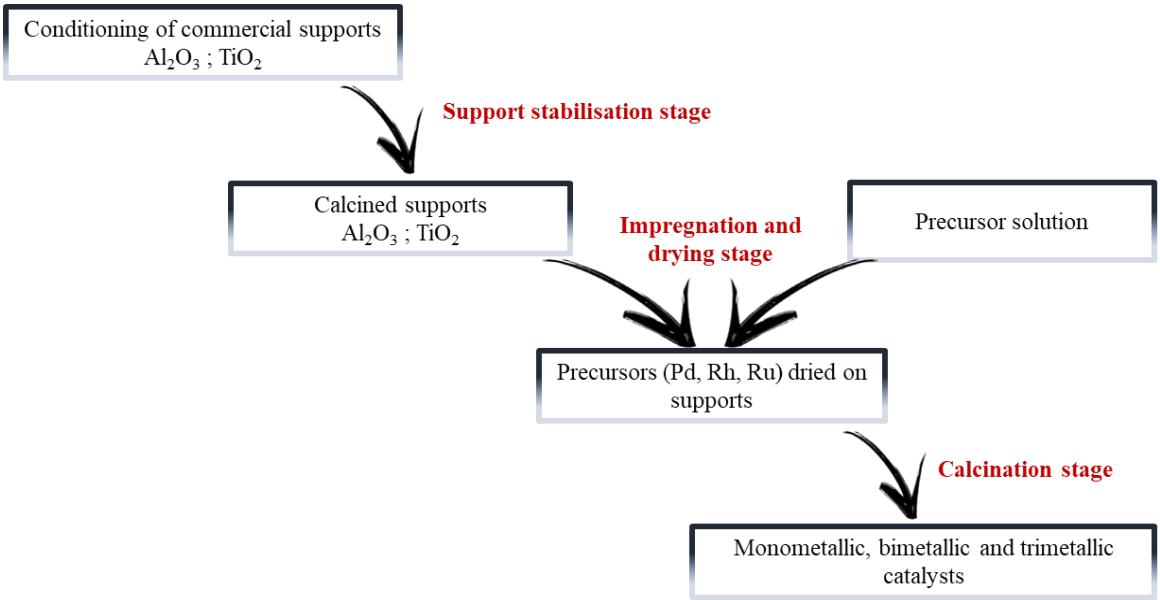

Figure 2-1:*Schematic synthesis of the catalysts.*

2.2.1.1. The support stabilisation stage

The commercial supports used in the preparation of the catalysts are: Al_2O_3 (SA-61138, University of Birmingham) and TiO_2 (ST-61120, University of Birmingham). Before use 15 g of each support are grinded with a porcelain mortar until a fine powder is obtained. The powder obtained is then sieved to 212 µm to homogenise the grain size. Afterwards, in order to ensure the absence of moisture and impurities, the sieved products were calcined in a muffle furnace at 500°C for 6 hours, with a heating ramp of 1.4°C·min^{-1}. Finally, the recovered supports were stored in plastic bottles before being used for the synthesis of the catalysts.

2.2.1.2. Impregnation and drying stage

- *Non-Radioactive catalyst*

All the prepared catalysts are impregnated in the same way with an excess of solvent. The metal precursors used are: $Pd(NO_3)_2*xH_2O$ (Alfa Aesar, CAS: 10102-05-3, 99.95% of purity where 39% min of Pd); $Ru(NO)(NO_3)_x(OH)_y$ (Alfa Aesar, CAS: 34513-98-9, 99.98% of purity where 39% min of Ru) and $Rh(NO_3)_3$ solution (Alfa Aesar, CAS: 10139-58-9, Rh 10-15% wt.%).

First, the impregnation solution is prepared by solubilising a specific amount of the target metal precursor, in a volume of 15 mL of water using a 100 mL beaker. The mixture is kept stirred for 30 minutes, until a homogeneous solution is obtained, which we named S_1. Afterwards, 0.5 g of support is weighed and placed in a 30 mL vial. The S_1 solution is then added to the vial containing the support. This vial is kept closed under agitation for 20 hours at room temperature. The product obtained is transferred to a 100 mL beaker allowing the evaporation of the solvent, under stirring for 6h at 60°C. The temperature of the liquid is monitored during the whole evaporation stage by means of an infrared thermometer. Finally, the beaker is covered with a perforated aluminium sheet and placed in an oven for 12 hours at 60°C. This procedure was carried out for each of the non-radioactive catalysts prepared.

Additionally, a serie of non-radioactive catalysts (5%Pd/TiO_2-acid and 5%Pd/Al_2O_3-acid) were synthesized in order to simulate more accurately the radioactive catalysts. For this purpose, a non-radioactive solution was prepared, with the approximate composition of the recovered and purified nuclear fuel solution containing ^{107}Pd (Table 2-1). This solution, which we call acidic S, was used as the impregnation solution for this series of catalysts. Both the impregnation step and the other steps of the protocol were carried out following the non-radioactive catalyst synthesis protocol.

- *Radioactive catalyst*

The radioactive catalysts were all impregnated using a solution that was recovered and purified from spent nuclear fuel, in the framework of the studies being carried out by Orano in collaboration with CEA, for the utilisation of the fines from the recycling of nuclear fuel. The general composition of the radioactive solution is shown in Table 2-1.

Table 2-1: *Composition of recovered and purified radioactive solution.*

	Molar mass	***C [g·L^{-1}]***	***M [mol·L^{-1}]***	***wt.%***
		Metals		
Pd_{Total}	106	1.1E+00	1.0E-02	1.9E+00
^{107}Pd	107	2.2E-01	2.0 E-03	3.8 E-03
Ru	101	6.0E-05	5.9E-07	1.0E-04
Mo	96	5.0E-04	5.2E-06	8.7E-04
Ag	108	8.0E-04	7.4E-06	1.4E-03
Zr	91	5.0E-04	5.5E-06	8.7E-04
		Anions		
C_2O_4	80	1.0E-02	1.2E-04	1.7E-02
Cl	35	1.1E-01	3.2E-03	2.0E-01
F	19	1.0E-02	5.3E-04	1.7E-02
NO_2	46	1.0E-02	2.2E-04	1.7E-02
NO_3	62	5.6E-01	9.0E-04	9.8E+01
PO_4	95	1.0E-02	1.1E-04	1.7E-02
SO_4	96	1.0E-02	1.0E-04	1.7E-02

The synthesis of the radioactive catalyst was carried out using 17.5 mL of purified solution. According to the composition specified in Table 2-1, the solution contained 19.25 mg of Pd with 3.8 mg being ^{107}Pd. To obtain the catalyst with 5wt.% Pd (where 0.98wt.% are ^{107}Pd), 366 mg of support were required. From the mixture of the purified radioactive solution with the support in a 30 mL vial, the impregnation was carried out in a glove box following exactly the same protocol described in the previous section for the non-radioactive catalyst.

2.2.1.3. Calcination stage

The dried product is collected, grinded with a mortar until a fine powder is obtained, and calcined at 250°C for 6 hours with a heating ramp of 1.4°C·min^{-1}. The prepared samples are stored at room temperature in closed 10 mL vials.

2.2.2. Characterization techniques

2.2.2.1. Nitrogen physisorption

The phenomenon that occurs when a gas is brought into contact with the surface of a degassed solid is the formation of van der Waals bonds (physisorption). The nitrogen physisorption technique is the most commonly used for the determination of the surface areas and pore size distribution of the catalyst. As a result of the analysis, an adsorption isotherm is obtained, allowing the adsorbed volume to be found directly at a given pressure, in addition to the calculation of the surface area, pore size, and distribution, usually using the BET method, based on the Brunauer, Emmet and Teller isotherm [1,2].

The general protocol that is carried out for the surface analysis of catalysts using nitrogen physisorption is described below.

Initially, in order to obtain the actual quantity to be analyzed, the mass of each empty cell is measured with its respective cap which we will call m_1, then, 50-100 mg of sample are

introduced in the cell, the cell containing the powder with its support and its cap is weighed to obtain a new mass called m_2. Then, the samples are degassed at 150°C for materials with Pd and Rh and at 80°C for Ru, in order to avoid any loss of Ru. After 3 hours, the degassing stops and the cells are filled with N_2 gas and weighed again to obtain a mass called m_3. With the samples already prepared in the next step, it is necessary to assemble the cells in the equipment (Micromeritics TriStar II plus) and to start the analysis for a duration of 12 hours, the real mass of the sample to be analyzed is calculated by the software for which it is necessary to enter the masses m_1 and m_3 ($m_R = m_3-m_1$).

2.2.2.2. X-ray-diffraction (XRD)

X-ray diffraction (XRD) is one of the most widely used techniques for analysing the crystalline phases of any type of material. The technique involves passing an X-ray beam at an angle θ over the material to be analyzed, as shown in Figure 2-2a. The intensity of the diffracted radiation resulting from the interaction of the beam with the solid is a function of the distance between the crystal planes, the type of atoms that make up the structure and the diffraction angle θ. This results in each crystalline substance having its own diffraction patter and constitutes a true "fingerprint" of it, allowing its identification in any mixture where it is present [3,4].

The samples were analyzed in the Bruker D8 Advance Powder Diffractometer in Bragg-Brentano θ-θ configuration (Figure 2-2b). The analysis was performed for 2θ values from 10° to 80°, with steps of 0.05°. The EVA software subsequently allows the determination of the crystal phases by comparing the experimental diffractogram with databases.

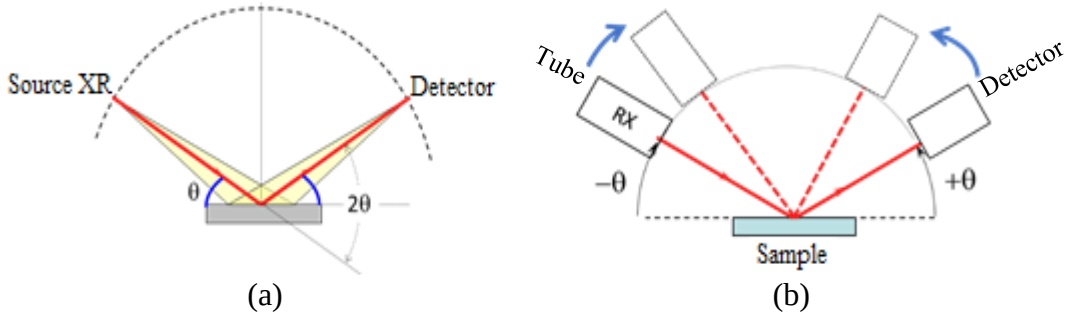

(a) (b)

Figure 2-2: *(a) Focusing Bragg-Brentano setup, (b) θ-θ Bragg-Brentano setup.*

2.2.2.3. Thermogravimetric analysis (TGA)

Thermogravimetry analysis (TGA) is a technique based on the measurement of the change in mass of a sample when subjected to a temperature change in a controlled atmosphere. This change can be a loss or a gain of mass. The analysis was notably performed to follow the thermal decomposition of the metal precursors during calcination.

TGA measurements were carried out on a SDT Q600 V20.9 Build 20. The experiments were performed under an air flow of 100 $mL \cdot min^{-1}$, applying a temperature ramp of 5 $°C \cdot min^{-1}$ up to 800 °C.

2.2.2.4. Temperature-programmed reduction (TPR)

Temperature programmed reduction (TPR) provides information on the number and type of reducible species present on the catalyst, their reduction temperature, reduction kinetics and metal-support interactions. In the TPR technique, the catalyst is subjected to a linear increase in temperature, while a mixture of reducing gas flows through it (usually hydrogen diluted in an inert gas such as argon). The reduction can be followed by monitoring the change in the composition of the gas mixture after passing through the cell.

The experiments were conducted on an Autochem chemisorption analyzer from Micromeritics, equipped with a TCD and coupled with a mass spectrometer (Omnistar, Pfeiffer) to follow

possible desorption (H_2O, O_2, CO_2 or others). About 100 mg of calcined catalyst was introduced into a U-shaped microreactor. Before the TPR run, the catalyst was pre-treated by degassing with a heating ramp of 10 ºC·min^{-1} to 400 ºC and then kept at this temperature for 30 min under Ar atmosphere at 50 mL·min^{-1}. After return to ambient conditions, the H_2-containing flow was stabilised (50 mL·min^{-1}, 5 vol.% H_2 in Ar) and the temperature programmed reduction was performed (from room temperature to 900 ºC, heating ramp of 10 ºC·min^{-1}).

2.2.2.5. X-ray Photoelectron Spectroscopy (XPS)

XPS is a technique based on the measurement of the kinetic energy of electrons emitted by a solid under the impact of a beam of X photons. The most commonly used beams are Mg and Al Kα with energies of 1253.6 and 1486.6 eV, respectively.

When a photon of energy hν interacts with an electron at a level with a binding energy (BE), the energy of the photon is completely transferred to the electron, resulting in the emission of a photoelectron with a kinetic energy (KE) [5].

The spectrum of the electrons in the nucleus in number and energy is characteristic of an atom in a given compound. XPS can analyse all elements of the periodic table except for hydrogen and helium.

The X-ray photoelectron spectroscopy (XPS) experiments were carried out in a Kratos AXIS Ultra DLD spectrometer using a monochromatic Al Kα radiation (1486.6 eV) operating at 180 W (12 mA, 15 kV). High-resolution spectra were collected using an analysis area of ≈ 300 μm × 700 μm and a 20 eV pass energy. Instrument base pressure was 5E−10 Torr. The Kratos charge compensation system was used for all analyses and the binding energies were corrected taking Alumina Al 2p peak (unresolved doublet) at 74.6 eV as reference. The C 1s/Ru 3d, O 1s, N 1s, Al 2p and Ru 3p spectra were analyzed using the CasaXPS software (version 2.3.17,

Casa Software Ltd.). Spectra decomposition and quantification was performed after a Shirley type background subtraction and Gaussian–Lorentzian profiles with 70/30 Gaussian/Lorentzian proportion.

2.3. Catalytic tests protocols

In the following, step-by-step reaction protocols for both CNA hydrogenation and methyl orange decolorization are described.

2.3.1. Hydrogenation of cinnamaldehyde

2.3.1.1. Non-Radioactive catalyst

- *Preparation of the reaction solution*

First, the reaction solution is prepared, for which 26 ml (20 g) of isopropanol (case: 67-63-0) are measured with a measuring cylinder and put into a beaker. Then 650 µL (0.68 g) of cinnamaldehyde (CNA, Alfa Aesar, CAS: 104-55-2, +98% of purity) are dissolved in isopropanol, which is equivalent to an initial CNA concentration of 0.2 M, finally the mixture is stirred until a homogeneous solution is obtained. In order to analyse the initial solution (t=0), 1 mL is taken before starting the reaction.

- *Set-up and operation of the PARR reactor*

To start the set-up, the stirrer and the sampling line are placed, then the reactor (PARR of 30 mL maximum capacity) is loaded with the solution already prepared (25 mL) and a quantity of catalyst of 20 mg to have an initial CNA/metal mass ratio equal to 680 $g \cdot g^{-1}$. The reactor is closed with a clamp, the screws are tightened and the closure of the valves is checked. After positioning the heating furnace, the gas inlet valve is opened, the system is purged and finally pressurised to the required pressure depending on the gas bottle used (4% or 100% of H_2). The final set-up of the reactor is shown in Figure 2-3.

The system is heated and stirred (1500 rpm), the reaction time is started as the system starts to heat up. The progress of the reaction is monitored by analysing samples (1 mL) taken from the reaction mixture every 30 and 60 minutes, the samples are immediately filtered using syringe and Agilent 0.2µm nylon filters.

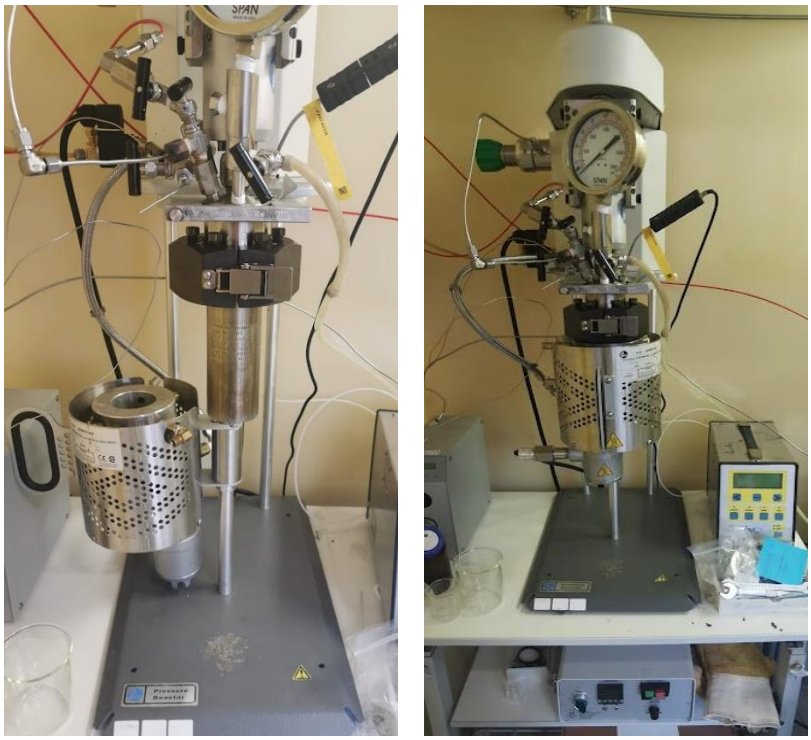

Figure 2-3: *PARR reactor set-up for the non-radioactive hydrogenation of CNA.*

- *Analysis of the catalytic results*

Samples were prepared with 400 µL of reaction solution and 10 µL of toluene used as internal standard. The samples were then analyzed by chromatography, using a GC-FID-MS gas chromatograph (Agilent technologies 5977B MSD) equipped with a CP-Wax 52 CB column (30 m x 250 µm x 0.25 µm) and a flame ionisation detector (FID) to calculate the conversion and selectivity. The analytical method used are given in Table 2-2.

Table 2-2: *GC analytical methods parameters.*

Injection	Injection mode	Split-Splitless Inlet
	Temperature	250 °C
	Carrier gas	He
	Pressure	17.2 psi
	Total flow	24.69 mL·min^{-1}
	Column flow	1.69 mL·min^{-1}
Oven	Initial Temperature, T_0	40 °C (4 min)
	T_1 (rate)	170 °C (25 °C·min^{-1}) / 5.2 min
	T_2 (rate)	240 °C (50 °C·min^{-1}) / 6.4 min
	Equilibration time	0.25 min
	Total program time	15.6 min
	Final temperature, T_F	240 °C
Detector (FID)	Temperature	270 °C
	H_2 flow	40 mL·min^{-1}
	Air flow	400 mL·min^{-1}

The identified reaction products were calibrated to determine the concentration which is directly proportional to the area determined by peak integration. The values obtained from the analysis of the initial solution, allowed the calculation of the conversion at each point using the equation 2-1.

$$X_t = \frac{n_{CNA}^0 - n_{CNA}^t}{n_{CNA}^0} \qquad \textit{Eq. 2-1}$$

Where X_t corresponds to the conversion at time t, n_{CNA}^0 corresponds to the concentration of cinnamaldehyde in the initial sample and n_{CNA}^t corresponds to the concentration of cinnamaldehyde in the sample at time t.

The selectivity can be defined by the equation 2-2.

$$S_i = \frac{n_i}{n_{CNA}^0 - n_{CNA}^t} \qquad \textit{Eq. 2-2}$$

Where n_i is the number of moles of product i.

2.3.1.2. Radioactive catalyst

- *Preparation of the reaction solution*

The preparation of the reaction solution was carried out in the same way as for the non-radioactive tests.

- *Set-up and operation of the PARR reactor*

After a lengthy administrative procedure, the reactor for the radioactive tests, whose characteristics were similar to those of the reactor used for the non-radioactive tests, was authorised for use and handling in fume hood. As a result, the assembly and operation of the reactor was slightly different from that of the non-radioactive tests. However, these variations did not affect in any way the development of the reaction.

The main difficulty was, as expected, the transfer of the radioactive catalyst from the glove box to the fume hood. In order to avoid any contamination, the following procedure was used:

- A new glass container with a lid, previously labelled, was taken to store the catalyst for each test. The fingers of the vinyl gloves commonly used in the laboratory were cut off and a finger was used to cover and protect each container and each lid. This greatly reduced the risk of contamination as the container does not come into direct contact with the contamination in the glove box.
- The previously prepared containers were placed in a sealable bag in the glove box.

- The 20 mg of radioactive catalyst for each test were pre-weighed in the glove box and carefully transferred separately into the glass containers protected by gloved fingers. The containers were closed and placed back into the airtight bag.
- The removal of the catalysts from the glove box was carried out with the use of a special plastic bag which was sealed and controlled to rule out alpha or beta contamination.
- The recovery of the catalysts required the help of another person and the use of a triple pair of gloves. The first person unzips the plastic bag, opens the airtight bag and checks the containers with the alpha and beta contamination detector. He then removes the gloved finger that was protecting the lid. The second person held the container with his clean gloves on the side of the lid, while the first person removed the second gloved finger protecting the rest of the container. The first person checked his hands with the detector and removed the first pair of gloves. The second person checks the container and cleans it with acid solution to rule out contamination. Finally, the whole area and the persons were checked thoroughly.
- After verifying that there is no contamination the containers are stored in a clean place in the fume hood ready for use.

The set-up of the reactor for the reaction is carried out in exactly the same way as described for the non-radioactive tests, taking great care when mixing the catalyst with the reaction solution. After completion of the set-up, for safety reasons, the reactor is covered by a metal mesh with a hatch to allow sampling (Figure 2-4).

After each test, the reactor and each of its components were thoroughly washed with acid solution and ethanol, until practically no alpha and beta contamination were detected.

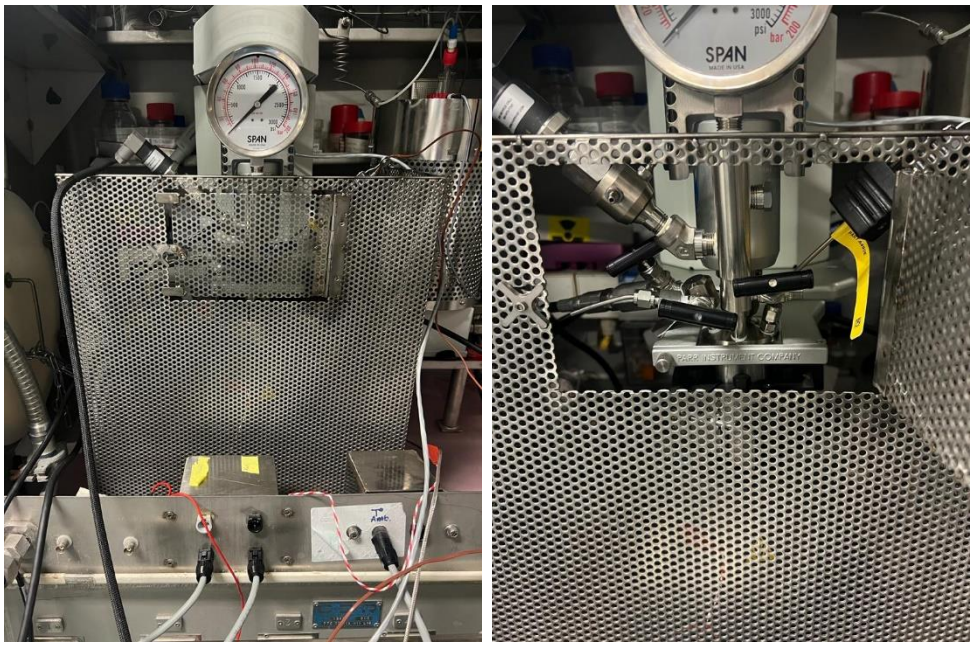

Figure 2-4: *Final set-up of the PARR reactor for radioactive tests.*

- *Analysis of the catalytic results*

Contrary to the non-radioactive tests, the aliquots sampled in the course of the reaction with radioactive catalyst, were analyzed by ^{1}H nuclear magnetic resonance (NMR) spectroscopy, since, as mentioned in the previous chapter, this is the only analysis technique available in the laboratory where the radioactive material tests are carried out, which is why this was one of the criteria to be taken into account in the selection of the model reaction.

NMR spectroscopy is an analytical technique used to determine the molecular structure and chemical composition of a sample. It is based on the property of some nuclei to absorb energy when exposed to radio frequencies, causing a transit between energy levels resulting from the interaction of an external magnetic field with the different orientations of the nuclear spin. Thus, the intensity, shape and position of the signals in the spectrum of a given nucleus are intimately related to its molecular structure, and a detailed analysis of the spectrum provides valuable information about the structure of the parent compound.

For the preparation of each sample, 400 µl of solution + 200 µl of D_2O (deuterated solvents) were mixed. The analyses were performed in an Agilent DD2 400MHz spectrometer with the 5mm "OneNMR" equipped with Z gradients. All NMR measurements are performed at 25°C.

The processing of the spectra obtained after the analysis of each sample was performed using ChemSketch-NMR Processor Academic Edition. Figure 2-5 shows a typical ^{1}H NMR spectrum of CNA hydrogenation with the identification of each of the protons present in the molecule.

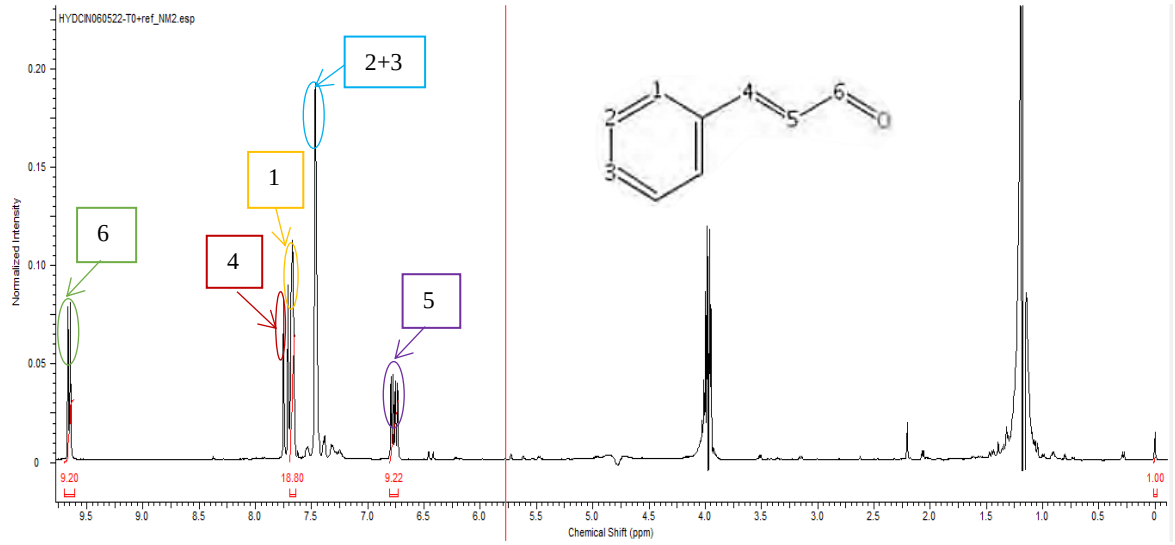

Figure 2-5: *Typical ^{1}H NMR spectrum of CNA hydrogenation.*

The H2+H3 proton peak is characteristic of carbons 2 and 3 of the aromatic ring present in both the cinnamaldehyde and the different reaction products, which means that it remains constant throughout the reaction. Thus, this peak was integrated and fixed directly to a value of 3, which corresponds to the 3 protons bound to carbons 2 and 3 (Figure 2-5). This hypothesis was used to compare all the spectra taking the H2+H3 proton peak as a reference and to normalise all the other values of the integration of the other peaks.

Finally, the integration of the H6 peak characteristic of the cinnamaldehyde molecule allowed the calculation of the conversion with the help of the equation 2-3.

$$X = \frac{I_{t_0} - I_{t_x}}{I_{t_0}} \qquad \textit{Eq. 2-3}$$

Where I_{t_0} is the integration value of the H6 peak at time zero and I_{t_x} is the integration value of the peak at time x.

2.3.2. Decolorization of methyl orange

- *Preparation of reaction solution*

The solution for the decolorization reactions was prepared by dissolving the required amount of methyl orange (CAS: 547-58-0) in distilled water to obtain a concentration of 1.52E-04 M. The mixture was stirred until a homogeneous orange coloured solution was obtained.

The reaction solutions were prepared in the same way as the non-radioactive tests and then placed in the glove box for the radioactive tests.

- *Set-up and operation*

30 mL of reaction solution and the amount of catalyst are placed in a 50 mL beaker on a magnetic hot plate, the beaker is completely covered with aluminium foil to avoid contact with light (Figure 2-6). The start of the reaction (t_0 or $t_{initial}$) is marked by stirring (400 rpm) and heating to 40°C. The reaction is monitored by taking 0.2 mL of sample every few minutes. Each sample is immediately centrifuged to separate and recover the supernatant. After the reaction time has elapsed, the heating and stirring are stopped.

For the preliminary tests carried out in the presence of light, a conventional 53 W tungsten halogen lamp was positioned over the beaker, in order to allow the light to have direct contact with the reaction mixture.

All the equipment necessary for the assembly and performance of the methyl orange decolorization tests was located in the glove box, so the only variation from the non-radioactive tests was the use of the radioactive catalyst. All tests with radioactive material were performed in the absence of light.

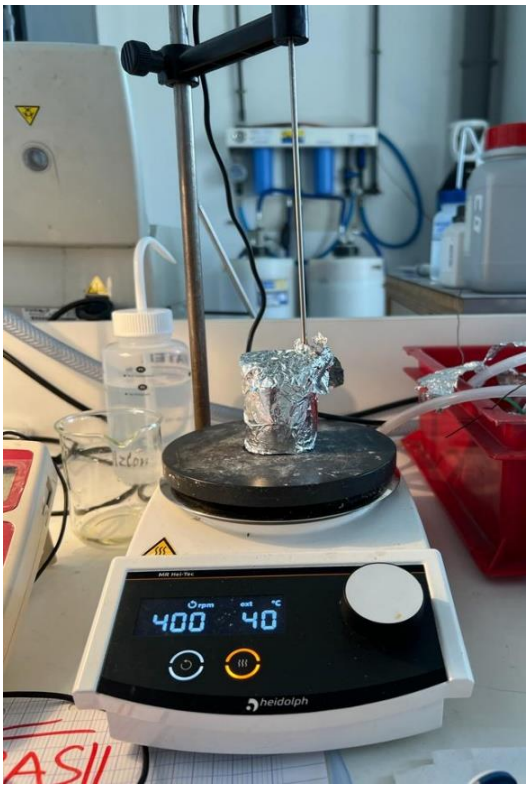

Figure 2-6: *General set-up for azo-dyes decolorization.*

- *Analysis of the catalytic results*

The initial solution together with all samples taken in the course of the reaction were diluted 10-fold in distilled water and analyzed with a Lambda 650 Perkin-Elmer UV-Visible Spectrometer. The absorbance intensity was used to calculate the conversion based on the Lambert-Beer Law, this law expresses the relationship between absorbance of monochromatic (fixed wavelength) and concentration of a chromophore in solution (Eq. 2-4).

$$\boldsymbol{A = \varepsilon \cdot c \cdot d} \qquad \textbf{Eq. 2-4}$$

The absorbance of a solution is directly proportional to its concentration (c), the greater the number of molecules the greater the interaction of light with them. Likewise, it depends on the distance the light travels through the solution at equal concentration (d), the greater the distance the light travels through the sample the more molecules it will encounter. Finally, it depends on ε, a proportionality constant called extinction coefficient, which is specific to each chromophore. In this study, samples were analyzed in 1 cm plastic cells, the MO concentration was followed at 469 nm (ε = 1917.6 L mol^{-1} cm^{-1}), which corresponds to the isobestic point of MO in order to eliminate the bathochromic shift in the acid pH regime as shown in Figure 2-7 [6,7]. "Peak-valley" differences in absorbance were measured to determine the concentration variations.

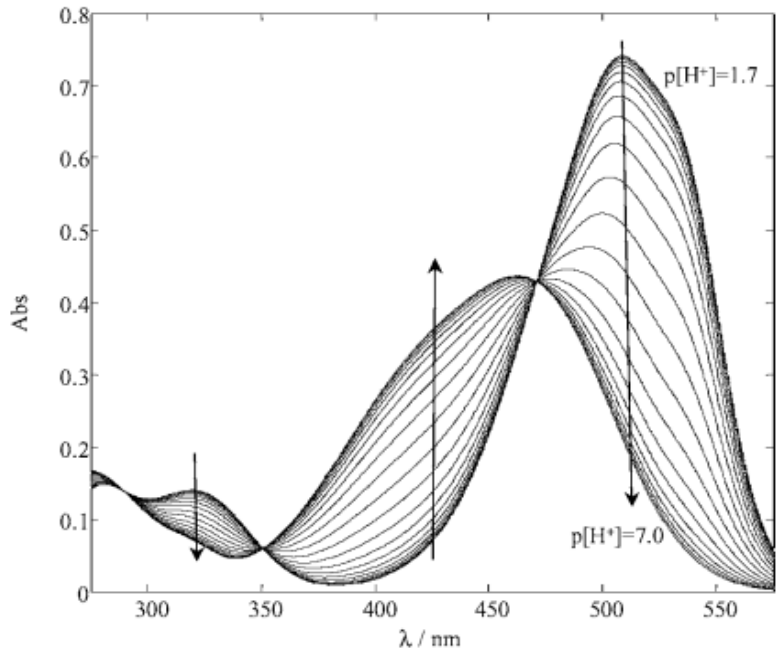

***Figure 2-7**: Isosbestic point for methyl orange. The spectra for pH 7–11 overlap and are represented by a single black line [7].*

Samples collected from the radioactive tests were analyzed by UV–vis absorption spectrophotometry (Shimadzu UV3600) in 1 cm plastic cells. Spectra were directly recorded in the glove box via optic fibers connected to the spectrometer situated outside the enclosure.

The concentration of MO was also followed at 469 nm ($\varepsilon = 1917.6\ L{\cdot}mol^{-1}{\cdot}cm^{-1}$). "Peak-valley" differences in absorbance were measured to determine the concentration variations.

2.3.3. Regeneration of catalyst

2.3.3.1. Catalyst deactivation

The deactivation of the catalysts as well as the hydrogenation of CNA was carried out in the PARR reactor. The reaction solution was prepared as follows: 40 g of fructose (CAS: 57-48-7) were dissolved in 200 mL of water to obtain a 20 wt.% solution which we will call S_1; 22 mL of solution S_1 were mixed with 11 mL of MIBK (CAS: 108-10-1) to obtain the reaction solution S_r; finally, the mixture, which will consist of an aqueous phase and an organic phase, is stirred for 10 min at 400 rpm. To analyse the initial solution (t=0), 3 mL of S_r solution is taken before starting the reaction.

The setup and operation of the PARR reactor was carried out in a similar way as described in section 2.3.1.1. The stirrer and the sampling line were placed, then the reactor (PARR with a maximum capacity of 30 mL) was loaded with the prepared S_r solution (30 mL) and a catalyst amount of 600 mg. After closing the reactor, the system is heated to 140°C and stirred (1500 rpm approx.) at atmospheric pressure, the reaction time is started when the system starts to warm up. After 3h of reaction, the final mixture is collected and filtered and the catalyst is recovered and dried under vacuum. In order to obtain a sufficient amount of catalyst for characterization and use in the model reaction, two experiments were carried out for each catalyst 5%Pd/Al_2O_3 and 5%Ru/Al_2O_3

2.3.3.2. Catalyst irradiation

The deactivated catalysts 5%Pd/Al_2O_3 and 5%Ru/Al_2O_3 were sent for irradiation in dry medium (250 mg each) to the ATALANTE facilities at CEA de Marcoule. A GRS-D1 Gamma-Service-

Médical-GmbH irradiation system with a calibrated Cs-137 irradiation source and a dose rate of approximately 0.6 $kGy \cdot h^{-1}$ was used for irradiation. Each sample was irradiated for 2 months corresponding to an approximate dose of 600 kGy, the catalysts were removed from the irradiator and sent back to the UCCS for further analysis and testing.

2.4. References

[1] W. Erika, Caractérisation des propriétés texturales et de transport de supports de catalyseurs Apport de la RMN du 129Xe. THESE DE DOCTORAT, Paris, 20 octobre/2015.

[2] B. Moulay-Rachid, Contribution à l'étude de l'adsorption physique de gaz sur les nanotubes de carbone mono- et multiparois. THESE DE DOCTORAT, Vandoeuvre-lès-Nancy, 07 Décembre/2004.

[3] A. Christophe, J. Erwann, DIFFRACTION DES RAYONS X TECHNIQUES ET ÉTUDES DES STRUCTURES CRISTALLINES, 2009, http://culturesciencesphysique.ens-lyon.fr/ressource/Diffraction-rayons-X-techniques-determination-structure.xml.

[4] B. ANDREI A., U. ELENA GABRIELA, A.-E. HASSAN Y., X-Ray Diffraction: Instrumentation and Applications, Critical Reviews in Analytical Chemistry (2015) 289–299.

[5] Mª del Valle, Martínez de Yuso García, "Aplicaciones de la Espectroscopía Fotoelectrónica de Rayos X en la Caracterización de Materiales Funcionales, Málaga, 2015.

[6] B. Jean-François, S. Terry M., On the Dissociation of Methyl Orange: Spectrophotometric Investigation in Aqueous Solutions from 10 to 90 ◦C and Theoretical Evidence for Intramolecular Dihydrogen Bonding, Journal ofSolution Chemistry (2005) 1387–1406.

[7] E. Sait, P. Aneta, S. Aneta Anna, V. Vasil, N. Thomas, T. Stephen, P. Craig, Photometric Sensing of Active Chlorine, Total Chlorine, and pH on a Microfluidic Chip for Online Swimming Pool Monitoring, Sensors (2020).

Chapter 3

Catalyst characterization

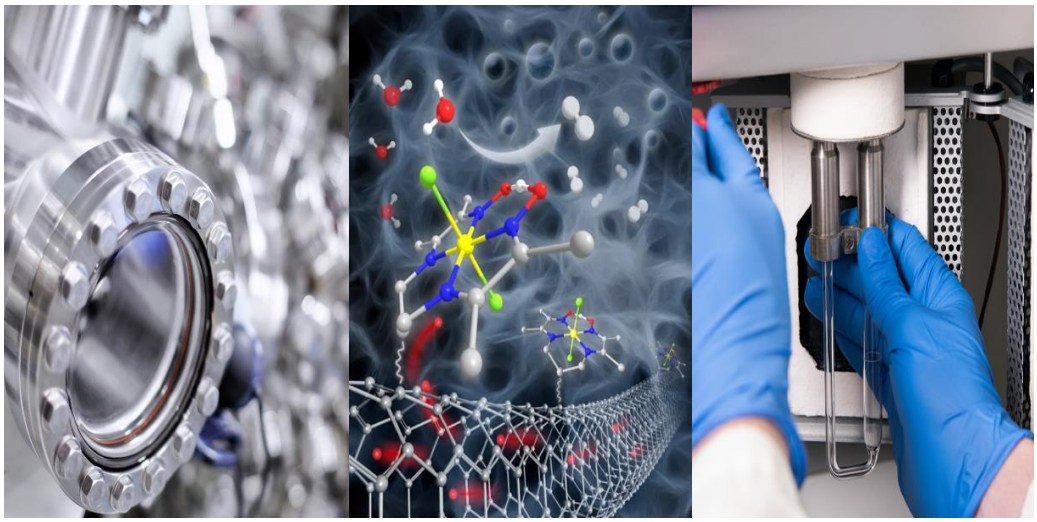

3.1. Introduction

The aim of this chapter is to present the results of the characterization carried out on the monometallic catalysts used in the different applications addressed in this work. In the first part, the results of the BET and XRD analyses will be shown, where the structural and textural properties of the different catalysts are evaluated, followed by the TPR analysis that sought to verify the Pd reduction in the acid catalysts, i.e. the non-radioactive catalysts synthesized with the solution similar to the radioactive solution. Then, the results of the TGA performed on the deactivated catalysts are presented in order to corroborate the presence of humins and finally, the results of the XPS analyses are shown, which allow to determine the oxidation state of the Ru-based catalysts used in the study of catalyst reactivation by γ-irradiation.

Table 3-1 shows the compilation of all the catalysts synthesized, specifying: the formulation, the metal loading, the reference and the application in which the catalyst was used. The synthesis of all catalysts was performed following the protocol described in section 2.2.1.

Table 3-1: *Compilation of synthesized catalysts.*

Formulation	***Metal charge***	***Reference***	***Application***
Monometallic	5% Pd	5%Pd/Al_2O_3	Hydrogenation of CNA and catalysts regeneration
	5% Ru	5%Ru/Al_2O_3	
	5% Rh	5%Rh/Al_2O_3	
Bimetallic	2.5% Pd 2.5%Ru	5%PdRu/Al_2O_3	Hydrogenation of CNA
	2.5% Pd 2.5%Rh	5%PdRh/Al_2O_3	
Trimetallic	3.3% Pd 3.3% Ru 3.3% Rh	5%Tri/Al_2O_3	Pre-studies of CNA hydrogenation

***Table 3-1**: Compilation of synthesized catalysts (Continuation).*

Formulation	*Metal charge*	*Reference*	*Application*
Monometallic	5% Pd	5%Pd/TiO_2	Decolorization of Methyl orange
Monometallic Acid solution	5%Pd	5%Pd/TiO_2-Acid	
	5%Pd	5%Pd/Al_2O_3-Acid	Hydrogenation of CNA
Monometallic Radioactive solution	5%Pd (where 17% ^{107}Pd)	5%Pd/TiO_2*	Decolorization of Methyl orange
	5%Pd (where 17% ^{107}Pd)	5%Pd/Al_2O_3*	Hydrogenation of CNA

This work was carried out under the supposition that, by replicating exactly the same synthesis protocol for the radioactive catalysts, they would retain the same characteristics as the non-radioactive catalyst. This is because, due to the constraints of handling radioactive material, it was technically not possible to characterise the catalyst prepared with ^{107}Pd.

3.2. Characterization of the catalysts

3.2.1. Nitrogen physisorption

Table 3-2 shows the textural properties of Pd-based catalysts supported on Al_2O_3. As can be seen, alumina has excellent textural properties (S_{BET} = 240.7 $m^2 \cdot g^{-1}$; V_p = 0.7 $cm^3 \cdot g^{-1}$), which makes it an ideal support for many studies in heterogeneous catalysis [1–3]. Impregnation of Pd (5wt.%) on alumina decreased the specific surface area, pore volume and mean pore size by 8.7%, 14.5% and 6.9%, respectively. This behaviour can be explained by the filling of the pores of the support by the palladium active phase, which leads to a decrease of the total pore volume and, consequently, of the specific surface area.

Meanwhile, the acid catalyst (5%Pd/Al_2O_3-Acid), reflects a more important decrease in S_{BET}, V_p and D_p (36%, 62.3% and 42.7% respectively), than observed with the non-acid catalyst

(5%Pd/Al_2O_3), this decrease may be caused either by the blocking of pores by larger Pd particles or by structural rearrangement of the support.

Table 3-2: *BET analysis results for Pd catalysts supported on Al_2O_3.*

Sample	***S_{BET} [$m^2 \cdot g^{-1}$]***	***V_p [$cm^3 \cdot g^{-1}$]***	***D_p [nm]***
Al_2O_3	240.7	0.69	11.57
5%Pd/Al_2O_3	220	0.59	10.8
5%Pd/Al_2O_3-Acid	153.7	0.26	6.63

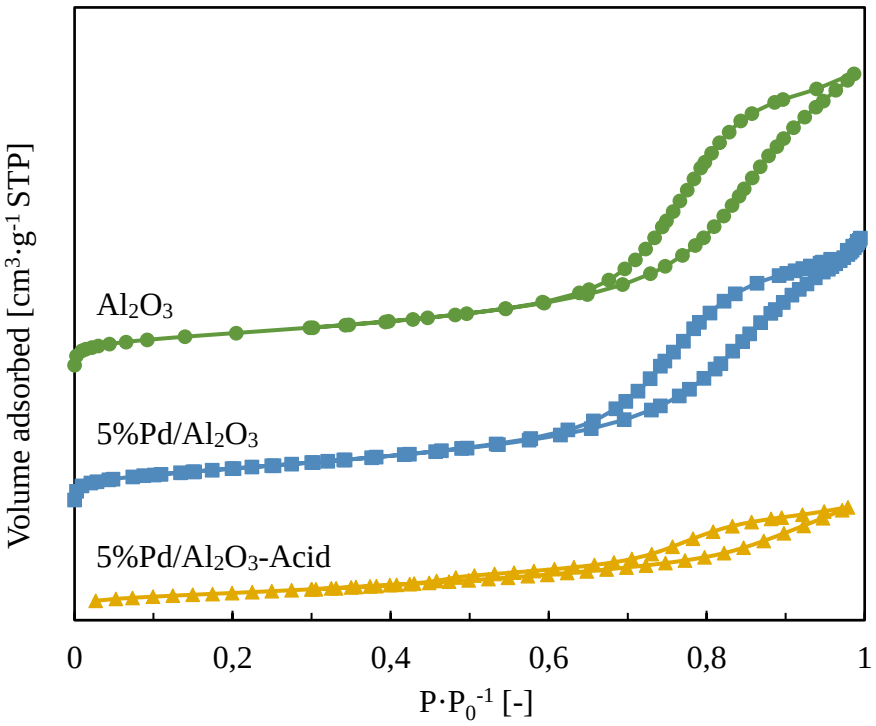

Figure 3-1**:** N_2-physisorption isotherms for *Pd catalysts supported on Al_2O_3.*

Figure 3-1 shows the nitrogen adsorption-desorption isotherms obtained for the Pd catalysts supported on Al_2O_3. As can be seen, the shape of the isotherms is very similar for the three samples and can be classified as type IV with H3 hysteresis according to the IUPAC classification, associated with the capillary condensation that takes place in the mesopores which, according to the hysteresis presented, are not ordered [4]. The fact that also the acid catalyst exhibits the same hysteresis indicates that the structure is not fundamentally different

from the parent support. On the other hand, the acid catalyst (yellow curve), presents between P/P_0 = 0.4-0.7 a notable delay in desorption, which strongly suggests the presence of larger Pd particles blocking the pores, leading to a decay of the N_2 desorption.

Compared to Al_2O_3, titanium dioxide (Table 3-3), exhibited lower specific surface area (89 $m^2 \cdot g^{-1}$) and pore volume (0.4 $cm^3 \cdot g^{-1}$). The impregnation of Pd on TiO_2 caused a decrease in S_{BET} from 89 $m^2 \cdot g^{-1}$ to 78 $m^2 \cdot g^{-1}$ (-12.4%), in V_p from 0.35 $cm^3 \cdot g^{-1}$ to 0.28 $cm^3 \cdot g^{-1}$ (-20%) and in mean pore size from 16.2 nm to 14.3 nm (-11.7%). This behaviour can be explained by the homogeneous filling of the pores of the support by the palladium active phase, which leads to a decrease of the total pore volume and, consequently, of the specific surface area. Contrary to the alumina based catalyst, the impregnation using an acid solution, did not significantly affect the textural properties in case of TiO_2 as a support.

Table 3-3: *BET analysis results for Pd catalysts supported on TiO_2.*

Sample	S_{BET} $[m^2 \cdot g^{-1}]$	V_p $[cm^3 \cdot g^{-1}]$	D_p [nm]
TiO_2	89	0.35	16.22
5%Pd/TiO_2	78	0.28	14.32
5%Pd/TiO_2-Acid	81.6	0.23	10.76

Figure 3-2 shows the nitrogen adsorption-desorption isotherms obtained for the Pd catalysts supported on TiO_2. As can be seen, titanium oxide also shows a type IV isotherm and H3 hysteresis according to the IUPAC classification, which indicates the presence of mesopores [4]. Comparing the isotherms of the catalysts with their respective supports, it is evident that there is no modification of the pore shape. However, the amount of adsorbed nitrogen decreases, which means that the pore volume and the specific surface area decrease in the presence of Pd, which blocks the pores of the support as already evidenced.

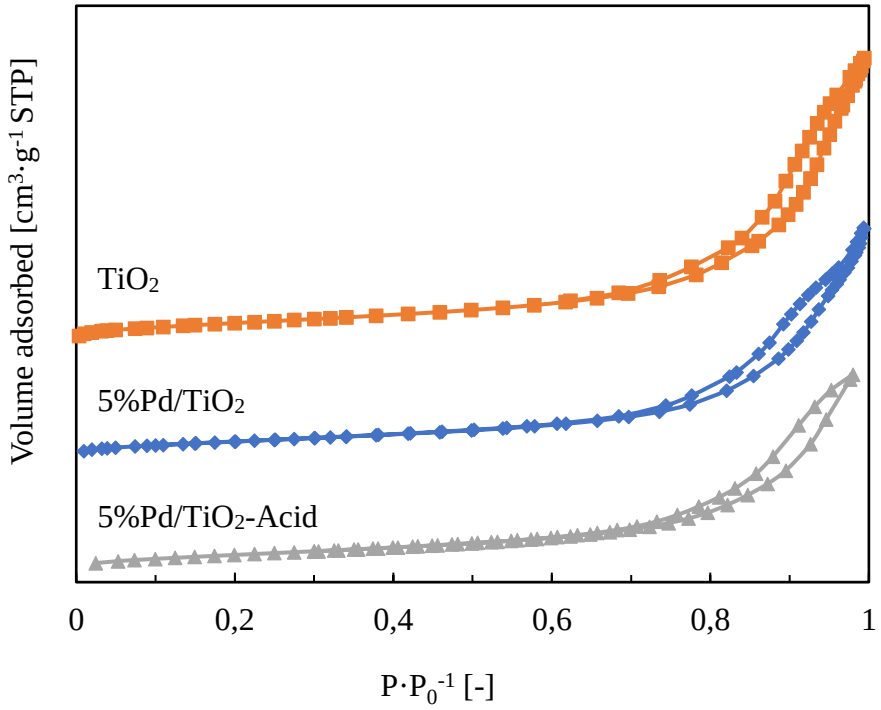

Figure 3-2:*N_2-physisorption isotherms for Pd catalysts supported on TiO_2.*

Table 3-4*: BET analysis results for deactivated catalysts.*

Sample	S_{BET} $[m^2 \cdot g^{-1}]$	V_p $[cm^3 \cdot g^{-1}]$	D_p [nm]
5%Pd/Al_2O_3	220	0.59	10.8
5%Pd/Al_2O_3-Deact.	19.1	0.06	5.63
5%Pd/Al_2O_3-Deact.-IR	31.7	0.1	11.07
5%Ru/Al_2O_3	228.3	0.5	9.52
5%Ru/Al_2O_3-Deact.	3.3	0.03	33.9
5%Ru/Al_2O_3-Deact.-IR	1.1	0.01	46.5

Table 3-4 shows the results of the physisorption analysis for the Pd catalysts (Table 3-1) employed in the regeneration study (meaning with artificial deactivation). A large decrease in pore volume (0.06 $cm^3 \cdot g^{-1}$ vs. 0.55 $cm^3 \cdot g^{-1}$) and specific surface area (19 $m^2 \cdot g^{-1}$ vs. 220$m^2 \cdot g^{-1}$) is observed for the deactivated catalyst, due to the clogging of pores by the presence of

carbonaceous species of the humins type. On the other hand, a slight increase in the pore volume (0.1 $cm^3 \cdot g^{-1}$ *vs.* 0.06 $cm^3 \cdot g^{-1}$) and specific surface area (32 $m^2 \cdot g^{-1}$ *vs.* 19 $m^2 \cdot g^{-1}$) is observed after irradiation of the catalyst. This result could imply that the irradiation is decomposing the humins molecules. The deactivated ruthenium-based catalyst also shows a large decrease in pore volume and specific surface area, however, the irradiated catalyst, contrary to the Pd catalyst, does not show evidence of possible humin decomposition.

3.2.2. X-ray-diffraction (XRD)

X-ray diffraction was used to estimate the size of the crystals, as well as to determine the structure and crystallinity of the synthesized catalysts.

Figure 3-3 shows the diffractograms of the catalysts supported on Al_2O_3 with 5wt.% metal. In the case of 5%Pd/Al_2O_3, the XRD patterns are mostly attributable to γ-alumina (PDF 46-1131, Annex 1), which means that there are no major changes in the crystalline structure of the support due to metal impregnation. A small peak at 34°, attributed to palladium oxide (PDF 41-1107, Annex 1), indicates that when alumina was used as a support, the metal is not very well dispersed on the support surface, but presents agglomerations. In the case of 5%Pd/Al_2O_3-Acid the peaks at 34° and 55°, attributed to PdO, are more intense suggesting the formation of larger particles.

In this sense, the crystallite size was determined on the most intense reflection of each sample using the EVA software. For the 5%Pd/Al_2O_3 catalyst a crystal size of 5 nm for PdO. On the other hand, in the case of the acid catalyst, a crystal size of 7.4 nm was found for PdO. These results indicate that the impregnation using an acid solution led to the formation of larger Pd particles. These results confirm the BET analysis, where the specific area and pore size strongly decreased when the catalyst was synthesized with the acid solution.

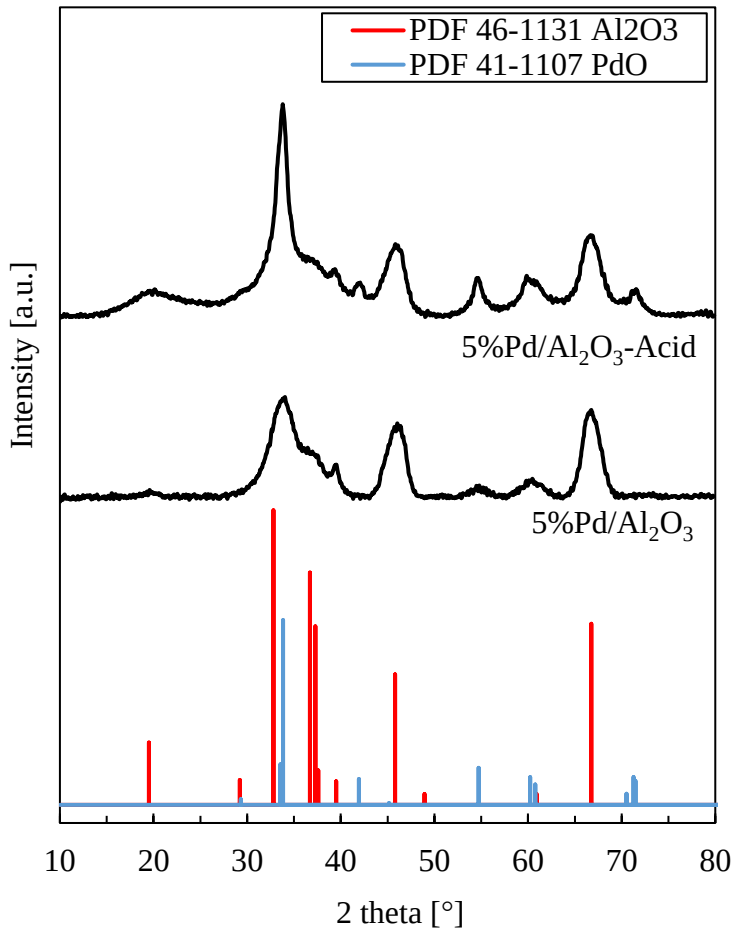

Figure 3-3: *Diffractograms XRD of the Pd catalysts supported on Al_2O_3.*

Meanwhile, diffractograms for Pd (5wt.%) supported on TiO_2 (Figure 3-4) show no diffraction peaks attributable to PdO, but exclusively the characteristic peaks of the anatase phase of TiO_2 (PDF 65-5714, Annex 1) [5], indicating a good dispersion of the Pd on the support. This result agrees with the BET analysis which only showed a small decrease in S_{BET}, V_p and D_p due to the presence of Pd on the support surface.

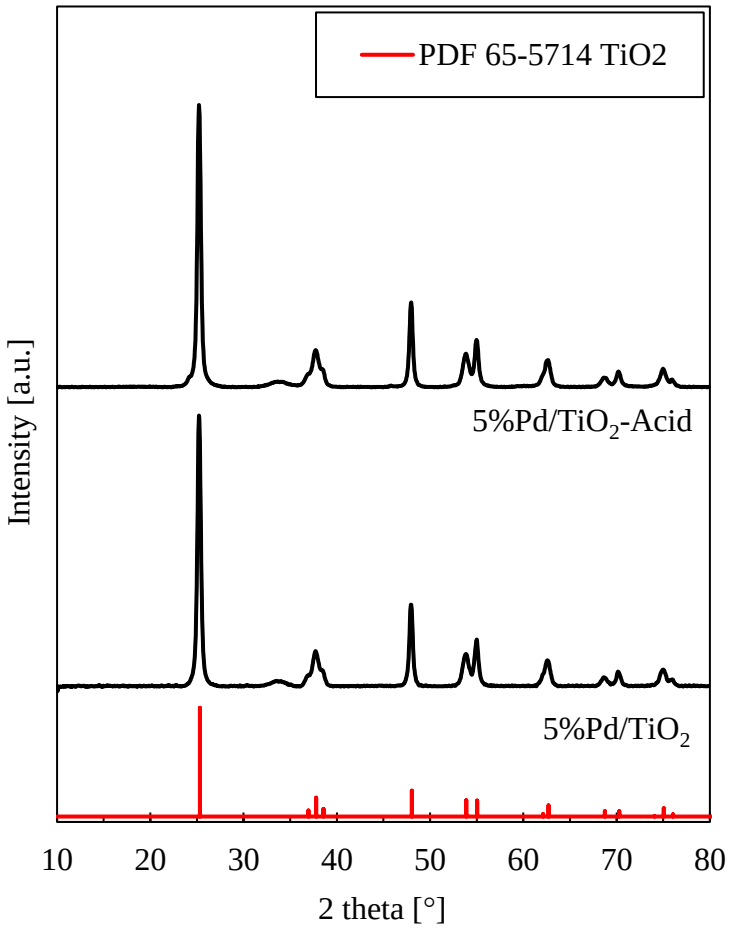

Figure 3-4: *Diffractograms XRD of the catalysts used on the on the decolorization of azo-dyes.*

3.2.3. Temperature programmed reduction (TPR)

TPR analysis was carried out on the 5%Pd/Al_2O_3-Acid and 5%Pd/TiO_2-Acid catalyst samples, the H_2 TPR profiles are shown in Figure 3-5. As can be seen for both catalysts, hydrogen production is present, which is identified with the negative peak at 77°C. According to the literature, the presence of this negative reduction peak is related to the decomposition of Pd-hydride (PdH_x) that occurs after the reduction of Pd, which took place below room temperature [6]. Different studies have reported the same behaviour with this type of catalyst [7,8]. Unfortunately, it was technically not possible to perform the analysis at lower temperature, which would allow to observe the Pd reduction in detail. However, these results corroborate that in both catalysts Pd is completely reduced and that additionally the particle size is large enough to be reduced at low temperature, otherwise we would observe a hydrogen consumption

between 350 and 370°C which is the reduction temperature range of the of smaller size PdO [9]. Thus, the TPR results agree with BET and XRD analyses, suggesting the formation of well dispersed Pd species.

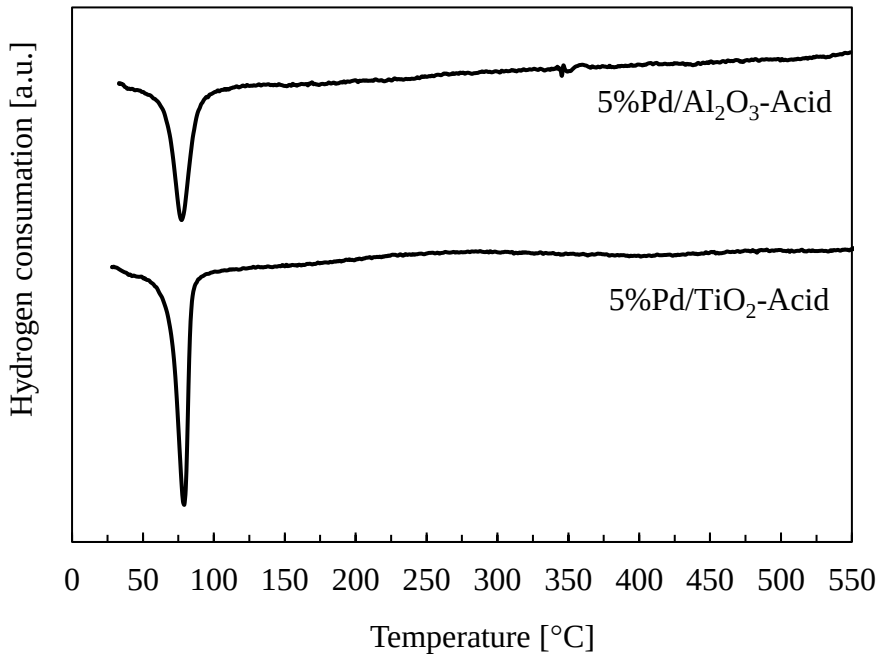

Figure 3-5: *TPR profiles for 5%Pd/Al_2O_3-Acid and 5%Pd/TiO_2-Acid.*

3.2.4. Thermogravimetric analysis (TGA)

Figure 3-6 and Figure 3-7 shows the curves obtained in the TGA analysis for fresh and deactivated Pd and Ru catalysts respectively. The curves for both Pd and Ru catalysts can be divided into 3 zones. Zone 1 (10-150°C) corresponds to the mass loss linked to water molecules or impurities that may be present on the catalyst. Zone 2 (150-500°C) is related to mass loss linked to the thermal decomposition of carbon molecules (humins) [10]. Finally, for zone 3 (over 500°C) no mass loss is evidenced. Zone 2 of the deactivated Pd/Al_2O_3 catalyst (Figure 3-6) showed a mass loss of 37.7% compared to a mass loss of 4.8% for the fresh catalyst, likewise, the deactivated Ru/Al_2O_3 catalyst (Figure 3-7), showed a mass loss of 53.5% while only a loss of 9.4% was observed for the fresh catalyst. With respect to the rather low

temperature of the decomposition, one can conclude that the deposed carbonaceous species exhibit rather low degree of polymerisation excluding notably the formation of graphite type carbon, which should facilitate the regeneration by γ-irradiation.

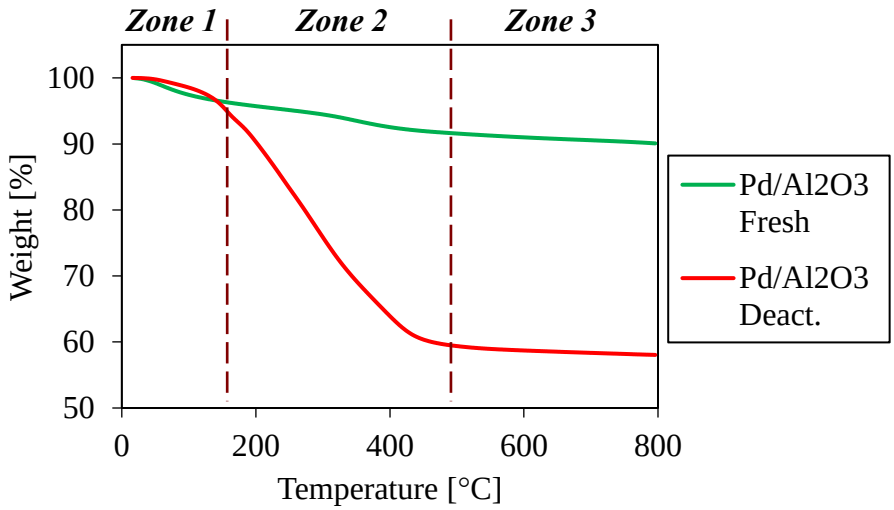

Figure 3-6: *TGA analysis for fresh and deactivated Pd and catalysts.*

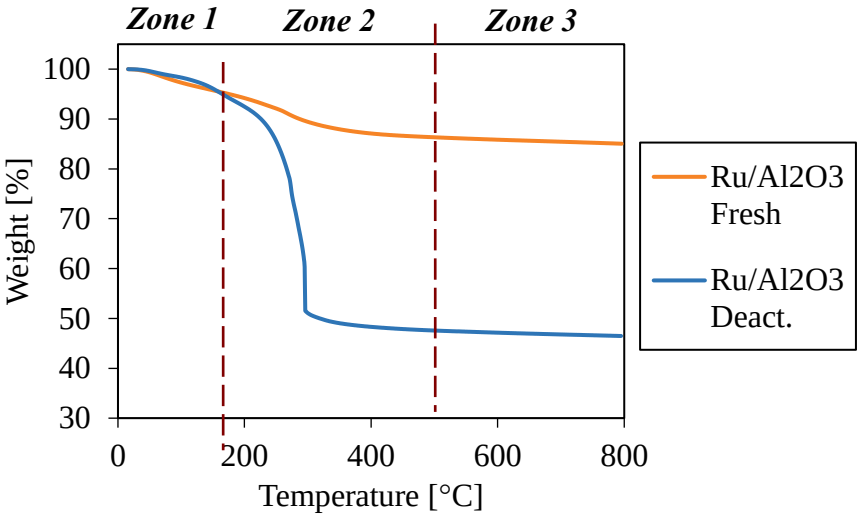

Figure 3-7: *TGA analysis for fresh and deactivated Ru catalysts.*

3.2.5. X-ray Photoelectron Spectroscopy (XPS)

The results of the XPS analysis performed on the samples of Ru-based catalysts used for the study of catalyst regeneration from γ-irradiation are shown below. Table 3-5 gathers the values obtained from the data processing of the C 1s spectra.

Table 3-5: *C 1s XPS results of Ru catalysts.*

Sample	***BE [eV] and FWHM of C 1s (deconvoluted)***			***BE [eV] and FWHM of Ru 3d 5/2***	***BE [eV] and FWHM of Ru 3d 3/2***	***% Ru/Al***	***% Ru/C***	***% Al/C***
	C_{C-C}	C_{C-OH}	C_{O-C-O}					
5%Ru/Al_2O_3_ Fresh	284.7 (1.5)	286.2 (2.1)	288.4 (1.9)	283 (1.6)	287.2 (2.1)	7.9	7.9	98.8
5%Ru/Al_2O_3_ Deact.	284.6 (1.4)	286.1 (2)	288.5 (1.4)	281.7 (1.8)	285.9 (1.8)	10.3	0.3	3.0
5%Ru/Al_2O_3_ Deact.-IR	284.7 (1.6)	286.2 (2.3)	288.4 (2)	281.8 (1.8)	285.9 (1.8)	9.8	0.5	5.4

The Ru/C and Al/C ratios of 7.9 and 98.8% respectively in the fresh catalyst strongly decrease (Ru/C = 0.3% and Al/C = 3%) after the deactivation of the catalyst. These results highlight the large amount of carbon that is present on the catalyst surface after deactivation. Similarly, the irradiated catalyst with Ru/C = 0.5% and Al/C = 5.4% also reflects the amount of carbon that remains on the surface even after regeneration by γ-irradiation.

Meanwhile, the Ru 3d 5/2 observed on the fresh catalyst has a BE of 283 eV, which corresponds to the energy of $Ru(NO)(NO_3)_3$ [11]. However, after deactivating the catalyst, the Ru 3d 5/2 changes to a BE of 281.7 eV +/- 0.1. This change can also be seen in the spectrum where the Ru 3d 5/2 peak shifts to a lower BE (Figure 3-8). The Ru 3d 3/2 also shifts from 287.2 eV to 285.9 eV for both the deactivated and irradiated catalysts. These results suggest that there was indeed a change in the chemical environment of Ru. Unfortunately, the oxidation state of Ru cannot be clearly identified since the signal is of Ru 3d 5/2 and Ru 3p 3/2 are very weak, due to the significant carbon layer on the surface that prevents the exploitation of the results.

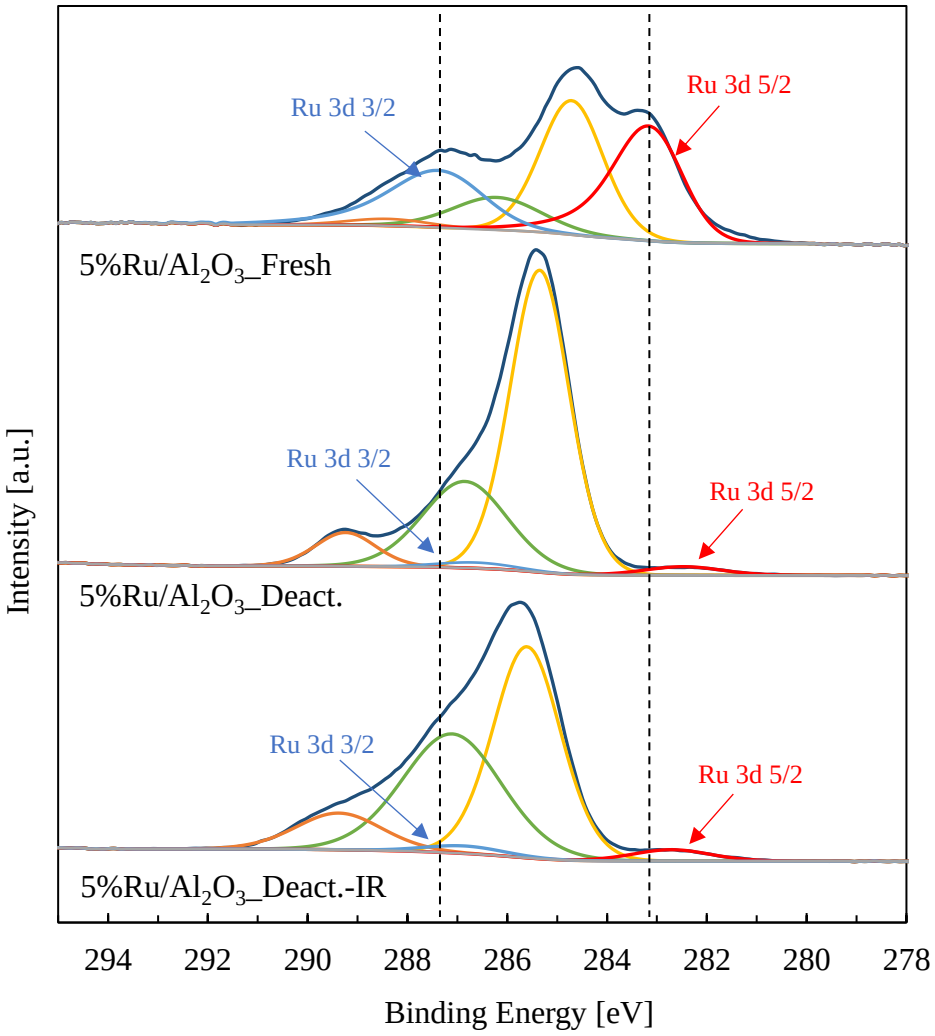

Figure 3-8: *C 1s XPS spectra of Ru catalysts.*

3.3. References

[1] E. Diaz, A.F. Mohedano, J.A. Casas, C. Shalaby, S. Eser, J.J. Rodriguez, On the performance of Pd and Rh catalysts over different supports in the hydrodechlorination of the MCPA herbicide, Applied Catalysis B: Environmental 186 (2016) 151–156. https://doi.org/10.1016/j.apcatb.2015.12.054.

[2] R. Jiménez, K. Fuentes, M.P. Medina, S. Godoy, F. Gracia, A. Karelovic, The kinetic effect of H2O pressure on CO hydrogenation over different Rh cluster sizes, International Journal of Hydrogen Energy 44 (2019) 768–777. https://doi.org/10.1016/j.ijhydene.2018.11.021.

[3] M. Munoz, Z.M. de Pedro, J.A. Casas, J.J. Rodriguez, Improved γ-alumina-supported Pd and Rh catalysts for hydrodechlorination of chlorophenols, Applied Catalysis A: General 488 (2014) 78–85. https://doi.org/10.1016/j.apcata.2014.09.035.

[4] M. Thommes, K. Kaneko, A.V. Neimark, J.P. Olivier, F. Rodriguez-Reinoso, J. Rouquerol, K.S. Sing, Physisorption of gases, with special reference to the evaluation of surface area and pore size distribution (IUPAC Technical Report), Pure and Applied Chemistry 87 (2015) 1051–1069. https://doi.org/10.1515/pac-2014-1117.

[5] T. A. Kandiel, L. Robben, A. Alkaim, D. Bahnemann, Brookite versus anatase TiO2 photocatalysts: phase transformations and photocatalytic activities, Photochem. Photobiol (2013) 602–609.

[6] C. Amairia, S. Fessi, A. Ghorbel, A. Rîves, Methane oxidation behaviour over sol–gel derived Pd/Al2O3-ZrO2 materials: Influence of the zirconium precursor, Journal of Molecular Catalysis A: Chemical (2010) 25–31.

[7] S. R. Akuri, C. Dhoke, K. Rakesh, S. Hegde, S. A. Nair, R. Deshpande, P. Manikandan, Decomposition of Methyl Formate over Supported Pd Catalysts, Catal Lett (2017) 1285–1293.

[8] H. P. Aytam, V. Akula, K. Janmanchi, S. R. R. Kamaraju, K. R. Panja, K. Gurram, J. W. Niemantsverdriet, Characterization and Reactivity of Pd/MgO and Pd/γ-Al2O3 Catalysts in the Selective Hydrogenolysis of CCl2F2, J. Phys. Chem (2002) 1024–1031.

[9] D.S. S. Bhogeswararao, Catalytic conversion of furfural to industrial chemicals over supported Pt and Pd catalysts, Journal of Catalysis (2015) 65–77.

[10] Alana P. Gomesa, Gabriel B. Sallesb, Marina G. Macedoa, Paula G. A. Gonzaleza, Yurany C. Ardilac, Jaiver E. Jaimes Figueroad, Viktor O. C. Conchaa, Laura P. Tovara, Pyrolysis of Humins Obtained from Acid-catalyzed Depolymerization of Rice Husk Cellulose: Model-Free Approach to Non-Isothermal Kinetics, Chemical Engineering Transactions 80 (2020) 211–216.

[11] D. J. Morgan, Resolving ruthenium: XPS studies of common ruthenium materials, Surf. Interface Anal. (2015).

Chapter 4

Impact of radioactivity on the hydrogenation of cinnamaldehyde

4.1. Introduction

Cinnamaldehyde is the main component of cassia oil (90%) and cinnamon oil (75% of cinnamon oil contains trans-cinnamaldehyde), but is also found in low concentrations in many other essential flower oils (e.g. hyacinth) [1]. Cinnamaldehyde consists of a phenyl group attached to an unsaturated aldehyde, 2-propenal (Figure 4-1). It is used as a flavouring agent in the food industry to create flavours in chewing gum, ice cream, candies and syrups (with concentrations between 9 and 4900 ppm).

The hydrogenation of cinnamaldehyde is a reaction widely used in research and industry [2,3]. It is highly sensitive to pressure, temperature, support and active phase of the catalyst, solvent, among others, which makes it an ideal reaction to evaluate the influence of these parameters, not only on the conversion but also on the selectivity towards the products of interest.

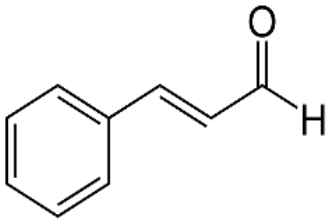

Figure 4-1:*Cinnamaldehyde structure.*

Hydrogenation of the C=C bond produces a saturated aldehyde, hydrocinnamaldehyde (HCNA), while that of the C=O bond produces an unsaturated alcohol, cinnamyl alcohol (CNOL), and the hydrogenation product of the latter, in turn, is a saturated alcohol, hydrocinnamyl alcohol (HCNOL) [4–6]. These products have industrial applications in pharmaceuticals and perfumery. In fact, HCNA has recently been found to be an important intermediate in the synthesis of pharmaceuticals used in the treatment of HIV [7]. Authors such as Jiang et al. [6] have reported Pd catalysts supported on Al_2O_3 and SiO_2 with conversions above 60% and high selectivity (≈ 60%)towards C=C bond hydrogenation at 60°C and 10 bar

pressure [3,8]. In addition to Pd, metals such as Ru and Rh supported metals have also been studied in the selective hydrogenation of cinnamaldehyde [3,8,12].

In the present study, the hydrogenation of cinnamaldehyde was chosen as the model reaction. It is a versatile and easy to carry out reaction, which favours its implementation in a glove box when using radioactive catalysts.

In this chapter, we seek to evaluate the impact of radioactivity on the model reaction of hydrogenation of cinnamaldehyde, using radioactive catalysts. For this, in a first part, the behaviour of the different reaction conditions and of the commonly used efficient catalysts will be evaluated. The optimal conditions meeting the above selection criteria will then be chosen and applied to the non-radioactive catalyst, synthesized under conditions close to those of the radioactive catalyst. In the second part, the results of the tests carried out with both the non-radioactive catalyst and the radioactive catalyst will be reviewed. Finally, the study of the effect of radiation β on the hydrogenation of CNA will be concluded by comparing these last results.

4.2. Preliminary tests

4.2.1. Reaction behaviour with variation of pressure, temperature and catalyst amount.

One of the most critical steps is the determination of the reaction conditions since, as already mentioned, these conditions must fulfil the safety requirements related to the use of a radioactive catalyst mentioned in section 1.2.3 and additionally allow the evaluation of the effect of the radiation to be studied. Therefore it is important to understand the impact of the conditions, such as pressure, temperature and amount of catalyst, in order to find the most suitable ones. The tests were carried out using the procedure described in section 2.3.1.1 with the trimetallic catalyst (5%Tri/Al_2O_3) (Table 3-1). The procedure was validated with blank tests

which showed no reactivity of the CNA without catalyst and only in the presence of the support (Al_2O_3).

4.2.1.1. Pressure

Figure 4-2 shows the CNA conversion results as a function of time at different values of H_2 pressure for the trimetallic catalyst 5%Tri/Al_2O_3 of (Table 3-1).

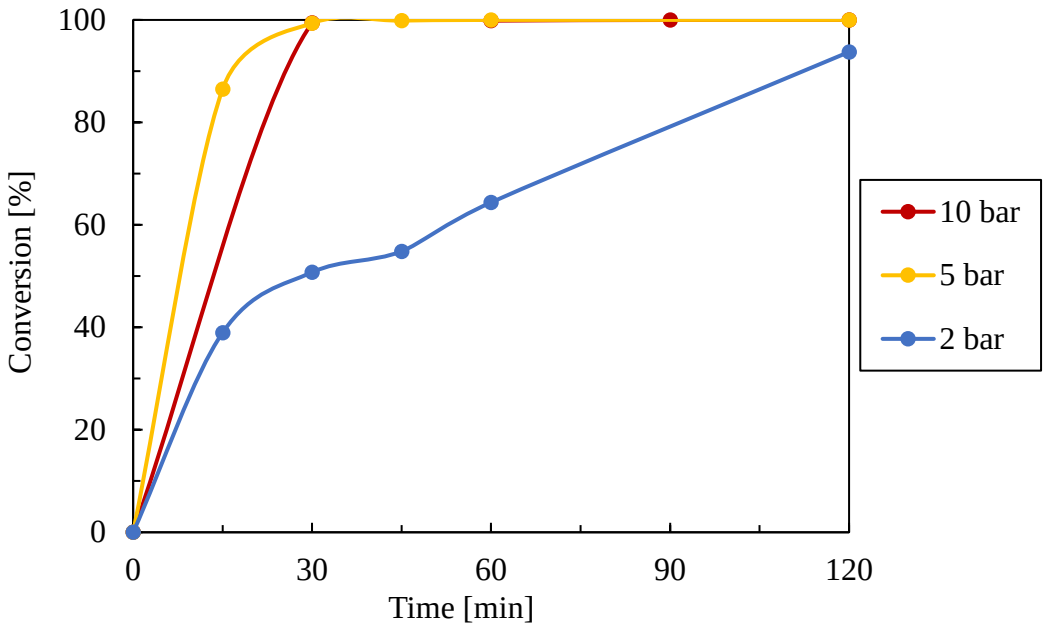

Figure 4-2: *Evolution of CNA conversion as a function of time for different H_2 pressures.*
(T= 130°C ; M= 2M ; m_{cata}= 50mg ; solvent, isopropanol 5%Tri/Al_2O_3)

The hydrogen pressure of the system is one of the most important parameters to take into account. As can be seen in Figure 4-2, increasing the pressure increases the rate at which cinnamaldehyde is converted, confirming the literature [4]. According to the reaction, the ratio of CNA to H_2 is 1:1, which means that for 5.16E-03 moles of CNA, 5.16E-03 moles of H_2 are needed to convert all the CNA molecules. However, it is usual to work with an excess of hydrogen to guarantee the transfer in the system and to achieve a complete conversion. Figure 4-2 shows that at H_2 pressures of 10 and even 5 bar, the hydrogen transfer allowed a complete conversion to be achieved in only 30 min. In fact, no significant differences in the evolution of

the conversion were observed with the use of these two pressures. On the contrary, at a hydrogen pressure of 2 bar, a slower increase in conversion is observed, reaching 95% only after 2 hours of reaction. This behaviour is related to the limitation in hydrogen transfer, since at this pressure there are only 1.8E-03 moles of hydrogen available to react with the same 5.16E-03 moles of CNA, which does hydrogen the limiting reactant and thus the reaction slower. Despite the limitation in hydrogen transfer, for the following preliminary tests, a pressure of 2 bar H_2 was set in order to keep the pressure low enough to be implemented in the ATALANTE installations, and which in turn will allow to evaluate more clearly the effect of other parameters, in particular the possible impact of radioactivity.

4.2.1.2. Temperature

The second parameter evaluated was the reaction temperature at 2 bar hydrogen pressure and 100 mg of catalyst. Figure 4-3 shows the behaviour of the CNA conversion over time at different temperatures. On the one hand, the decrease in temperature from 130°C to 60°C (almost half) shows no difference in conversion as the reaction progresses, which is attributed to the limitation in the amount of hydrogen, discussed in the previous section, when working at low H_2 pressures. If this were not the case, it would not be normal that the conversion behaviour at 130°C to 60°C would be similar. On the other hand, a large decrease in conversion (from 100% to 15%) is observed in 180 min, when the temperature is lowered from 60°C to 25°C. These results lead us to infer that:

- Although the hydrogenation of cinnamaldehyde is efficient at room temperature [10,11], this is not an optimal temperature for our system with the 5%Tri/Al_2O_3 catalyst.
- The most convenient temperature for our tests is 60°C, since, in addition to complying with the restrictions of handling under radioactive conditions, it allows us to obtain

"exploitable" reaction kinetics, because additionally, it is considered that we are measuring the intrinsic kinetics of the reaction.

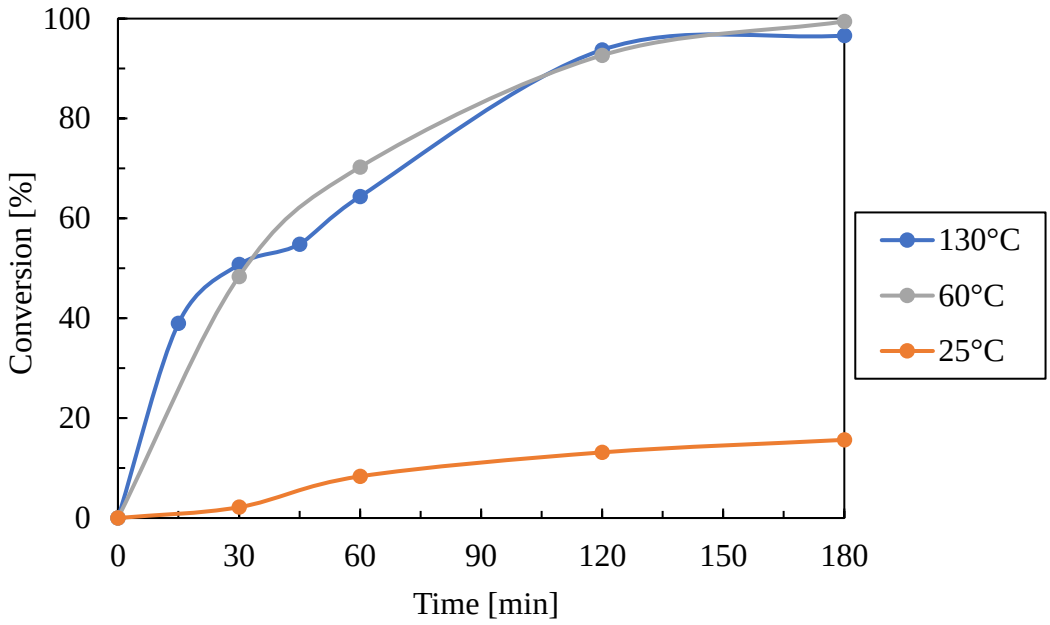

Figure 4-3: *Evolution of CNA conversion as a function of time for different temperatures.*
(P_{H_2} = 2 bar ; m_{cat}= 50mg ; M= 2M ; solvent, isopropanol 5%Tri/Al_2O_3)

4.2.1.3. Mass of catalyst

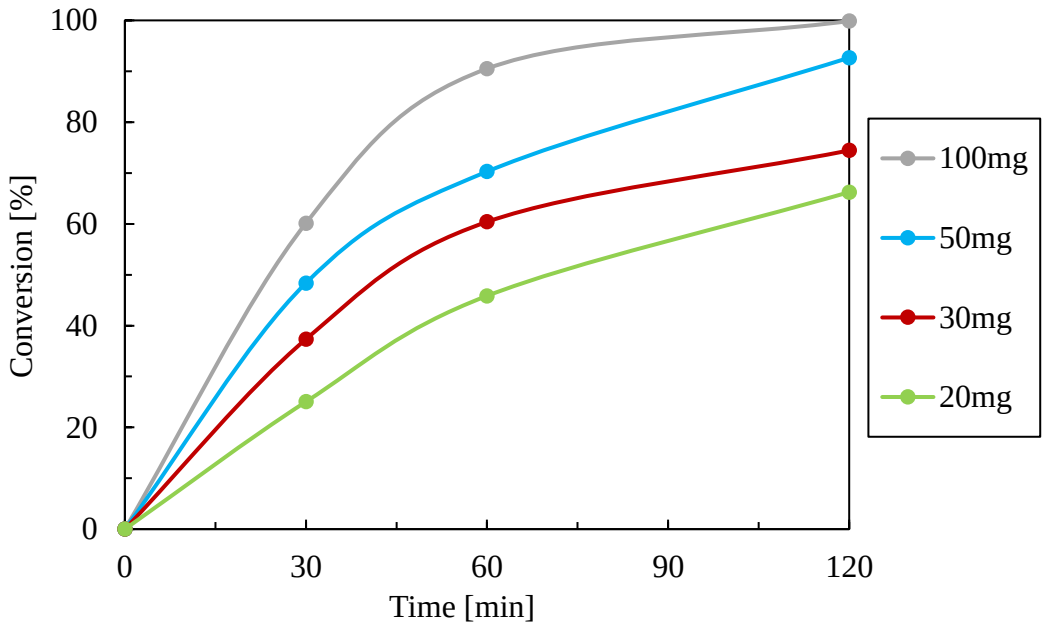

Figure 4-4: *Evolution of CNA conversion as a function of time for different amounts of catalyst mass.*
(P_{H_2} = 2 bar ; T= 60°C ; M= 2M ; solvent, isopropanol 5%Tri/Al_2O_3)

The mass of catalyst was varied between 20 and 100 mg for the same reaction conditions at fixed temperature of 60°C and 2 bar of hydrogen pression (Figure 4-4). As expected, increasing the amount of catalyst increases the conversion of cinnamaldehyde. However, increasing the amount of catalyst increases the amount of metals needed to prepare catalysts with 5% metal loading, both radioactive and non-radioactive, so 20 mg of catalyst is an amount that would economise the amount of metals available, especially the radioactive ones. Furthermore, by using 20 mg of catalyst, it is guaranteed to be below the permitted limits for handling radioactive material in a fume hood at ATALANTE.

4.2.2. Comparison of Pd catalyst performance with other noble metals (Ru and Rh) and their bimetallic formulations PdRu and PdRh

The performance of the model reaction with the use of monometallic and bimetallic catalysts with the above established conditions (section 4.2.1) is shown in the following.

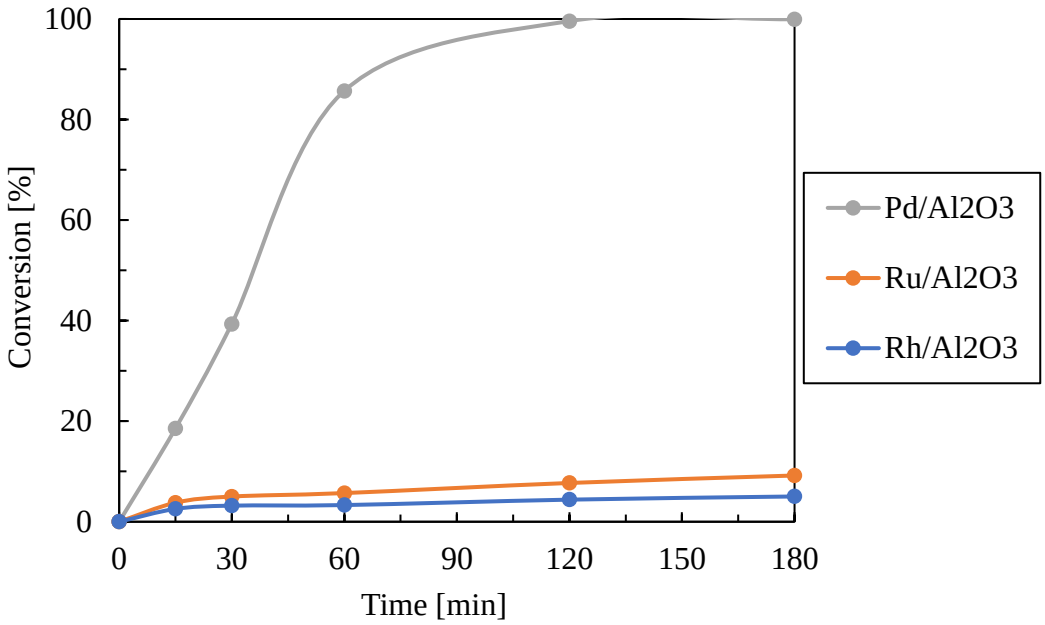

Figure 4-5: *Conversion as a function of time for 5wt.% monometallic catalysts.* *(P_{H_2} = 2 bar ; T= 60°C ; M= 2M ; m_{cata}= 20mg ; solvent, isopropanol)*

Figure 4-5 shows the conversion vs. time for the 5% monometallic catalysts based on Pd, Ru and Rh supported on alumina. It can be observed that the 5%Pd/Al_2O_3 catalyst, reaches complete conversion after 2h of reaction, contrary to what is observed with the catalysts

5%Ru/Al_2O_3 and 5%Rh/Al_2O_3 which in the same time presented a conversion of 5 and 9% respectively. This agrees with the reports of different authors, claiming high conversions for Pd catalysts and low conversions for Rh and Ru catalysts [3,6,8,12].

The selectivity of the 5%Pd/Al_2O_3 catalyst at different conversions are presented in Figure 4-6. As reported in other studies [8], the Pd-based catalyst shows a high selectivity towards HCNA formation, with an almost constant trend after 40% conversion, while products such as hydrocinnamylalcohol (HCNOL) and cinnamylalcohol (CNOL) are observed in small quantities and only at low conversions (X=18%). In turn, the selectivity towards product B (product not yet identified), tends to decrease at the same rate as HCNA increases, suggesting that this product is an intermediate to the formation of HCNA.

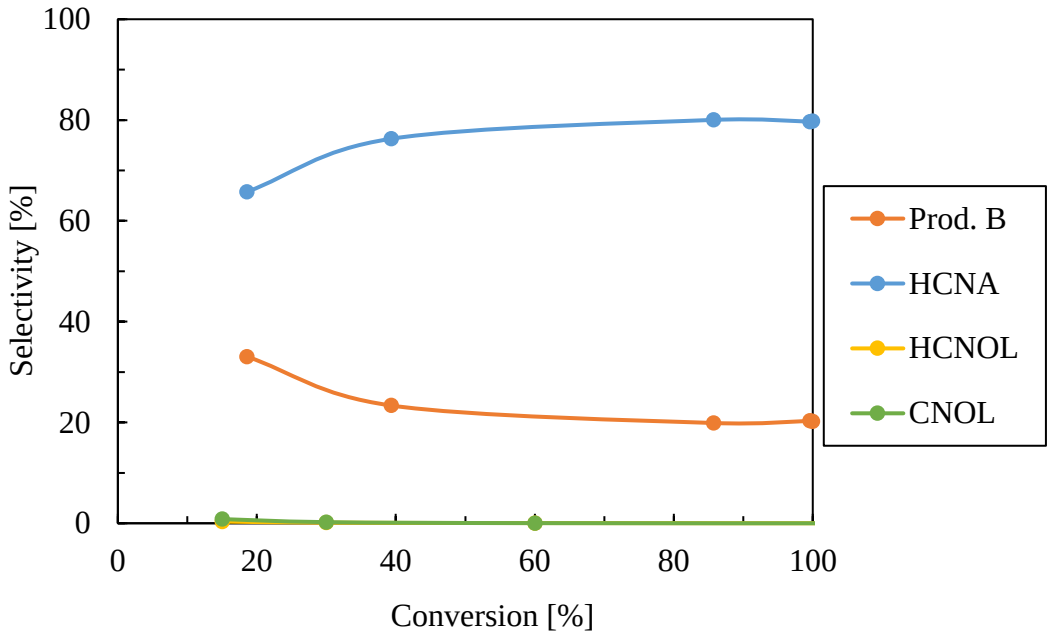

Figure 4-6: *Selectivity vs. conversion with the catalyst 5%Pd/Al_2O_3.*
(P_{H_2} = 2 bar H_2 ; T= 60°C ; M= 2M ; m_{cata}= 20mg ; solvent, isopropanol)

As for the selectivity for the Rh and Ru catalysts, although they are highly selective to HCNA, it is also found that contrary to the Pd catalyst, they are more selective towards the HCNOL and CNOL products and less towards Prod B (Figure 4-7). This result coincides with the previously mentioned fact suggesting a better selectivity of Ru towards the hydrogenation of the C=O bond

[13], however, the selectivity shown by the Rh catalyst at 5% conversion is unexpected considering that it is known to favour the hydrogenation of the C=C bond [14,15]. Still, it shows higher selectivity towards HCNOL and CNOL than Ru. This behaviour may be due to the particle size since, as reported by several authors, claiming that a larger particle size infers a higher selectivity towards CNOL [12,14].

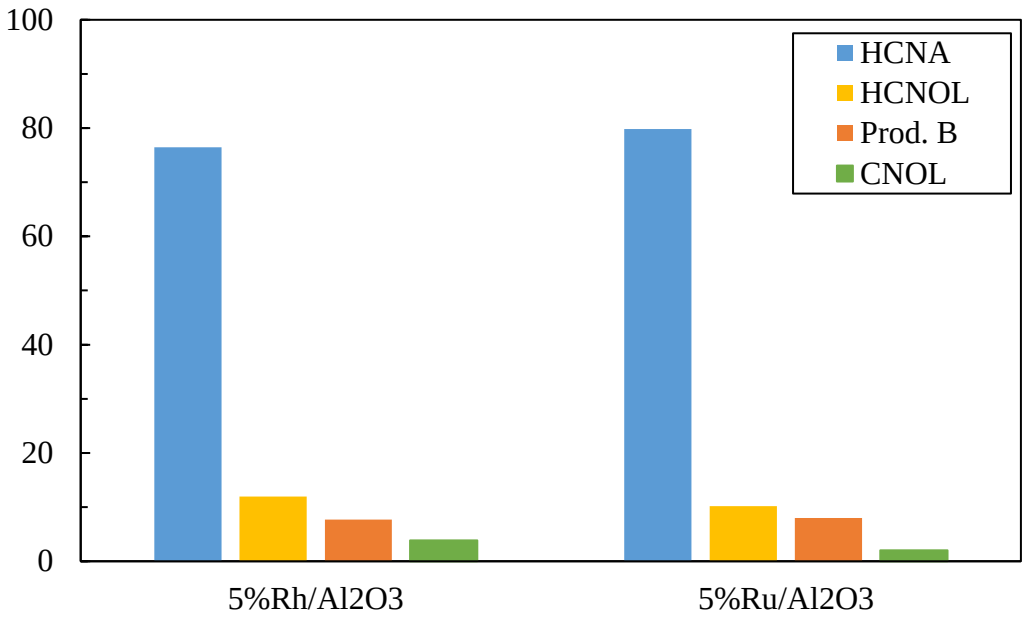

Figure 4-7: *Selectivity with 5%Ru/Al_2O_3 and 5%Rh/Al_2O_3 catalyst at 5% of conversion. (P_{H_2} = 2 bar ; T= 60°C ; M= 2M ; m_{cata}= 20mg ; solvent, isopropanol)*

In order to evaluate the effect of the presence of other metals on the catalytic activity of Pd, experiments were carried out using 5%PdRu/Al_2O_3 and 5%PdRh/Al_2O_3 bimetallic catalysts. The results of the conversion evolution of these catalysts compared to a 2.5%Pd catalyst (equivalent Pd metal loading in the bimetallic catalyst), are shown in Figure 4-8.

The results show that the 5%PdRh and 5%PdRu catalysts are much less active than the 2.5%Pd catalyst, suggesting a possible inhibition of palladium by the presence of Rh and Ru in the bimetallic catalyst. This result leads us to think that it may be due to an effect of the structuring of the catalyst. However, more detailed analysis is required to explain the lack of synergy in these formulations as there is no bibliographical evidence available.

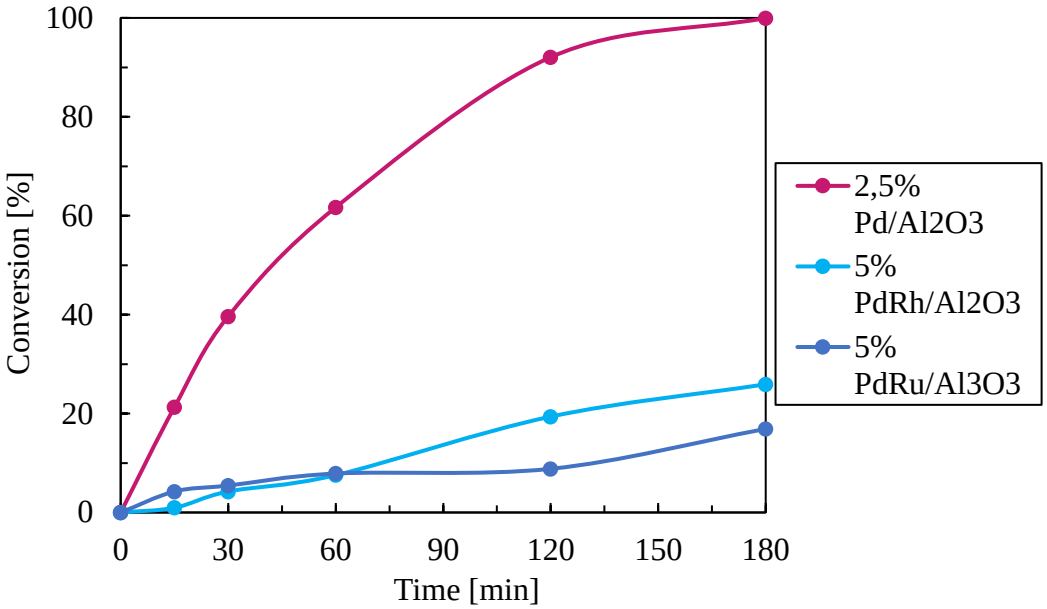

Figure 4-8: *Conversion as a function of time for bimetallic catalysts.*
(P_{H_2} = 2 bar ; T= 60°C ; M= 2M ; m_{cata}= 20mg ; solvent, isopropanol)

4.2.3. Implementation of the radioactive catalyst

As aforementioned, the test conditions employed before were chosen with respect to the safety conditions for working in glove boxes and fume hoods under radioactive conditions:

- A temperature of 60°C, which complies with the limits for working in the aforementioned conditions.
- To use a quantity of catalyst of 20 mg which not only economises the use of mainly radioactive metals but also complies with the radioactivity limits for handling in glove boxes and fume hoods.

When implementing these conditions, two main problems were encountered:

1) The solution containing the ^{107}Pd precursor comes from solutions of fines formed from the dissolution of nuclear fuel. The Pd is separated from the other species and purified, however, after said treatments, traces of different species prevail in the solution (Table 2-1), including nitrates, which make the recovered solution acidic. Since this could have

an effect on the synthesis of the catalyst and consequently on the performance, the initial synthesis protocol had to be adapted. In order to replicate these acid conditions, the new protocol (section 2.2.1.2) consists of using an impregnation solution with a composition similar to the recovered radioactive solution (Table 2-1).

2) Although the H_2 pressure for the initial experiments was chosen to be very low (2 bar), even if limited by the amount of hydrogen, safety regulations when using pressurised equipment in a radioactive environment limited the H_2 pressure to below 1 bar and restricted the use of pure H_2.

The impact of these two changes on the catalytic activity are detailed in the following.

Concerning the modification of the synthesis protocol, a series of characterizations were performed in order to see the impact of the acidic environment on the structure and composition of the catalyst. The nitrogen physisorption (BET) analysis presented in section 3.2.1 showed a significant decrease in the surface properties of the catalyst synthesized with the acidic solution, possibly related to pore blockage by larger Pd particles or structural rearrangement of the support. Meanwhile, XRD analysis of the acid catalyst (Figure 3-3, section 3.2.2), showed larger Pd particles (7.4 nm), than those found in the non-acidic catalyst (5 nm). The conversion results of the new 5%Pd/Al_2O_3_Acid catalyst, compared to the one used in the previous tests, are shown in Figure 4-9.

The results show, after 180 min of reaction, a decrease from 100 to 80% in the final catalytic activity, with the 5%Pd/Al_2O_3_Acid catalyst. As reported by Jiang et. al. [6], the particle size of Pd has a great influence on the hydroxylation of CNA, thus, with a larger particle size, the results showed a decrease in the conversion. In this sense, the decrease observed in this case with the acid catalyst is directly related to the increase in Pd particle size found in the characterization analyses mentioned above.

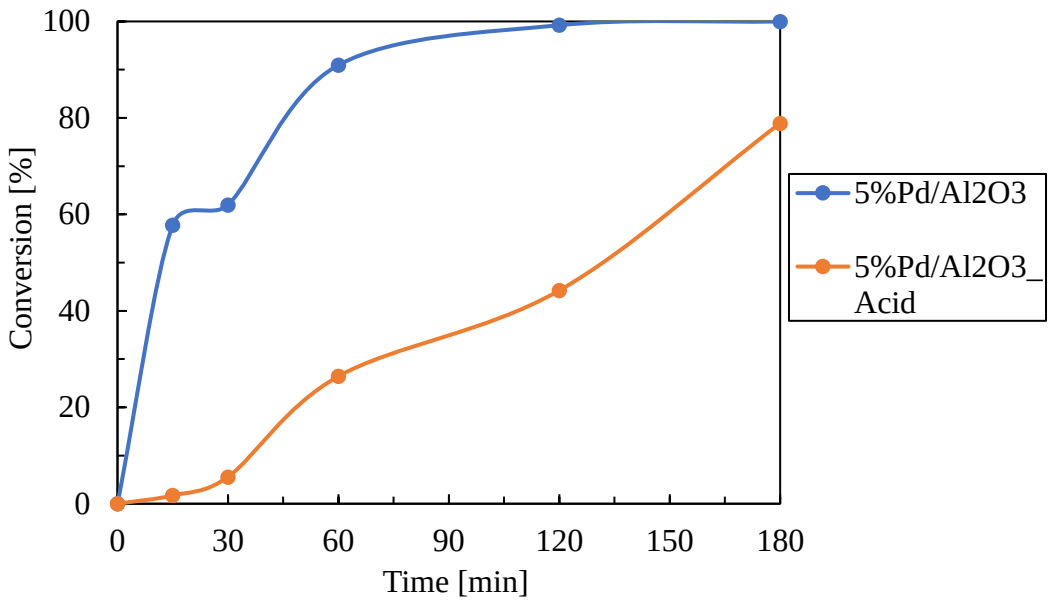

Figure 4-9: *Conversion comparison for the 5%Pd/Al_2O_3 and 5%Pd/Al_2O_3_Acid catalysts. (P= 2 bar 100%H_2 ; T= 60°C ; M= 2M ; m_{cata}= 20mg ; solvent, isopropanol)*

Concerning the H_2 pressure, in order to avoid working with pure hydrogen, it was decided to work with a mixture of 4% H_2 in Ar. Figure 4-10 shows the results of the tests carried out during 6 h of reaction, with pressures of 15 and 10 bar H_2/Ar mixture, which corresponds to a hydrogen pressure of 0.6 and 0.4 bar respectively, compared to the test carried out with a hydrogen pressure of 2 bar.

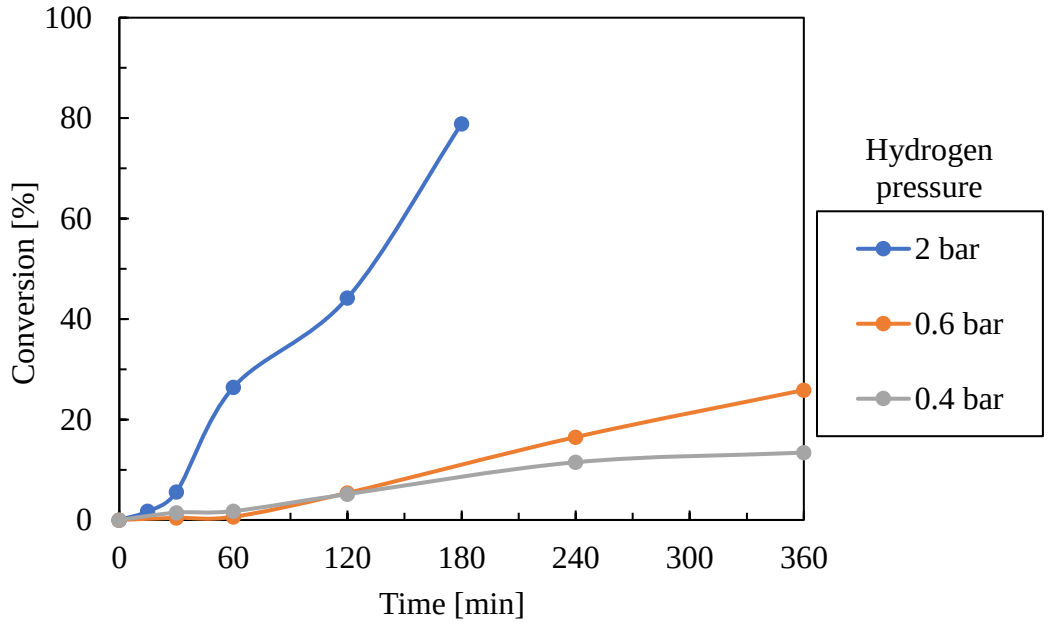

Figure 4-10: *Conversion evolution for 5%Pd/Al_2O_3_Acid catalyst using hydrogen pressure of 0.4, 0.6 and 2 bar. (T= 60°C ; M= 2M ; m_{cata}= 20mg ; solvent, isopropanol)*

The decrease of the hydrogen partial pressure in the system clearly decreases the conversion. Despite the increased reaction time, the conversion only reaches 26% at P_{H_2} = 0.6 bar and 14% at P_{H_2} = 0.4 bar H_2, compared to 80% at P_{H_2} = 2 bar. This underlines that the hydrogen became the limiting factor of the reaction. However, it is important to mention that due to a ban on the use of pure hydrogen in a glove box and fume hood and last minute technical problems linked to pressure control, it was not possible to work with a total pressure of 15 bar (P_{H_2} = 0.6 bar). For this reason, it was decided to work with a total pressure of 10 bar mixture of 4% H_2 in Ar, which is equivalent to a hydrogen pressure of 0.4 bar. Additionally, it was planned to test with the gas bottle open in order to allow a constant H_2 supply.

4.3. Performance of the hydrogenation of cinnamaldehyde in the fume hood system

The tests described below were carried out following the protocol described in section 2.3.1.2. As mentioned in the Experimental and analytical methods chapter, the only analytical method for monitoring the reaction behaviour of the tests performed at ATALANTE was ^{1}H Nuclear Magnetic Resonance (NMR) spectroscopy. In this sense, and in order to validate this technique, the initial (t_i) and final (t_f) samples of a preliminary test, which had been analyzed with GC, were taken and analyzed with the NMR equipment at ATALANTE. Table 4-1 shows the conversion results, using the two analysis techniques on the two samples: t_i and t_f. Both techniques resulted in a conversion of approximately 79%, thus validating NMR as the analysis technique for the tests carried out in the reactor installed at ATALANTE.

Table 4-1: *Validation of NMR analysis.*

	Samples GC	***Samples RMN***
Time	***Conversion (%)***	
t_i	*0*	*0*
t_f	*78.9*	*79.6*

As mentioned above, due to safety issues and technical inconveniences, 0.4 bar hydrogen pressure (10 bar total pressure) was used for the series of tests performed on the fume hood mounted reaction system. It was also mentioned that at this pressure we are strongly limited by the amount of hydrogen needed for the reaction to occur, which does it the limiting reagent. From the point of view of catalysis and more specifically chemical engineering, with hydrogen as the limiting reagent, we would not be measuring the performance of the catalyst correctly. Thus, the results will be exploited only for the beginning of the reaction, when the amount of hydrogen is sufficient. In this sense, we calculate the initial rate of the reaction which is the number of moles of CNA converted per minute, during the first 60 minutes.

The hydrogenation campaign at ATALANTE consisted of a series of tests, which are numbered below:

1. Test with 5%Pd/Al_2O_3-acid catalyst (non-radioactive) with closed H_2/Ar bottle.
2. Test with 5%Pd/Al_2O_3* catalyst (radioactive) with closed H_2/Ar bottle.
3. Test with 5%Pd/Al_2O_3-acid catalyst (non-radioactive) with open H_2/Ar bottle.
4. Test with 5%Pd/Al_2O_3* catalyst (radioactive) with open H_2/Ar bottle.
5. Test with 5%Pd/Al_2O_3-acid catalyst recovered (non-radioactive) with open H_2/Ar bottle.
6. Test with 5%Pd/Al_2O_3* catalyst recovered (radioactive) with open H_2/Ar bottle.

Unfortunately, at the moment of the treatment and interpretation of the results and after discarding the error of the analysis of the samples (E_a = ±1.5% max. in the conversion), it is found that the trend of the data of tests 3 and 4 is erroneous and does not coincide with the behaviour of the reaction, reason for which the results of these tests were discarded. This inconsistency could be due to technical failures at the time of the tests or even handling errors. The results of the other tests are presented below.

4.3.1. Results of the hydrogenation of cinnamaldehyde with non-radioactive catalysts

Table 4-2 shows the results of tests 1 and 5 mentioned above. Recall that the test with the fresh catalyst and open bottle was discarded.

Table 4-2: *Non-radioactive catalyst results.*

		CNA [mol]	***Time [min]***	***Rate [mol·min^{-1}]***
5%Pd/Al$_2$O$_3$-acid	*Closed bottle*	*4.80E-03*	*0*	***-4.18E-06***
		4.55E-03	*60*	
5%Pd/Al$_2$O$_3$-acid recovered	*Open bottle*	*4.80E-03*	*0*	***-5.88E-06***
		4.45E-03	*60*	

The rate, expressed in mol·min^{-1}, represents the consumption of cinnamaldehyde per minute of reaction, which is why it takes a negative value, indicating that CNA is consumed.

As one can see from these values, the test performed with the open bottle test showed a higher initial rate (5.88E-06 mol·min^{-1}), which is related to the fact that there is more hydrogen available to react than in the test with the closed bottle (4.18E-06 mol·min^{-1}). Since the results for the test with the open bottle was obtained using the recycled catalyst, one can clearly expect that the same test using a fresh catalyst would certainly not exhibit a lower initial rate than 5.88E-06 mol·min^{-1}, whereby our conclusion on the influence of the open or closed bottle is not compromised.

4.3.2. Results of the hydrogenation of cinnamaldehyde with radioactive catalysts

The results of tests 2 and 6 mentioned above are presented in Table 4-3. Recall that, as with the non-radioactive catalyst, the test with the fresh radioactive catalyst and open bottle had to be discarded.

Table 4-3: *Radioactive catalyst results*

		CNA [mol]	***Time [min]***	***Rate [mol·min^{-1}]***
5%Pd/Al$_2$O$_3$*	*Closed bottle*	*5.26E-03*	*0*	***-4.17E-06***
		5.01E-03	*60*	
5%Pd/Al$_2$O$_3$* recovered	*Open bottle*	*4.80E-03*	*0*	***-5.24E-06***
		4.49E-03	*60*	

As in the case of the non-radioactive catalyst, again the use of a continuous H-supply (open bottle) resulted in a higher rate (rate of 5.24E-06 mol·min^{-1}) than the test with the closed bottle and fresh radioactive catalyst (rate of 4.17E-06 mol·min^{-1}). The results again evidence that the amount of hydrogen plays an important role in the initial reaction rate. Having a constant supply of hydrogen increases the H_2 available to come into contact with the cinnamaldehyde, thus increasing the reaction rate.

4.3.3. Comparison of radioactive and non-radioactive catalysts

The comparison of the radioactive and non-radioactive catalysts is presented in Figure 4-11. Figure 4-11a shows the conversion after the first hour using a continuous H-supply (open bottle) over the recovered catalyst in both cases. As can be seen, the non-radioactive catalyst (green graph) has a slightly higher conversion (X=7.3%) than the radioactive catalyst (blue graph; X=6.5%) which implies that the rate is also higher (5.88E-06 mol·min^{-1} vs. 5.24E-06 mol·min^{-1}). However, this small difference is within the absolute error of the conversion, which is ±1.5%. Correspondingly, it seems the β radiation yielding from the ^{107}Pd in the radioactive catalyst, does not have any significant effect on the hydrogenation of CNA, since this catalyst presents the same behaviour as the non-radioactive catalyst under the same conditions.

Comparably, the tests with the two catalysts and with closed bottle (Figure 4-11b) show practically the same rate and the same behaviour, reaching a conversion of 5.2% for the non-

radioactive catalyst and 4.8% for the radioactive catalyst (rate of 4.18E-06 mol·min^{-1} vs. 4.17E-06 mol·min^{-1}). Again, this difference in conversion is within the maximum absolute error value, so we can infer that the result for the two catalysts is the same, underlining that the β radiation from ^{107}Pd had no effect on the catalytic activity.

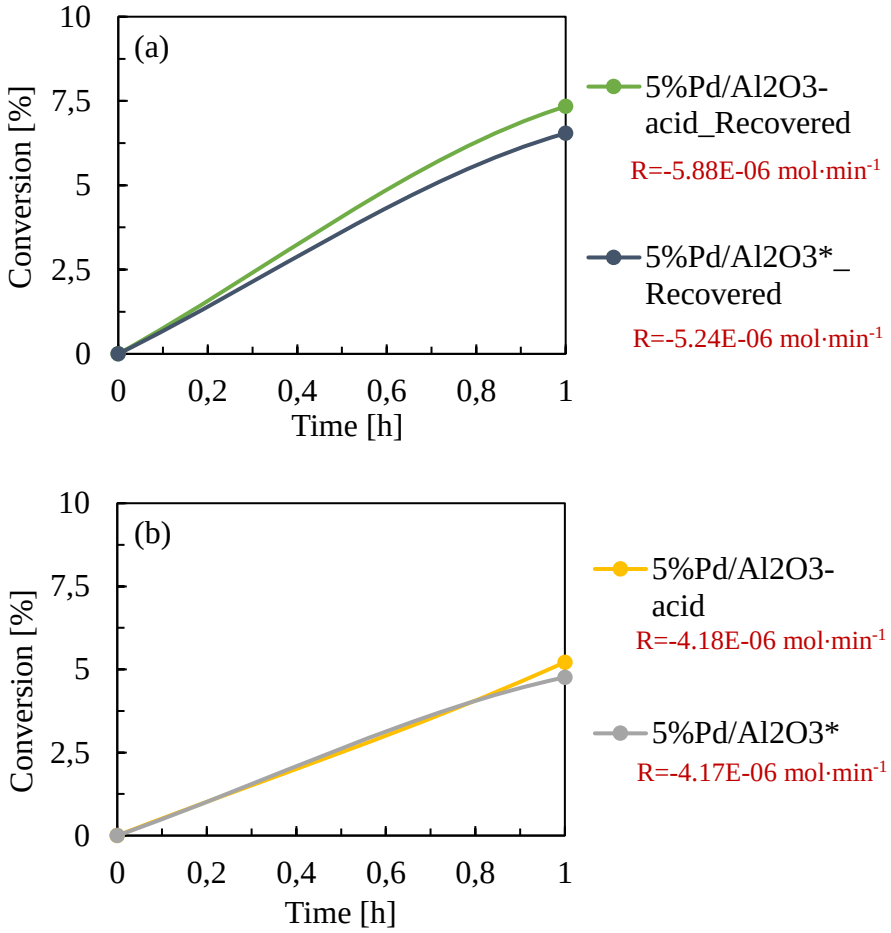

Figure 4-11: *Comparison of radioactive and non-radioactive catalyst with (a) Open bottle and (b) Closed bottle. (P= 0.4 bar H_2 ; T= 60°C ; M= 2M ; m_{cata}= 20mg ; solvent, isopropanol)*

4.4. Conclusion of impact of radioactivity on the hydrogenation of cinnamaldehyde

The impact of radioactivity, specifically β-radiation, on the hydrogenation of cinnamaldehyde was evaluated using an Al_2O_3-based catalyst, which was impregnated with a ^{107}Pd-containing solution.

Preliminary tests, besides allowing the optimisation of the reaction protocol, revealed technical problems (safety, permits, etc.), which, among others, did not allow the use of pure hydrogen under pressurized conditions at ATALANTE facilities. This forced us to adjust the protocol and to take the CNA consumption rate (during the first hour of reaction) for comparison between the different tests carried out. The aim was to reduce the limitation in the amount of H_2 caused by the decrease in pressure.

Tests were carried out with continuous feeding of the 4% H_2/Ar mixture (recovered catalyst) and without continuous feeding (fresh catalyst). In both cases, the results with the radioactive catalyst (5%Pd/Al_2O_3*) showed the same behaviour as the 5%Pd/Al_2O_3-acid catalyst. It can therefore be said that there is neither a positive nor a negative effect of the presence of β-radiation in the catalyst on the hydrogenation of cinnamaldehyde.

The catalysts recovered with continuous H_2 feed showed a better performance despite having completed 1 cycle of use. It would be interesting to carry out tests with fresh catalyst at the same conditions, in order to evaluate a possible effect of β-radiation on catalyst regeneration. Unfortunately, in the present study, such tests had to be discarded and at the time of writing this manuscript it was not possible to repeat them. Thus, the influence of irradiation on the catalyst regeneration had to be studied ex-situ.

4.5. References

[1] Fahlbusch K.G., Hammerschmidt F.J., Panten J., Pickenhagen W., Schatkowski D., Bauer K., Garbe D., Surburg H., Wiley-VCH (2012) 163.

[2] HAJEK, J. N. Kumara, P. Mäki-Arvela, T. Salmi, D.Yu. Murzin, I. Paseka, T. Heikkilä, E. Laine P. Laukkanend, J. Väyrynen, Ruthenium-modified MCM-41 mesoporous molecular sieve and Y zeolite catalysts for selective hydrogenation of cinnamaldehyde, Applied Catalysis A: General 251 (2003) 385–396. https://doi.org/10.1016/S0926-860X(03)00345-4.

[3] P. Mäki-Arvela, J. Hájek, T. Salmi, D. Murzin, Chemoselective hydrogenation of carbonyl compounds over heterogeneous catalysts, Applied Catalysis A: General 292 (2005) 1–49. https://doi.org/10.1016/j.apcata.2005.05.045.

[4] S. Bhogeswararao, D. Srinivas, Chemoselective Hydrogenation of Cinnamaldehyde over Pd/CeO_2–ZrO_2 Catalysts, Catal Lett 140 (2010) 55–64. https://doi.org/10.1007/s10562-010-0423-z.

[5] H.G. Manyar, B. Yang, H. Daly, H. Moor, S. McMonagle, Y. Tao, G.D. Yadav, A. Goguet, P. Hu, C. Hardacre, Selective Hydrogenation of α,β-Unsaturated Aldehydes and Ketones using Novel Manganese Oxide and Platinum Supported on Manganese Oxide Octahedral Molecular Sieves as Catalysts, ChemCatChem 5 (2013) 506–512. https://doi.org/10.1002/cctc.201200447.

[6] F. Jiang, J. Cai, B. Liu, Y. Xu, X. Liu, Particle size effects in the selective hydrogenation of cinnamaldehyde over supported palladium catalysts, RSC Adv. 6 (2016) 75541–75551. https://doi.org/10.1039/C6RA17000E.

[7] T. Szumełda, A. Drelinkiewicz, R. Kosydar, J. Gurgul, Hydrogenation of cinnamaldehyde in the presence of PdAu/C catalysts prepared by the reverse “water-in-oil” microemulsion method, Applied Catalysis A: General 487 (2014) 1–15. https://doi.org/10.1016/j.apcata.2014.08.036.

[8] M. Lashdaf, A. Krause, M. Lindblad, M. Tiitta, T. Venäläinen, Behaviour of palladium and ruthenium catalysts on alumina and silica prepared by gas and liquid phase deposition

in cinnamaldehyde hydrogenation, Applied Catalysis A: General 241 (2003) 65–75. https://doi.org/10.1016/S0926-860X(02)00423-4.

[9] Y. Kume, K. Qiao, D. Tomida, C. Yokoyama, Selective hydrogenation of cinnamaldehyde catalyzed by palladium nanoparticles immobilized on ionic liquids modified-silica gel, Catalysis Communications 9 (2008) 369–375. https://doi.org/10.1016/j.catcom.2007.07.012.

[10] S. Fujiwara, N. Takanashi, R. Nishiyabu, Y. Kubo, Boronate microparticle-supported nano-palladium and nano-gold catalysts for chemoselective hydrogenation of cinnamaldehyde in environmentally preferable solvents, Green Chem 16 (2014) 3230–3236. https://doi.org/10.1039/C4GC00383G.

[11] M. Jahjah, B. Caron, S. Menuel, E. Monflier, L. Djakovitch, C. Pinel, Hydrogenation of cinnamaldehyde with heterogeneous catalyst in the presence of cyclodextrins, Arkivoc 2011 (2011) 406–415. https://doi.org/10.3998/ark.5550190.0012.733.

[12] T. Shimizu, M. Ota, Y. Sato, H. Inomata, Effect of pore structure on catalytic properties of mesoporous silica supported rhodium catalysts for the hydrogenation of cinnamaldehyde, Chemical Engineering Research and Design 104 (2015) 174–179. https://doi.org/10.1016/j.cherd.2015.08.004.

[13] P.N. Rylander, Catalytic hydrogenation in organic syntheses, Academic Press, New York, 1979.

[14] P. Reyes, C.Rodrıguez G. Pecchi and J.L.G. Fierro, Promoting effect of Mo on the selective hydrogenation of cinnamaldehyde on Rh/SiO_2 catalysts, Catal Lett 69 (2000) 27–32.

[15] F. Zhao, Y. Ikushima, M. Chatterjee, M. Shirai, M. Arai, An effective and recyclable catalyst for hydrogenation of α,β-unsaturated aldehydes into saturated aldehydes in supercritical carbon dioxide, Green Chem 5 (2003) 76–79. https://doi.org/10.1039/B209252M.

Chapter 5

Impact of radioactivity on the decolorization of azo-dyes

5.1. Introduction

Azo-dyes are by far the most important dye class for textile dyeing, especially water-soluble dyes, which are used to dye hydrophilic textiles such as cotton and viscose rayon. Cotton is the most widely used textile fabric in the world, so the tonnages of these water-soluble dyes are extremely large [1]. This is why many researches have been directed to study the toxicity and to create processes aimed at removing these non-biodegradable dyes from the effluents of these industries, as they pollute our water sources and the whole ecosystems. Today, there are several physico-chemical and biological methods for the treatment of textile wastewater. Unfortunately, these processes have a high operational cost and are of limited applicability [2].

Heterogeneous photocatalysis is a promising advanced oxidation-reduction process in which free radicals are generated in situ due to the interaction of light and light-active catalysts (photocatalysts). In heterogeneous photocatalysis, the catalyst acts as an active surface for the generation of free radicals that are able to completely neutralize pollutants through complex mechanisms [3–6]. Moreover, the photocatalytic reaction can take place at ambient temperature and pressure without significant reduction in catalytic efficiency or production of additional sludge. Due to the sustainable characteristics of photocatalysis, it has been widely used for wastewater treatment using photocatalysts such as TiO_2, ZnO or CuO [7,8]. However, compared to other semiconductor materials, TiO_2 has been most widely studied due to its high photocatalytic activity, non-toxicity, low cost and chemical stability [6].

In the present study, we chose a model reaction that is widely studied and could easily be implemented to the glove box where the tests involving the handling of radioactive material must be carried out. Furthermore, as mentioned above, studies have shown promising results of proton and gamma irradiation in the decay of methyl orange [9,10].

This chapter, divided into two main parts, aims to study the impact of radioactivity, particularly the β radiation provided by ^{107}Pd, on the decolorization of the azo molecule - methyl orange - by radio-catalysis. In this sense, in the first part, catalytic tests with non-radioactive catalysts will be addressed, starting with preliminary tests. Subsequently, radioactive catalysts synthesized in glove boxes will be tested following protocol described in section 2.2.1, where their effect on MO decomposition will be evaluated.

5.2. Preliminary tests

This section presents the results obtained in the preliminary tests carried out for the decolorization of methyl orange (MO), using the protocol described in section 2.3.2 with the non-radioactive catalysts 5%Pd/TiO_2 (Table 3-1). It is important to mention that previously, blank tests were performed with the supports and catalysts that showed no evidence of significant decolorization in the absence of photochemical initiation (light).

5.2.1. Optimisation of protocol and conditions

Preliminary tests allowed the optimisation of the established protocol in such a way that it was simple and reproducible under radioactive conditions as mentioned above. In addition, optimal conditions were sought to evaluate the effect of the radioactivity using the lowest amount of radioactive material. This measure was taken, not only in order to economise on the available radioactive material, but also to respect the limits for safe handling of radioactive material in glove boxes. For this purpose, tests were carried out with 20 and 50 mg of non-radioactive catalyst, with a reaction time of 2 h and photochemical initiation (light). Figure 5-1 shows the UV-Vis spectra obtained for the mentioned amounts of catalyst. For each test a different initial solution (S_i) was used, which is why the curves of the initial solutions are shown in a darker colour than their respective final solutions.

The absorption in the visible band at 469 nm, besides being the isosbestic point, is attributed to the absorption of the N=N group present in MO, while the aromatic ring absorbs in the 220-270 nm range [4,11]. In this sense, the decrease of absorption in the 469nm band is related to the degradation of methyl orange. As one can see, the final solutions (S_f) for both 50 mg (blue curves) and 20 mg (green curves) show a decrease in absorbance compared to their respective initial solutions (S_i). This decrease is, of course, more important when using 50 mg of catalyst (20%) than when using 20 mg of catalyst (16%).

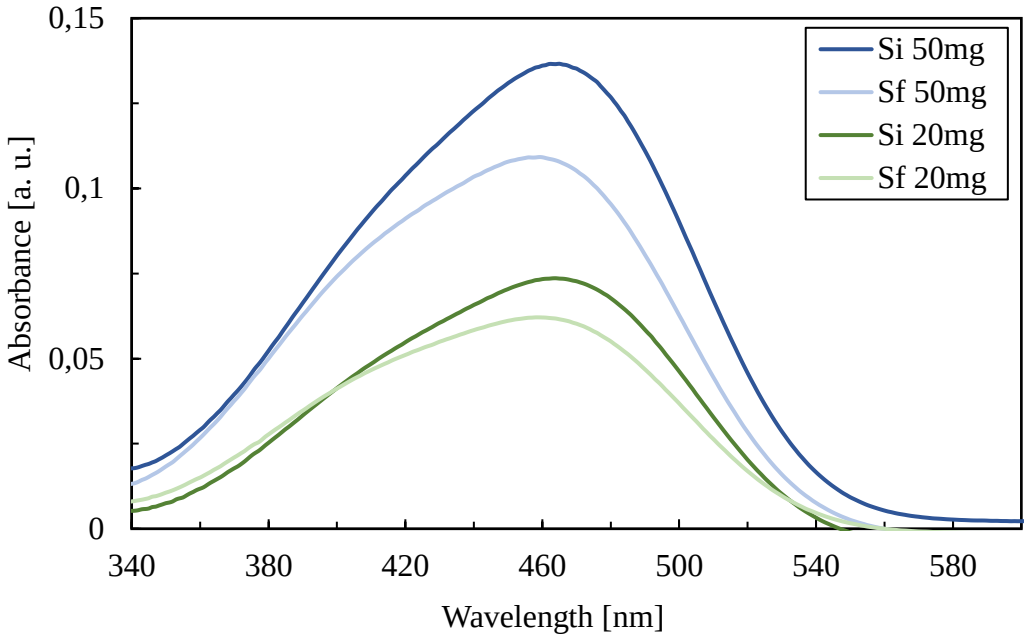

Figure 5-1:*UV-vis spectra for MO decolorization with different amounts of non-radioactive catalyst 5%Pd/TiO₂. Reaction conditions: 30mL of aqueous solution MO (1.54E-4 M); 40°C; 1bar; 400rpm; 2h; light.*

In a second series of tests, the reaction time was varied between 2 and 5 h with a fixed amount of catalyst of 20 mg (Figure 5-2). The spectra showed 33% decrease in the intensity of the 469 nm band when the reaction time was increased to 5 h (red curves) versus a 21% at 2h of reaction (grey curves).

These preliminary tests clearly show that the non-radioactive 5%Pd/TiO_2 catalyst works in the presence of light, even with small amounts of catalyst (20 mg).

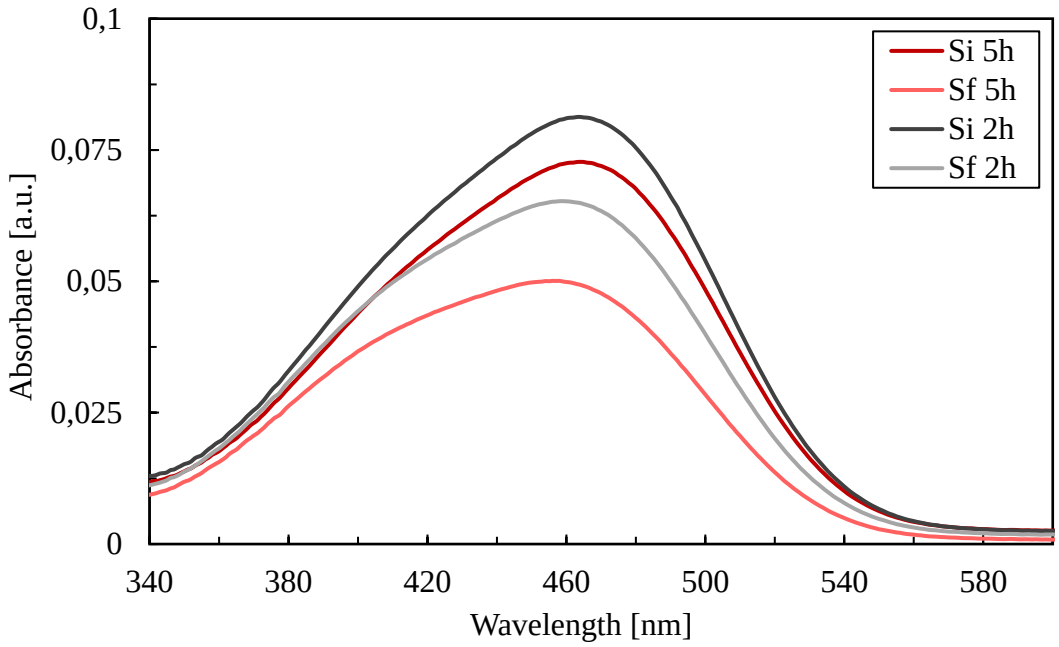

Figure 5-2: *UV-vis spectra for MO decolorization for different reaction times with 5%Pd/TiO₂*
Reaction conditions: *20 mg of catalyst*; *30mL of aqueous solution MO (1.54E-4 M); 40°C; 1bar; 400rpm; light.*

5.2.2. Non-radioactive tests with 5%Pd/TiO₂ and 5%Pd/TiO₂-acid catalyst

As mentioned above, a non-radioactive catalyst with a similar composition to the radioactive catalyst was synthesized. This catalyst, referenced as 5%Pd/TiO₂-acid, was tested in the decolorization of methyl orange in order to evaluate the effects of other characteristics, independent of radioactivity, possibly present later in the radioactive tests.

Figure 5-3 shows the absorbance at 469 nm during the reaction with the acid catalyst compared to the "non-acid" catalyst. The two tests were performed under the same conditions, using the maximum amount of catalyst envisaged for the radioactive tests (100 mg) in the absence of light. The behaviour of the 5%Pd/TiO₂ catalyst did not show any significant variation in absorbance after 1h of reaction, and a sample was even taken after 15 days in which the solution was in contact with the catalyst. Figure 5-3 represents two points: one at one hour and the other after 6h of reaction, however, the trend shows that the absorbance did not change with respect to the absorbance found in the first sample.

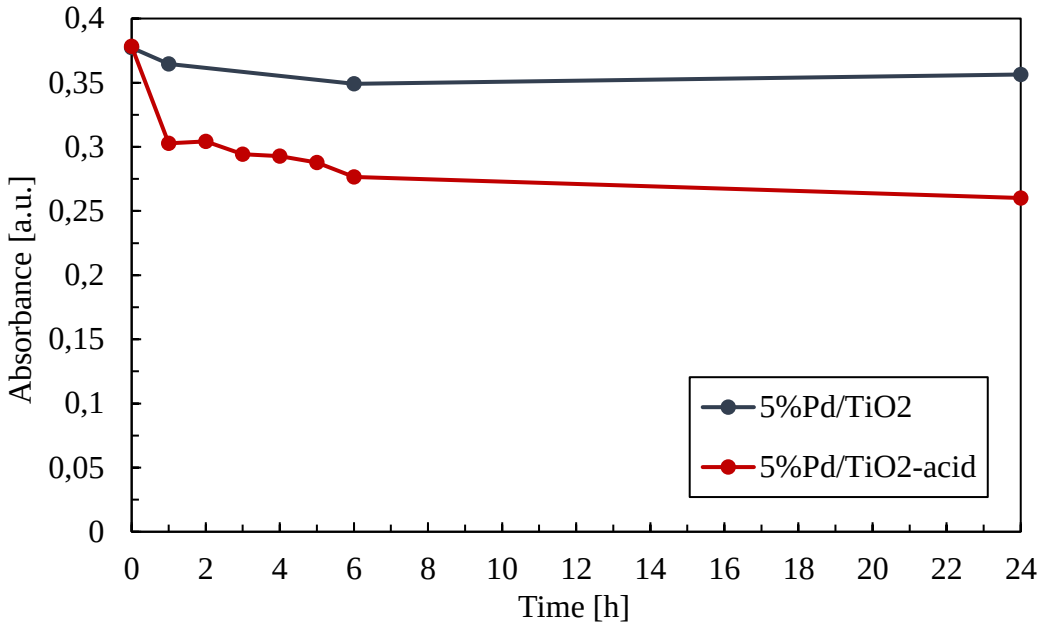

Figure 5-3: *Evolution of the absorbance over time for acid and non-acid 5%Pd/TiO₂*
Reaction conditions: 100 mg of catalyst; 30mL of aqueous solution MO (1.54E-4 M); 40°C; 1bar; 400rpm; non-light.

On the other hand, with the 5%Pd/TiO₂-acid catalyst a decrease of the absorbance from 0.38 to 0.26 in 24h of reaction was observed, which corresponds to a total decrease of 31%, although, it is interesting to note that after 1h of reaction there is a decrease of 20% in absorbance, meaning that the main decrease takes place in the first hour. This behaviour is attributed to the adsorption of the methyl orange that takes place on the catalyst surface, more precisely over protonated TiO₂.

The adsorption phenomenon of methyl orange on the TiO₂ surface has been demonstrated by several authors. Guettaï et al. [4] found that the pH has a strong influence on the adsorption of MO, which is explained by the change of the surface charge properties of TiO₂ with changing pH values according to the following reactions:

$$\boldsymbol{TiOH + H^+ \leftrightarrow TiOH_2^+ \; ; \; pH < pH_{pzc}}$$

$$TiOH + OH^- \leftrightarrow H_2O + TiO^- \; ; \; pH > pH_{pzc}$$

The pH of zero charge (pH_{pzc}) of TiO_2 is known to be close to pH = 6.8 [12], in this sense when pH is higher than pH_{pzc} the TiO_2 surface is negatively charged (TiO^-), on the contrary when pH is lower than pH_{pzc} the surface is positively charged ($TiOH_2{}^+$). The pKa of methyl orange in aqueous solution is equal to 3.4 [13] and in alkaline solution, the MO molecules are negatively charged, which implies that when the pH is between 3.4 and 6.8, the number of $TiOH_2{}^+$ groups on the surface increases and the MO (which would be negatively charged) is electrostatically attracted. Consequently, the adsorption of MO increases with increasing $TiOH_2{}^+$ groups, hence with decreasing pH. Moreover, authors such as N. Barka et al. [12] and H. Ayoub et al. [14] also observed that large amounts of MO were adsorbed at pH 3.

In our case, the fact of having synthesized the catalyst with the acidic solution, similar in composition to the radioactive solution, had an effect on the surface charge of the catalyst which led to the adsorption of MO. This is reflected by the decrease in absorbance observed in the test with the acid catalyst, in contrast to the test with the "non-acidic" catalyst where the absorbance remains almost constant. Additionally, tests were performed in the absence of light with a SiO_2-supported catalyst (non-semiconducting support) synthesized in acidic conditions, which reported no variation in absorbance at the isosbestic point, the results are shown in Annex 2. These results serve as a reference to evaluate the effect of the β radiation, which will eventually bring the ^{107}Pd present in the radioactive catalyst, which will be discussed in the following section.

5.3. Radio-catalysis decolorization activity

The results for the tests carried out with the radioactive catalysts are shown below. These catalysts (labelled 5%Pd/TiO_2*) were synthesized in glove box using the ^{107}Pd solution recovered and purified by CEA-Marcoule (Table 2-1), as described in the protocol in section

2.2.1. Likewise, the radioactive tests that will be discussed in the following, were carried out in a glove box following the protocol described in section 2.3.2.

5.3.1. Reproducibility test

Figure 5-4 shows the reproducibility to validate the tests carried out in the glove box assembly. Both tests were carried out under the same conditions of temperature, pressure, catalyst and catalyst mass. At the same time, different samples were taken during the course of the reaction, which allowed the evolution of the absorbance to be closely monitored. The results show the reproducibility of the protocol implemented in the glove box, as the two tests showed the same behaviour.

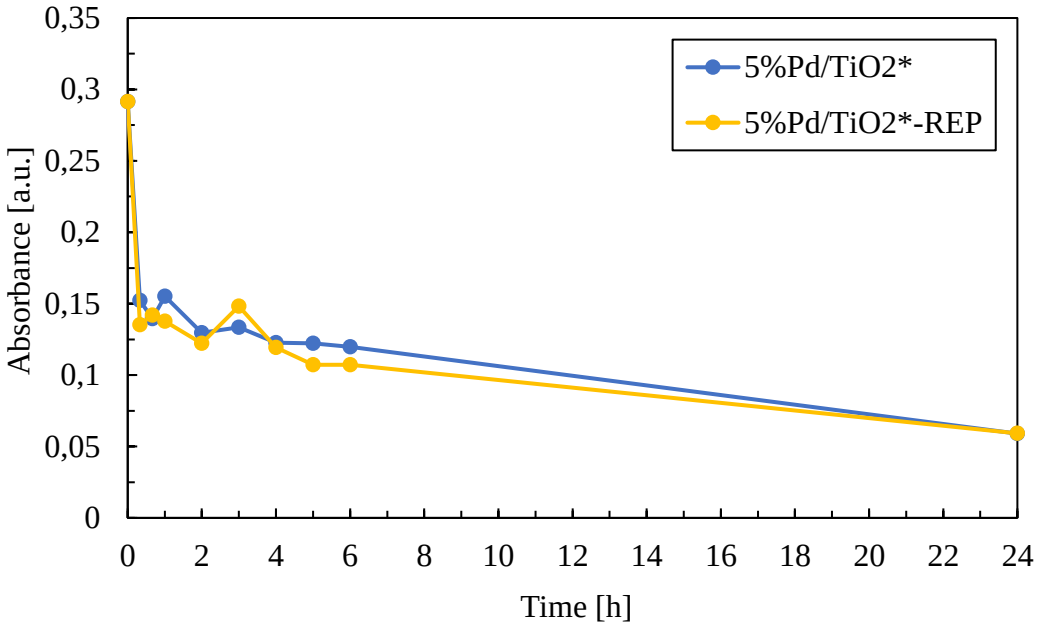

Figure 5-4: *Reproducibility of glove box tests with 5%Pd/TiO_2* catalyst.*
Reaction conditions: 50 mg of catalyst; 30ml of aqueous solution MO (1,54E-4 M); 40°C; 1bar; 400rpm; non-light.

5.3.2. Effect of radioactive catalyst on the decolorization of methyl orange.

The effect of the radioactive catalyst on the decolorization was evaluated with the maximum amount of catalyst estimated for the glove box tests.

In Figure 5-5, the evolution of the absorbance during 24h of reaction is compared between the non-radioactive catalyst 5%Pd/TiO_2-acid and 5%Pd/TiO_2 and the radioactive catalyst 5%Pd/TiO_2*. The three tests were carried out with the same amount of catalyst (100 mg) and at the same reaction conditions, except for the radioactive catalyst where a new initial solution preparation was used, which is why the starting point does not overlap with that of the other two tests shown in the figure. As can be seen, the absorbance for 5%Pd/TiO_2* (green curve) decreases rapidly during the first 20 minutes of reaction, then it decreases progressively until it reaches a value of 0, after 24h of reaction. This absence of absorbance is also illustrated by the clear solution obtained after 24 (Figure 5-5) as observed by naked eye. Precisely, the radioactive catalyst, showed 70% decrease in absorbance at 469 nm after 20 minutes of reaction and continues to reach 99% in 24h (Absorbance$_{469nm}$ = 0.0027).

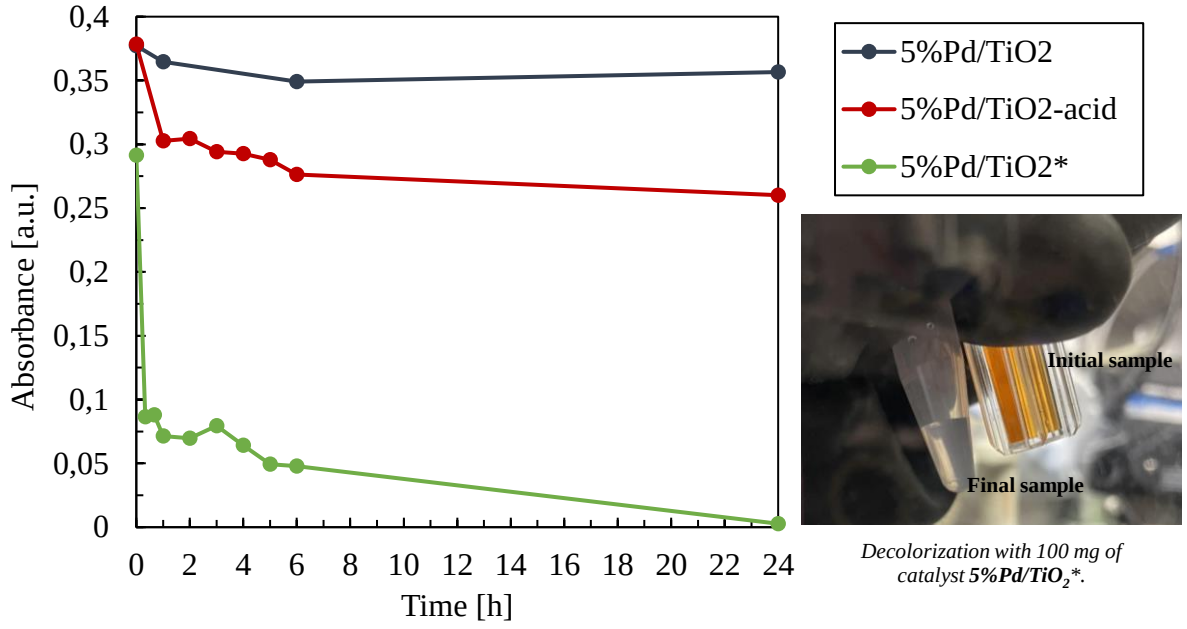

*Decolorization with 100 mg of catalyst **5%Pd/TiO_2***.*

Figure 5-5: *Evolution of the absorbance over time, comparison of 5%Pd/TiO_2, 5%Pd/TiO_2-acid and 5%Pd/TiO_2* catalyst.*
Reaction conditions:100 mg of catalyst; 30mL of aqueous solution MO (1.54E-4 M); 40°C; 1bar; 400rpm; non-light

As discussed previously, the acidic pH that characterises the radioactive solution recovered from the nuclear fuel favours the adsorption of the MO on the TiO_2 surface, which could be responsible for the rapid decrease of the absorbance during the first 20 minutes of reaction.

Recall that the non-radioactive acid catalyst (red curve), had a 31% reduction in 24h of reaction, contrary to the non-radioactive catalyst which seems to remain constant (blue curve). The reduction observed with the radioactive catalyst is therefore a little more than three times the reduction of the non-radioactive catalyst. Discriminating the adsorption of MO by TiO_2, which represents 31% of the absorbance, and taking into account that the only difference between the two catalysts (5%Pd/TiO_2-acid and 5%Pd/TiO_2*) is the presence of ^{107}Pd, we can deduce that the β radiation promotes the decomposition, i.e. on the decolorization of MO.

5.3.3. Effect of different amounts of radioactive catalyst on the decolorization of methyl orange

In order to confirm that the radiation was responsible for the decolorization, tests with different amounts of catalysts where performed, since the radiation doses is directly correlated to the amounts of ^{107}Pd. For this purpose, experiments were carried out with 20 and 50 mg of catalyst. The results are shown below.

Figure 5-6 summarises the results of the evolution of the absorbance of the band at 469 nm as a function of time for 20, 50 and 100 mg of 5%Pd/TiO_2* catalyst and 100 mg of 5%Pd/TiO_2-acid catalyst. The observed trend coincides with that found in the tests with 100 mg of catalyst (Figure 5-5), where increasing the reaction time promoted the decomposition of the MO.

The test increasing the amount of radioactive catalyst to 50 mg, i.e. the amount of ^{107}Pd and thus the amount of radiation in the system, also showed a progressive decrease in absorbance over the course of the reaction time (blue curve in Figure 5-6), while increasing the amount of catalyst caused the MO decay to be higher than that found with 20 mg of catalyst. In addition, a decrease in colouring was observed between the initial and final solution, although it was not the same as that of the final solution of the 100 mg catalyst test, it was noticeable to the naked eye when the sample was taken.

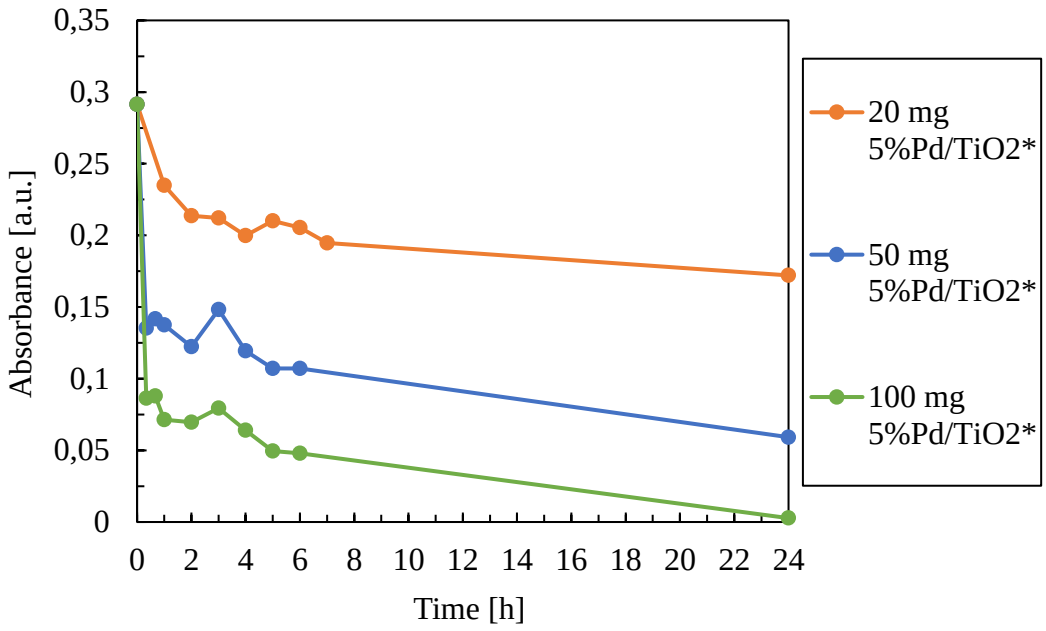

Figure 5-6: *Evolution of the absorbance over time, comparison of different amounts of 5%Pd/TiO₂* catalyst. Reaction conditions: 30ml of aqueous solution MO (1,54E-4 M); 40°C; 1bar; 400rpm; non-light.*

The comparison of the evolution of the absorbance of the different quantities of radioactive catalyst and acid catalyst allows us to see in more detail the effect of the β radiation present in the radioactive tests. As we have already mentioned, the increase in the mass of catalyst and, therefore, of radioactive matter, contributes to the progressive decrease in absorbance over time, being more significant with 100 mg of catalyst than with the other quantities. In fact, for 100 mg, the absorbance decreased from 0.29 to 0.0027 during 24h, reaching 99% of MO decay, compared to 79% and 40% achieved with 50 and 20 mg of 5%Pd/TiO₂* respectively.

Moreover, it is striking that by increasing the amount of radioactive ^{107}Pd, not only the decomposition increases in the first 20 minutes, but from then on, the decomposition rate increases as well, being 100 mg (decrease of 1.21% in 1h) > 50 mg (decrease of 1.10% in 1h) > 20 mg (decrease of 0.94% in 1h). These results show a positive effect of the β radiation on the decolorization of the MO due to the degradation process of the molecule, leaving aside the adsorption of the catalyst.

The effect of the presence of β-radiation on the catalyst, which was observed in the decolorization of methyl orange, could be interpreted in two ways, which will be described below:

- β-radiation "replaces" UV-light

The first thing one can think about the effect of β-radiation on the decolorization is that β-radiation fulfils the function of light in a traditional photocatalytic reaction (Figure 5-7), i.e. it strikes the TiO_2 surface directly and absorbs photons with an energy equal to or greater than the difference between the valence (V_B) and conduction (C_B) bands of the photocatalyst. This absorption of photons allows the excitation of the valence electrons e^-, which consequently move from V_B to C_B, giving rise to positive holes h^+. The h^+ react with H_2O to form hydroxyl radicals (·OH), while the e^- react with O_2 to form superoxide ($\cdot O_2^-$). Finally, it is ·OH and $\cdot O_2^-$ that are directly involved in the degradation of methyl orange [15]. This is an indirect effect of the β-radiation, which requires the presence of the semiconductor to decompose the MO.

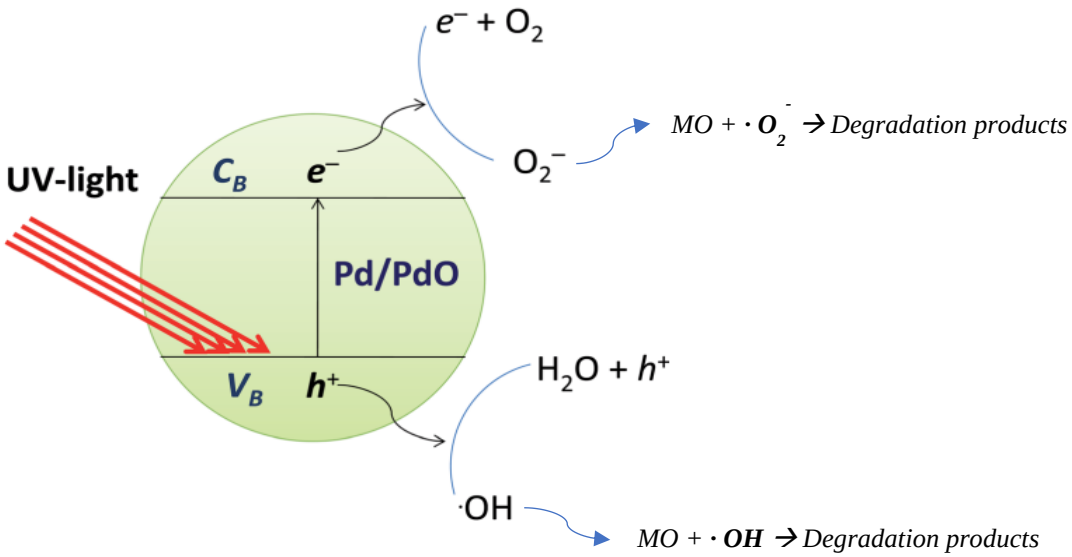

Figure 5-7: *Mechanism of photocatalytic degradation of azo-dyes by catalysts Pd-γ-Al_2O_3 et PdO-γ-Al_2O_3 [15]*

- β-radiation reacts directly with the MO solution

It can also be thought that the β-radiation, upon contact with the aqueous solution, directly decomposes the MO. This is due to the fact that hydroxyl radicals (·OH) are the main oxidising species produced in the radiolysis of aqueous solutions [16]. Therefore, the decomposition of the MO molecule would take place via oxidative degradation, in which the ·OH reacts with the -N=N- double bond, which is mainly responsible for the decolorization, according to the following reaction [10]:

$$-N=N- \; + \cdot OH \rightarrow -N\cdot -N(OH) \xrightarrow{+H_2O} -N^{\cdot} - NH- \; + OH^-$$

In this case it would be the β-radiation that acts directly in the decomposition, without the need for the presence of the semiconductor material, which in our case is the TiO_2. Tests with a non-semiconducting support such as SiO_2 impregnated with ^{107}Pd, or even contacting the MO solution with a β emitter such as ^{90}Y, would give a good indication of the possibility of β-radiation having a direct effect on the discolouration. However, at the time of writing it was not technically possible to perform such tests.

Although so far, there are no reports of photocatalytic tests with catalysts impregnated with radioactive metals with β-radiation, our results are consistent with those found in other studies, where other methods using ionising radiation to promote the decolorization of MO have been successfully tested. These studies showed, for example, that gamma irradiation promotes the decomposition of MO and that this decomposition is accelerated by increasing the dose or the exposure time of the solution [9,17,18]. Similarly, proton and electron irradiation also showed a positive effect on MO decolorization by promoting the decomposition of the molecule [9,10,17].

5.4. Conclusion of impact of radioactivity on the decolorization of methyl orange

The impact of radioactivity on the decolorization of methyl orange (azo-dye molecule) was evaluated with the use of a TiO_2-based catalyst, impregnated with a solution recovered directly from nuclear fuel, containing ^{107}Pd, a β-emitter.

The preliminary tests allowed, on the one hand, to validate the protocol created specifically for the development of the tests under radioactive conditions. On the other hand, to evaluate with non-radioactive tests, the effect that the acidity present in the radioactive solution. As a result, it was found that MO is adsorbed on the protonated TiO_2 surface at pH <6.8.

The results with the radioactive catalyst, after leaving aside the adsorption, showed an effect of the β-radiation on the decolorization of methyl orange, which is evidenced by the decrease in the absorbance value at the isosbestic point (469 nm). This decrease was more significant when the amount of catalyst was increased, which in turn increased the amount of ^{107}Pd present in the system. As a result, a completely transparent solution was obtained in the test where the higher amount of radioactive catalyst (100mg) was used. Additionally, it was observed that increasing the amount of ^{107}Pd also promoted the rate at which the MO decomposes after 1h of reaction.

It is clear that there is an effect of the presence of β-radiation on the decolorization of methyl orange, however, it could not be determined whether this is a direct effect or an indirect effect that requires the presence of a semiconductor. It would be interesting to analyse in more detail with tests where a semiconductor material is not included or where the solution is put in contact with another β-emitter.

5.5. References

[1] R.B. Chavan, Environmentally friendly dyes, in: M. Clark (Ed.), Handbook of textile and industrial dyeing, Woodhead Publishing Limited, Oxford, Philadelphia, 2011, pp. 515–561.

[2] B. Neppolian, S. Sakthivel, B. Arabindoo, M. Palanichamy, V. Murugesan, Photocatalytic degradation of textile dye commonly used in cotton fabrics, Studies in Surface Science and Catalysis 113 (1998) 329–335. https://doi.org/10.1016/S0167-2991(98)80304-2.

[3] W.S. Kuo, P.H. Ho, Solar photocatalytic decolorization of methylene blue in water, Chemosphere 45 (2001) 77–83. https://doi.org/10.1016/S0045-6535(01)00008-X.

[4] N. Guettaï, H. Ait Amar, Photocatalytic oxidation of methyl orange in presence of titanium dioxide in aqueous suspension. Part II: kinetics study, Desalination 185 (2005) 439–448. https://doi.org/10.1016/j.desal.2005.04.049.

[5] B. Neppolian, H.C. Choi, S. Sakthivel, B. Arabindoo, V. Murugesan, Solar light induced and TiO_2 assisted degradation of textile dye reactive blue 4, Chemosphere 46 (2002) 1173–1181. https://doi.org/10.1016/S0045-6535(01)00284-3.

[6] M. Huang, C. Xu, Z. Wu, Y. Huang, J. Lin, J. Wu, Photocatalytic discolorization of methyl orange solution by Pt modified TiO_2 loaded on natural zeolite, Dyes and Pigments 77 (2008) 327–334. https://doi.org/10.1016/j.dyepig.2007.01.026.

[7] M. Ghorbanpour, M. Yousofi, S. Lotfiman, Photocatalytic Decolorization of Methyl Orange by Silica- Supported TiO_2 Composites, Journal of Ultrafine Grained and Nanostructured Materials 50 (2017).

[8] F. Masoom, F. Robina, L. Rakel W., S. Muhammad, A review on biocatalytic decomposition of azo dyes and electrons recovery, Journal of Molecular Liquids 246 (2017) 275–281. https://doi.org/10.1016/j.molliq.2017.09.063.

[9] Y. Ling, G. Wang, T. Chen, X. Fei, S. Hu, Q. Shan, D. Hei, H. Feng, W. Jia, Irradiation-catalysed degradation of methyl orange using BaF_2–TiO_2 nanocomposite catalysts prepared by a sol–gel method, Royal Society Open Science (2019).

[10] R. Huszank, G. Nagy, I. Rajta, A.M. Czeglédi, In-air proton beam irradiation induced radiolysis of methyl orange in aqueous solution, Radiation Physics and Chemistry (2021).

[11] S. Al-Qaradawi, S.R. Salman, Photocatalytic degradation of methyl orange as a model compound, Journal of Photochemistry and Photobiology A: Chemistry 148 (2002) 161–168. https://doi.org/10.1016/S1010-6030(02)00086-2.

[12] N. Barka, A. Assabbane, A. Nounah, J. Dussaud, Y. Ait Ichou, Photocatalytic degradation of methyl orange with immobilized TiO_2 nanoparticles: effect of ph and some inorganic anions, Phys. Chem. News (2008) 85–88.

[13] J. Oakes, P. Gratton, Kinetic investigations of the oxidation of Methyl Orange and substituted arylazonaphthol dyes by peracids in aqueous solution, J. Chem. Soc., Perkin Trans. (1998) 2563–2568.

[14] H. Ayoub, M. Kassir, M. Raad, H. Bazzi, A. Hijazi, Effect of Dye Structure on the Photodegradation Kinetic Using TiO2 Nanoparticles, Journal of Materials Science and Chemical Engineering (2017) 31–45.

[15] A.P. Kumar, D. Bilehal, A. Tadesse, Photocatalytic degradation of organic dyes: Pd-γ-Al_2O_3 and PdO-γ-Al_2O_3 as potential photocatalysts, Royal Society of Chemistry (2021) 6396–6406.

[16] M. Taguchi, T. Kojima, Yield of OH radicals in water under heavy ion irradiation. Dependence on mass, specific energy, and elapsed time, Nuclear Science and Techniques (2007) 35–38.

[17] R. M.A., S.A. S, Radiation induced degradation of dyes—An overview, Journal of Hazardous Materials (2009) 6–16.

[18] Y.-P. Chen, S.-Y. Liu, H.-Q. Yu, H. Yin, Q.-R. Li, Radiation-induced degradation of methyl orange in aqueous solution, Chemosphere (2008) 532–536.

Chapter 6

Catalyst regeneration by γ-irradiation

6.1. Introduction

The deactivation of catalyst by carbonaceous species is a phenomenon widely observed in chemical industry. Classical methods for the regeneration of these deactivated catalysts are mainly based on oxidative treatment (calcination in air). Studies dating back to the 1960s showed that the irradiation of catalysts with X-rays, neutrons, protons and gamma rays affected the catalytic activity, whereby it was not clear if the latter actually affected the active sites of the catalyst or only hindered the deactivation of the catalysts [1,2]. The present study aims to determine the effect of γ-irradiation on the regeneration of deactivated catalysts. For this purpose, Pd and Ru-based catalysts with Al_2O_3 as a support were synthesized and deliberately deactivated by humin deposition using the synthesis of 5-hydroxymethylfurfural (5-HMF) from fructose as a model reaction. Subsequently, these deactivated catalysts were subjected to γ-irradiation for a given time. Finally, the catalytic activity of these irradiated catalysts in the hydrogenation of cinnamaldehyde (CNA) was evaluated and compared with fresh and non-irradiated catalysts.

6.2. Palladium catalyst tests.

In this section the results of the regeneration study for the 5%Pd/Al_2O_3 catalyst are presented. The catalyst was synthesized with the usual protocol (section 2.2.1), then it was deliberately deactivated by the deposition of humins, using the synthesis of 5-HMF, a reaction known to produce these carbonaceous spices. Humins deposition was confirmed by TGA analysis, which evidenced the presence of these species on the deactivated catalyst, corresponding to a 38% mass loss the temperature range 105-500°C (section 3.2.4). The detailed protocol of the deactivation was presented in section 2.3.3.1 of the chapter "Experimental and analytical methods". Subsequently, the deactivated catalyst was submitted gamma irradiation according to the protocol (section 2.3.3.2). The three catalysts: fresh, deactivated (Deact.) and deactivated-

irradiated (Deact.-IR) were tested in the hydrogenation of CNA using the protocol described above (section 2.3.1.1). The conversion results as a function of time are shown in Figure 6-1.

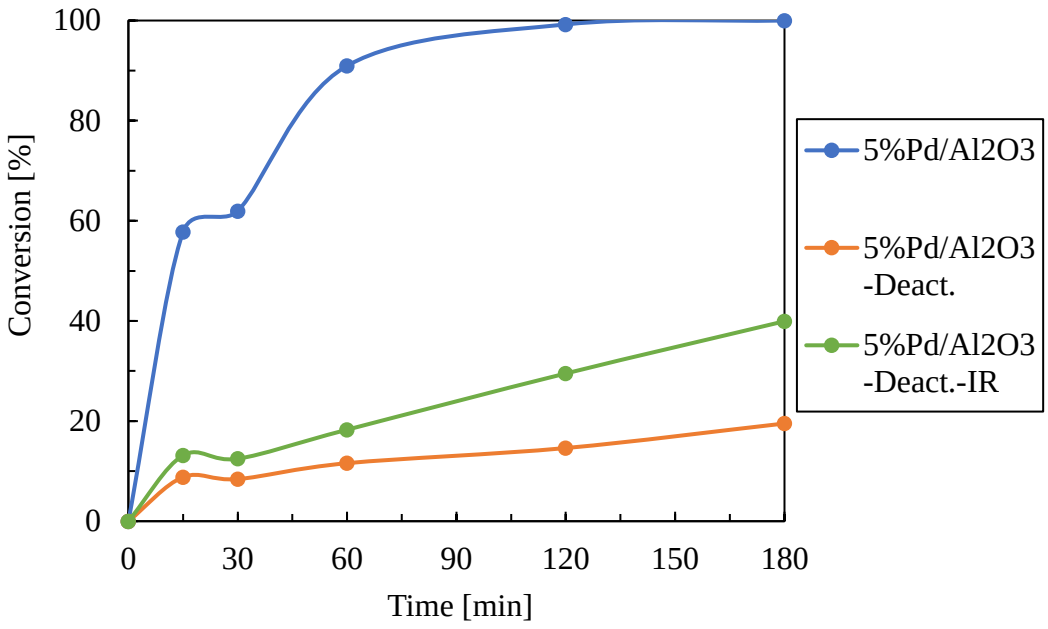

Figure 6-1: *Conversion as a function of time of fresh, deactivated and irradiated 5%Pd/Al_2O_3 catalysts. (P_{H_2} = 2 bar ; T= 60°C ; M= 2M ; m_{cata}= 20mg ; solvent, isopropanol)*

The 5%Pd/Al_2O_3 catalyst, as already known, has a high catalytic activity for the hydrogenation of CNA, reaching a complete conversion after 2h of reaction. As expected, a significant decrease of the conversion of the deactivated catalyst (X=19.5% in 3h) was detected, which is directly related to the accumulation of carbon molecules (humins) on the catalyst surface, which induces losses in the catalytic activity. This result agrees with the results obtained in the BET (Table 3-4; section 3.2.1) and TGA (Figure 3-6; section 3.2.4) analyses that show the presence of these species. Meanwhile, the catalyst that was deactivated and then irradiated showed an increase in its catalytic activity, being twice as active as the deactivated catalyst (X=40%), which is a consequence of the possible decomposition of the deposed carbon molecules (humins) by the γ-irradiation. The results of the nitrogen physisorption analysis confirm this decomposition, since the analysis showed an increase in the specific area (from 19 to 32 $m^2 \cdot g^{-1}$) and the porous volume (from 0.06 to 0.1 $cm^3 \cdot g^{-1}$), after irradiation of the deactivated catalyst.

These results are in agreement with the findings of Sokol'skii et. al. [3] claming, that γ-irradiation restored the catalytic activity of supported Pd-, Pt- and Rh-based catalysts, which had been previously poisoned with 2-methylthiophene. The authors conclude that "Under irradiation, the catalyst-chimisorbed organosulfur compound system can reach radiolysis and then the oxidised radiolysis products with oxygen from the air lose the role of catalytic poison". In our particular case, further analyses are needed to highlight the causes of this behaviour and to reach a concrete conclusion on the effect of γ-irradiation, whether it acts exclusively on the deposed humin species or also alters the active sites. Unfortunately, at the time of writing this manuscript, it was not possible to perform such analyses.

6.3. Ruthenium catalyst tests.

The results of the regeneration study of the 5%Ru/Al_2O_3 catalyst are presented below. The catalyst was synthesized, deactivated and irradiated using the same steps and protocols as for the palladium catalyst (previous section). The deposition of humins was corroborated by TGA analysis, which confirmed the presence of these species on the deactivated catalyst, with a mass loss of 53.5% (Figure 3-7; section 3.2.4). The conversion results as a function of time for the fresh, deactivated (Deact.) and deactivated-irradiated (Deact.-IR) catalysts are shown in Figure 6-2.

As with the results for the Ru-based catalyst shown in the hydrogenation chapter, the catalytic activity of the fresh 5%Ru/Al_2O_3 catalyst is very low (3%), in fact, it almost matches the catalytic activity of the deactivated catalyst (2%). Surprisingly, the catalytic activity observed in the test with the deactivated and then irradiated catalyst increased to 9%, which even exceeds the performance of the fresh catalyst. This unexpected result was confirmed by a repetition of the test carried out with the 5%Ru/Al_2O_3-Deact.-IR catalyst (red curve).

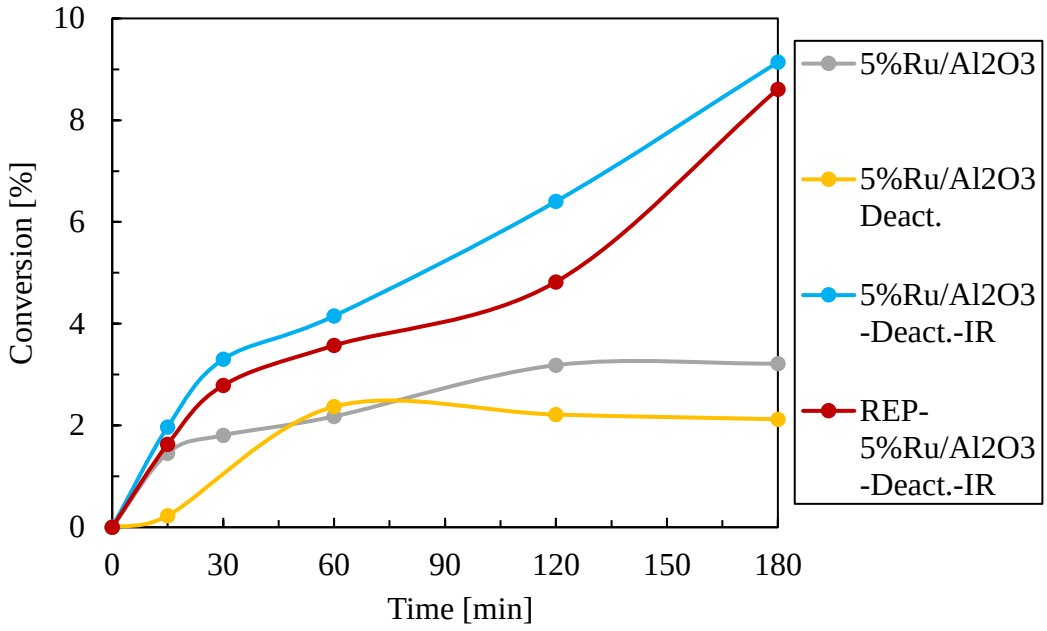

Figure 6-2: *Conversion as a function of time of fresh, deactivated and irradiated 5%Ru/Al_2O_3 catalysts. (P_{H_2} = 2 bar ; T= 60°C ; M= 2M ; m_{cata}= 20mg ; solvent, isopropanol)*

Contrary to the results with the Pd-based catalyst, the BET analysis for the ruthenium catalyst did not show any significant modification neither in specific surface area nor in pore volume (Table 3-4; section 3.2.1), which suggests that the increased performance was not related to the removal of deposed carbonaceous species but to the alteration of the active site. Correspondingly the Ru active site was analyzed by XPS in order to detect changes in the oxidation state. The results presented in section 3.2.5 allow us to deduce that:

- Indeed, the increase in yield of 5%Ru/Al_2O_3-Deact.-IR cannot be explained by carbon decomposition since the carbon peak remains very intense.
- Ru is no longer found as nitrate.
- Ru is not in metallic form.

Nevertheless, it would be wrong to state that Ru changes its oxidation state. What is suggested is that in both cases there is a change in the chemical environment of Ru. However, this is a hypothesis that remains to be validated, so it is not possible to conclude on the effect of the γ-

irradiation on the deactivated catalyst and how this benefited to the catalytic activity. In this sense, further analysis is required with a pre-treatment to remove the carbonaceous species, such as plasma.

6.4. Conclusion of experimental and analytical methods

The impact of γ-irradiation on the regeneration of Pd- and Ru-based catalysts, arbitrarily deactivated with 5-HMF synthesis and tested in the hydrogenation of CNA, was evaluated.

Nitrogen physisorption analysis (BET) and thermogavimetric analysis (TGA) of the catalysts confirmed the presence of Humins-type carbonaceous species on the surface of the deactivated catalyst.

The deactivation of the Pd catalyst induced a decrease in conversion from 100 to 20%, however, it was observed that after γ-irradiation, the catalyst recovered a part of the initial catalytic activity reaching a conversion of 40% in 3h. The fresh and deactivated Ru catalysts showed no relevant catalytic activity, however, after γ-irradiation, the deactivated catalyst showed a slight increase in conversion. XPS analyses performed on the irradiated and non-irradiated deactivated catalysts suggest a change in the chemical environment of Ru compared to the fresh catalyst. However, no concrete conclusion was reached on the positive effect of γ-irradiation on the deactivated and irradiated Ru catalyst.

These results show positive effects of γ-irradiation on the Pd and Ru catalysts, which will require further analysis to determine the cause of their behaviour. It is also suggested to evaluate the effect of different irradiation doses.

6.5. References

[1] Vikt. I. Spitsyn, G. N. Pirogova, and I. E. Mikhailenko, The effect of ionizing radiation on the catalytic dehydration of N-dodecyl alcohol, The Institute of Physical Chemistry, Acad. Sci., USSR 9 (1962) 1515–1520.

[2] A. A. Balandin, Vikt. Spitsyn and N. P. Dobrosel'skaya, Cracking of cumene on a radioactive tricalcium phosphate catalyst, Institute of Physical Chemistry, Academy of Sciences of the USSR 12 (1965) 2095–2100.

[3] Sokol'skii D. V., Nadykto B. T., and D'yakova, G. A., Effect of ionizing radiation on regeneration of hydrogenation catalysts. [Gamma rays]., Journal ID: CODEN: IVUKA (1979) 1415–1417.

Chapter 7

General conclusions and perspectives

7.1. General conclusion

In the search for a way to valorise potentially recoverable noble metals (mainly Pd, Ru, Rh) after the dissolution process of recycled nuclear fuel, Orano has been interested in investigating possible applications where the radioactivity contained in these metals plays a beneficial role. That is why in this doctoral thesis the effect of radiation was evaluated in different applications, namely heterogeneous catalysis, photocatalysis and regeneration of catalysts.

The bibliographic introduction showed that, although there are some works where the effect of radiation is studied (mainly developed in the 60's), there is no concrete answer of its contribution in catalytic systems. That is why in this work we present the effect of radioactivity present in catalysts supported on Al_2O_3 and TiO_2, impregnated with ^{107}Pd (main mode of decay: β-emission) on the hydrogenation of cinnamaldehyde (CNA) and the decolorization of methyl orange (MO), as well as the effect of γ-irradiation on deactivated catalysts using the synthesis of 5-Hydroxymethylfurfural. The study ranges from catalyst design, characterization and evaluation of the catalytic activity in the respective reactions.

Several protocols for the catalyst synthesis and for the reactions were elaborated and validated, especially for their implementation under radioactive conditions. These protocols, besides being simple and reproducible, rigorously complied with the technical limitations and the different safety requirements of handling radioactive substances, in this case, an acid solution, of known composition, recovered and purified from nuclear fuel, containing ^{107}Pd. The protocols were implemented satisfactorily in glove box and fume hood as appropriate.

The characterizations of the catalysts presented in chapter 3 showed good textural properties for the non-acidic catalysts, however, the analysis of the 5%Pd/Al_2O_3-acid catalyst, synthesized with a non-radioactive solution of similar composition to the ^{107}Pd solution, resulted in an increase in the particle size of Pd. The 5%Pd/TiO_2-acid, on the other hand, showed similar

characteristics to the non-acidic catalyst. The deactivation of the 5%Pd/Al_2O_3 and 5%Ru/Al_2O_3 catalysts was verified by TGA analysis which evidenced the presence of humins, a result that was also corroborated by XPS on 5%Ru/Al_2O_3 where a large carbon layer was seen which, in fact, did not allow to see clearly the behaviour of Ru after deactivation and irradiation.

In Chapter 4 the results of the hydrogenation of CNA were presented. Preliminary tests validated the protocol, established the optimal conditions that met the constraints for its implementation under the fume hood, and additionally showed a superior performance of the 5%Pd/Al_2O_3 with respect to the Ru and Rh-based catalysts. The 5%Pd/Al_2O_3-acid catalyst had a 20% decrease in conversion with respect to the non-acid catalyst, which was related to the increase in Pd particle size found in the characterization analyses. The results of the tests with the radioactive 5%Pd/Al_2O_3* catalyst were compared in terms of the initial reaction rate, where H_2 is not limiting. After discarding the tests with the fresh non-radioactive catalyst, whose results did not coincide with the reaction behaviour, the results of the analyses allow concluding that the presence of β-radiation had no effect on the hydrogenation of cinnamaldehyde as there was no significant difference between the initial rate of the non-radioactive catalyst and the radioactive catalyst.

The impact of β-radiation on a photocatalytic reaction, such as MO decolorization, was presented in chapter 5. All results were compared at the isosbestic point (469nm) at which pH-related effects are discarded. The preliminary tests allowed to validate the protocol created for the radioactive conditions and additionally to verify the adsorption effect on the TiO_2 surface. The results with the radioactive catalyst showed an effect of β-radiation on the decolorization of MO, which is evidenced by a decrease in absorbance that increases with increasing catalyst mass, i.e. ^{107}Pd. This effect could be due to the fact that β radiation directly decomposes the MO in solution, as β-radiation replaces the UV light that traditionally activates the reaction.

Finally, in chapter 6, the effect of γ-irradiation on the regeneration of arbitrarily deactivated Pd and Ru-based catalysts is presented. The catalytic activity evaluated in the hydrogenation of CNA showed that the Pd-based catalyst decreased its activity from 100 to 20% after deactivation and increased its activity after gamma irradiation from 20 to 40%. Whereas, in the case of Ru catalysts, the deactivated and then irradiated catalyst showed even better activity than the fresh catalyst. The XPS analysis allowed inferring that possibly, after deactivation, there is a change in the chemical environment of Ru that could explain this behaviour, however, due to the presence of the huge carbon layer on the surface, it was not possible to obtain concrete results about the oxidation state of Ru.

In conclusion, on the one hand, β-radiation has no effect on the hydrogenation of CNA, however, it has an important effect on the decolorization of MO. On the other hand, gamma irradiation seems to have a positive effect on the regeneration of deactivated catalysts.

7.2. Perspectives

In this work the effect of radioactivity on the hydrogenation of CNA, the decolorization of MO and the regeneration of catalysts deactivated by the presence of humins was studied. From the results presented, it is concluded that there is no effect on the hydrogenation of CNA, on the contrary, an effect of β-radiation on the discolouration of MO and of γ-irradiation on the regeneration of catalysts is observed. In this sense, it is suggested for future work:

To implement the decolorization of MO using another β-radiation emitter in the absence of the semiconductor, to determine if the effect found is directly from the radiation on the MO or if on the contrary it requires the presence of a semiconductor such as TiO_2.

Perform more detailed characterization analyses to explain the behaviour of the 5%Pd/Al_2O_3_Desact-IR catalyst after irradiation, in addition to evaluating the effect of different irradiation doses.

Pre-treat the catalyst to clean the surface and at the same time not affect the Ru. It would be interesting to further investigate the origin of the behaviour of the 5%Ru/Al_2O_3_Desact-IR catalyst, and why not, like the Pd-based catalyst, evaluate the effect of different irradiation doses.

Annexes

8.1. Annex 1: PDF DATA CARDS

PDF# 00-046-1131

00-046-1131 Oct 4, 2022 1:56 PM (CHEV-C3-2)

PDF Card

Status: Primary **Quality Mark:** Blank **Environment:** Ambient
Temperature of Data Collection: 298.0 K (Assigned by ICDD editor) **Phase:** δ
Chemical Formula: Al2 O3 **Empirical Formula:** Al2 O3 **Weight %:** Al52.93 O47.07
Atomic %: Al40.00 O60.00 **Compound Name:** Aluminum Oxide
Mineral Name: Deltalumite, syn **Alternate Name:** δ-Al2 O3 **CAS Number:** 1344-28-1
Entry Date: 09/01/1996 **Modification Date:** 09/01/2005 **Modifications:** DBstatus

Experimental

Radiation: CuKα (1.5418 Å) **d-Spacing:** Diffractometer **Cutoff:** 17.70 Å
Intensity: Diffractometer - Integrated

Physical

Crystal System: Tetragonal **SPGR:** P-4m2 (115)

Author's Unit Cell

a: 5.599(10) Å	**c:** 23.657(50) Å	**Volume:** 741.62 Å³
Z: 12.00	**MolVol:** 61.80	**c/a:** 4.225

Calculated Density: 2.74 g/cm³ **SS/FOM:** F(30) = 4.8(0.0897, 70)

Crystal

ICDD Calculated Parameters

Space Group: P-4m2 (115) **Molecular Wt:** 101.96 g/mol

Crystal Data

a: 5.599 Å	**b:** 5.599 Å	**c:** 23.657 Å
α: 90.00°	**β:** 90.00°	**γ:** 90.00°
Volume: 741.62 Å³	**Z:** 12.00	**c/a:** 4.225
a/b: 1.000	**c/b:** 4.225	

Reduced Cell

a: 5.599 Å	**b:** 5.599 Å	**c:** 23.657 Å
α: 90.00°	**β:** 90.00°	**γ:** 90.00°
Volume: 741.62 Å³		

 Page 1 / 3

00-046-1131 Oct 4, 2022 1:56 PM (CHEV-C3-2)

Structure

Crystal (Symmetry Allowed): Non-centrosymmetric

Classifications

Subfiles: Cement and Hydration Product, Forensic, Inorganic, Metal & Alloy, Mineral Related (Mineral, Synthetic), Pharmaceutical (Excipient)

Pearson Symbol: tP60.00 **Prototype Structure (Formula Order):** Al2.67 O4

Prototype Structure (Alpha Order): Al2.67 O4

LPF Prototype Structure (Formula Order): Al2.67 O4,tP84,115

LPF Prototype Structure (Alpha Order): Al2.67 O4,tP84,115

Cross-references

Cross-Ref PDF #'s: 00-016-0394 (Deleted)

References

Type	DOI	Reference
Primary Reference		Repelin, Y., Husson, E. Mater. Res. Bull. 1990, 25, 611.

Comments

Database Comments: Additional Patterns: To replace 00-016-0394. General Comments: Reference reports reflection 1.9294 out of order between 1.9132 and 1.8178. Sample Preparation: Prepared by calcining δ-"Al2 O3". Warning: Lines with abs(delta 2Theta)>0.2 DEG. Unit Cell Data Source: Powder Diffraction.

d-spacings (73) - Al2 O3 - 00-046-1131 (Stick, Fixed Slit Intensity) - X-ray (Cu Kα1 1.54056

2θ (°)	d (Å)	I	h	k	l	*	2θ (°)	d (Å)	I	h	k	l	*
16.201	5.4666	3	0	1	1		39.502	2.2794	50	0	2	6	
17.501	5.0633	2	0	1	2		41.782	2.1601	3	0	2	7	
19.501	4.5483	15	0	1	3		44.982	2.0136	45	1	2	7	
21.801	4.0733	<1	0	1	4		45.162	2.0060	60	0	1	11	
24.641	3.6099	<1	0	1	5		45.642	1.9860	70	2	2	0	
27.601	3.2291	2	0	1	6		46.064	1.9688	30	2	2	1	
29.262	3.0495	6	1	1	5		46.602	1.9473	36	2	2	2	
31.022	2.8804	29	0	1	7		47.060	1.9294	<1	2	2	3	
31.802	2.8115	32	0	2	0		47.483	1.9132	16	2	0	9	
32.102	2.7859	30	0	2	1		50.142	1.8178	2	0	3	3	
32.802	**2.7280**	71	0	2	2		50.493	1.8060	4	2	0	10	
34.602	2.5901	22	1	1	7		51.105	1.7858	4	0	3	4	
36.003	2.4925	37	1	2	1		51.563	1.7710	4m	1	3	0	
36.763	2.4427	56	1	2	2		51.563	1.7710	4m	2	2	6	
37.302	2.4086	43	0	2	5		56.462	1.6284	3	1	2	11	
37.643	2.3876	38	1	2	3		57.163	1.6101	4	2	0	12	
37.883	2.3730	34	1	0	9		60.106	1.5381	19	2	3	2	
38.863	2.3154	37	1	2	4		61.026	1.5171	16m	1	3	8	

00-046-1131 Oct 4, 2022 1:56 PM (CHEV-C3-2)

2θ (°)	d (Å)	I	h	k	l	*	2θ (°)	d (Å)	I	h	k	l	*
61.026	1.5171	16m	2	2	10		87.807	1.1108	1m	0	5	3	
63.886	1.4559	17	2	2	11		88.166	1.1072	3m	2	3	15	
64.406	1.4454	16	0	2	14		88.166	1.1072	3m	2	4	10	
66.783	1.3996	56	0	4	0		88.813	1.1008	2	0	5	4	
66.983	**1.3959**	90m	0	4	1		89.213	1.0969	1	1	5	0	
66.983	**1.3959**	90m	2	2	12		94.650	1.0477	3m	0	4	15	
67.245	**1.3911**	100	0	4	2		94.650	1.0477	3m	0	5	8	
73.208	1.2918	4	0	4	7		95.067	1.0442	4	1	5	7	
73.746	1.2837	4	2	2	14		95.599	1.0398	3m	2	5	0	
75.449	1.2589	5m	1	4	7		95.599	1.0398	3m	3	3	14	
75.449	1.2589	5m	2	3	11		96.112	1.0356	5	2	5	2	
77.810	1.2265	2	3	3	7		96.808	1.0300	3	3	4	9	
78.526	1.2171	<1	2	3	12		99.855	1.0066	8m	2	4	14	
84.051	1.1506	9	2	4	8		99.855	1.0066	8m	2	5	6	
84.611	1.1444	10	2	3	14		100.813	0.9996	7	1	4	16	
85.005	1.1401	5	0	4	12		101.245	0.9965	8	1	5	10	
85.404	1.1358	4	1	3	16		101.767	0.9928	7	0	5	11	
87.609	1.1128	1	0	5	2		104.453	0.9745	3	3	4	12	
87.807	1.1108	1m	0	4	13								

PDF# 00-041-1107

00-041-1107 Oct 4, 2022 1:59 PM (CHEV-C3-2)

PDF Card

Status: Primary **Quality Mark:** Star **Environment:** Ambient
Temperature of Data Collection: 298.0 K (Assigned by ICDD editor) **Chemical Formula:** Pd O
Empirical Formula: O Pd **Weight %:** O13.07 Pd86.93 **Atomic %:** O50.00 Pd50.00
Compound Name: Palladium Oxide **Mineral Name:** Palladinite **Entry Date:** 09/01/1991

Experimental

Radiation: CuKα (1.5418 Å) **Filter:** Graph Mono **Internal Standard:** Si
d-Spacing: Diffractometer **Cutoff:** 15.00 Å **Intensity:** Diffractometer - Peak

Physical

Crystal System: Tetragonal **SPGR:** P42/mmc (131)

Author's Unit Cell

a: 3.0456(6) Å	**c:** 5.3387(45) Å	**Volume:** 49.52 Å³
Z: 2.00	**MolVol:** 24.76	**c/a:** 1.753

Calculated Density: 8.21 g/cm³ **Color:** Black **SS/FOM:** F(30) = 42.3(0.0182, 39)

Crystal

ICDD Calculated Parameters

Space Group: P42/mmc (131) **Molecular Wt:** 122.42 g/mol

Crystal Data

a: 3.046 Å	**b:** 3.046 Å	**c:** 5.339 Å
α: 90.00°	**β:** 90.00°	**γ:** 90.00°
Volume: 49.52 Å³	**Z:** 2.00	**c/a:** 1.753
a/b: 1.000	**c/b:** 1.753	

Reduced Cell

a: 3.046 Å	**b:** 3.046 Å	**c:** 5.339 Å
α: 90.00°	**β:** 90.00°	**γ:** 90.00°
Volume: 49.52 Å³		

00-041-1107 Oct 4, 2022 1:59 PM (CHEV-C3-2)

Structure

Atomic parameters are cross-referenced from PDF entry 04-007-4016

AC Space Group: P42/mmc (131)

AC Unit Cell

a: 3.042(1) Å	**b:** 3.042(1) Å	**c:** 5.351(3) Å
α: 90°	**β:** 90°	**γ:** 90°

Space Group Symmetry Operators:

Seq	Operator	Seq	Operator	Seq	Operator	Seq	Operator
1	x,y,z	5	-y,x,z+1/2	9	-x,y,-z	13	y,x,-z+1/2
2	-x,-y,-z	6	y,-x,-z+1/2	10	x,-y,z	14	-y,-x,z+1/2
3	-x,-y,z	7	y,-x,z+1/2	11	x,-y,-z	15	-y,-x,-z+1/2
4	x,y,-z	8	-y,x,-z+1/2	12	-x,y,z	16	y,x,z+1/2

Atomic Coordinates:

Atom	Num	Wyckoff	Symmetry	x	y	z	SOF	IDP	AET
Pd	1	2c	mmm.	0.0	0.5	0.0	1.0		4#c
O	2	2e	-4m2	0.0	0.0	0.25	1.0		4-a

Crystal (Symmetry Allowed): Centrosymmetric **AC Space Group:** P42/mmc (131)

Classifications

Subfiles: Common Phase, Inorganic, Metal & Alloy, Mineral Related (Mineral, Natural), Superconducting Material (Superconductor Reaction Product)

Pearson Symbol: tP4.00 **Prototype Structure (Formula Order):** Pt S

Prototype Structure (Alpha Order): Pt S

LPF Prototype Structure (Formula Order): Pt S,tP4,131

LPF Prototype Structure (Alpha Order): Pt S,tP4,131

Cross-references

Cross-Ref PDF #'s: 00-006-0515 (Alternate), 04-002-4417 (Primary), 04-005-4781 (Alternate), 04-006-5918 (Alternate), 04-007-4016 (Alternate), 04-007-6608 (Alternate)

References

Type	DOI	Reference
Primary Reference		Welton-Holzer, J., McCarthy, G., North Dakota State University, Fargo, North Dakota, USA. ICDD Grant-in-Aid 1989.
Crystal Structure		Crystal Structure Source: LPF.

00-041-1107 Oct 4, 2022 1:59 PM (CHEV-C3-2)

Comments

Database Comments: Additional Patterns: To replace 00-006-0515. General Comments: Average relative standard deviation in intensity of the ten strongest reflections for three specimen mounts = 4%. Validated by a calculated pattern. Sample Source or Locality: Sample obtained from ROC/RIC.

d-spacings (30) - Pd O - 00-041-1107 (Stick, Fixed Slit Intensity) - X-ray (Cu Kα1 1.54056 Å)

2θ (°)	d (Å)	I	h	k	l	*	2θ (°)	d (Å)	I	h	k	l	*
29.316	3.0440	3	1	0	0		99.720	1.0076	5	1	0	5	
33.549	**2.6690**	22	0	0	2		100.263	1.0036	5	2	0	4	
33.836	**2.6470**	100	1	0	1		100.938	0.9987	5	2	2	2	
41.927	2.1530	14	1	1	0		101.162	0.9971	5	3	0	1	
45.138	2.0070	1	1	0	2		106.236	0.9630	2	3	1	0	
54.715	**1.6762**	20	1	1	2		107.805	0.9533	<1	2	1	4	
60.218	1.5355	15	1	0	3		116.528	0.9057	4	3	1	2	
60.782	1.5226	11	2	0	0		119.943	0.8897	<1	0	0	6	
70.521	1.3343	6	0	0	4		121.790	0.8816	1	3	0	3	
71.251	1.3224	15	2	0	2		130.881	0.8469	1	3	1	3	
71.457	1.3191	13	2	1	1		131.568	0.8446	2	3	2	0	
85.534	1.1344	3	1	1	4		132.889	0.8403	4	2	1	5	
90.834	1.0815	5	2	1	3		133.584	0.8381	5	2	2	4	
91.353	1.0767	5	2	2	0		134.816	0.8343	4	3	2	1	
98.721	1.0151	2	3	0	0		138.984	0.8224	2	1	1	6	

PDF# 03-065-5714

03-065-5714 Oct 4, 2022 2:00 PM (CHEV-C3-2)

PDF Card

Status: Alternate **Quality Mark:** Star **Environment:** Ambient
Temperature of Data Collection: 298.0 K (Assigned by ICDD editor) **Chemical Formula:** Ti O2
Empirical Formula: O2 Ti **Weight %:** O40.06 Ti59.94 **Atomic %:** O66.67 Ti33.33
Compound Name: Titanium Oxide **Mineral Name:** Anatase, syn **Entry Date:** 09/01/2003

Experimental

Radiation: CuKα1 (1.5406 Å) **d-Spacing:** Calculated **Intensity:** Calculated - Peak

Physical

Crystal System: Tetragonal **SPGR:** I41/amd (141)

Author's Unit Cell

a: 3.785(1) Å	**c:** 9.514(6) Å	**Volume:** 136.30 Å³
Z: 4.00	**MolVol:** 34.08	**c/a:** 2.514

Calculated Density: 3.892 g/cm³ **Structural Density:** 3.89 g/cm³
SS/FOM: F(30) = 614.8(0.0014, 35) **I/Ic:** 5.04 **I/Ic - CW ND:** 1.06

Crystal

ICDD Calculated Parameters

Space Group: I41/amd (141) **Molecular Wt:** 79.86 g/mol

Crystal Data

a: 3.785 Å	**b:** 3.785 Å	**c:** 9.514 Å
α: 90.00°	**β:** 90.00°	**γ:** 90.00°
Volume: 136.30 Å³	**Z:** 4.00	**c/a:** 2.514
a/b: 1.000	**c/b:** 2.514	

Reduced Cell

a: 3.785 Å	**b:** 3.785 Å	**c:** 5.458 Å
α: 110.29°	**β:** 110.29°	**γ:** 90.00°
Volume: 68.15 Å³		

03-065-5714 Oct 4, 2022 2:00 PM (CHEV-C3-2)

Structure

AC Space Group: I41/amd (141)

AC Unit Cell

a: 3.785(1) Å	**b:** 3.785(1) Å	**c:** 9.514(6) Å
α: 90.0°	**β:** 90.0°	**γ:** 90.0°

Space Group Symmetry Operators:

Seq	Operator	Seq	Operator	Seq	Operator
1	x,y,z	7	-x+1/2,y,-z+3/4	13	-y+1/2,x+1/2,-z+1/2
2	-x+1/2,-y+1/2,z+1/2	8	x,-y+1/2,-z+1/4	14	y,-x,-z
3	x+1/2,y,-z+3/4	9	y+1/2,x+1/2,-z+1/2	15	-y,x+1/2,z+1/4
4	-x,-y+1/2,-z+1/4	10	-y,-x,-z	16	y+1/2,-x,z+3/4
5	-x,y,z	11	y,x+1/2,z+1/4		
6	x+1/2,-y+1/2,z+1/2	12	-y+1/2,-x,z+3/4		

Atomic Displacement Parameter Type: B **Origin Of Unit Cell:** O1

Atomic Coordinates:

Atom	Num	Wyckoff	Symmetry	x	y	z	SOF	Biso	AET
O	1			0.0	0.0	0.2064	1.0	0.664	
Ti	2			0.0	0.0	0.0	1.0	0.51	

Crystal (Symmetry Allowed): Centrosymmetric **AC Space Group:** I41/amd (141)

Classifications

Subfiles: Common Phase, Forensic, Inorganic, Metal & Alloy, Mineral Related (Mineral, Synthetic), Pharmaceutical (Excipient), Pigment/Dye

Pearson Symbol: tI12.00 **Prototype Structure (Formula Order):** Ti O2

Prototype Structure (Alpha Order): O2 Ti

LPF Prototype Structure (Formula Order): Ti O2,tI12,141

LPF Prototype Structure (Alpha Order): O2 Ti,tI12,141

Cross-references

03-065-5714 Oct 4, 2022 2:00 PM (CHEV-C3-2)

Cross-Ref PDF #'s: 01-070-6826 (Alternate), 01-070-7348 (Alternate), 01-071-1166 (Alternate), 01-071-1167 (Alternate), 01-071-1168 (Alternate), 01-071-1169 (Alternate), 01-073-1764 (Alternate), 01-075-1537 (Alternate), 01-075-2544 (Alternate), 01-075-2545 (Alternate), 01-075-2546 (Alternate), 01-075-2547 (Alternate), 01-075-2550 (Alternate), 01-075-2551 (Alternate), 01-075-2552 (Alternate), 01-075-2553 (Alternate), 01-076-7109 (Alternate), 01-076-8999 (Alternate), 01-083-2243 (Alternate), 01-083-5913 (Alternate), 01-083-5914 (Alternate), 01-083-5916 (Alternate), 01-084-1285 (Alternate), 01-084-1286 (Alternate), 01-085-5943 (Alternate), 01-089-4203 (Alternate), 04-001-7641 (Alternate), 04-002-2678 (Alternate), 04-002-2750 (Alternate), 04-002-2751 (Alternate), 04-002-8296 (Alternate), 04-006-1918 (Alternate), 04-006-9240 (Alternate), 04-007-0701 (Alternate), 04-011-0664 (Primary), 04-013-5313 (Alternate), 04-013-5967 (Alternate), 04-014-0246 (Alternate), 04-014-0490 (Alternate), 04-014-5762 (Alternate), 04-014-5764 (Alternate), 04-014-8515 (Alternate), 04-015-4102 (Alternate), 04-016-2837 (Alternate), 04-021-3587 (Alternate), 04-022-3337 (Alternate), 04-022-3338 (Alternate)

References

Type	DOI	Reference
Primary Reference		Calculated from NIST using POWD-12++.
Structure		Cromer, D.T., Herrington, K. "The structure of anatase and rutile". J. Am. Chem. Soc. 1955, 77, 4708.

Comments

Database Comments: NIST M&A collection code: A 50867 ST1243 1. Sample Preparation: Commercial pigmentary material was used. Calculated Pattern Original Remarks: Anatase-synthetic. Temperature Factor: TF Isotropic TF given by author. Unit Cell Data Source: Powder Diffraction.

d-spacings (41) - Ti O2 - 03-065-5714 (Stick, Fixed Slit Intensity) - X-ray (Cu Kα1 1.54056

2θ (°)	d (Å)	I	h	k	l	*	2θ (°)	d (Å)	I	h	k	l	*
25.303	**3.516900**	1000	1	0	1		98.322	1.018150	11	1	0	9	
36.948	2.430850	56	1	0	3		99.809	1.006940	7	2	0	8	
37.792	**2.378500**	175	0	0	4		101.233	0.996589	5	3	2	3	
38.565	2.332560	71	1	1	2		107.474	0.955315	24	3	1	6	
48.035	**1.892500**	238	2	0	0		108.984	0.946250	12	4	0	0	
53.884	1.700060	148	1	0	5		112.822	0.924675	2	3	0	7	
55.059	1.666530	146	2	1	1		113.863	0.919166	22	3	2	5	
62.105	1.493300	23	2	1	3		114.913	0.913754	13	4	1	1	
62.683	1.480920	103	2	0	4		118.467	0.896445	35m	1	1	10	
68.754	1.364210	49	1	1	6		118.467	0.896445	35m	2	1	9	
70.285	1.338200	49	2	2	0		120.112	0.888943	6	2	2	8	
74.051	1.279170	4	1	0	7		121.744	0.881797	5	4	1	3	
75.043	1.264700	74	2	1	5		122.348	0.879226	15	4	0	4	
76.030	1.250720	20	3	0	1		122.916	0.876846	10	3	3	2	
80.737	1.189250	3	0	0	8		131.043	0.846352	20	4	2	0	
82.153	1.172300	5	3	0	3		132.000	0.843175	5	1	0	11	
82.670	1.166280	35	2	2	4		135.988	0.830808	3	3	2	7	
83.152	1.160740	15	3	1	2		137.382	0.826805	19	4	1	5	
93.241	1.059790	5	2	1	7		142.869	0.812565	1	4	0	6	
94.199	1.051520	17	3	0	5		143.842	0.810285	7	3	0	9	
95.159	1.043440	19	3	2	1								

8.2. Annex 2: Evolution of the absorbance for SiO_2-supported catalyst (non-semiconducting support)

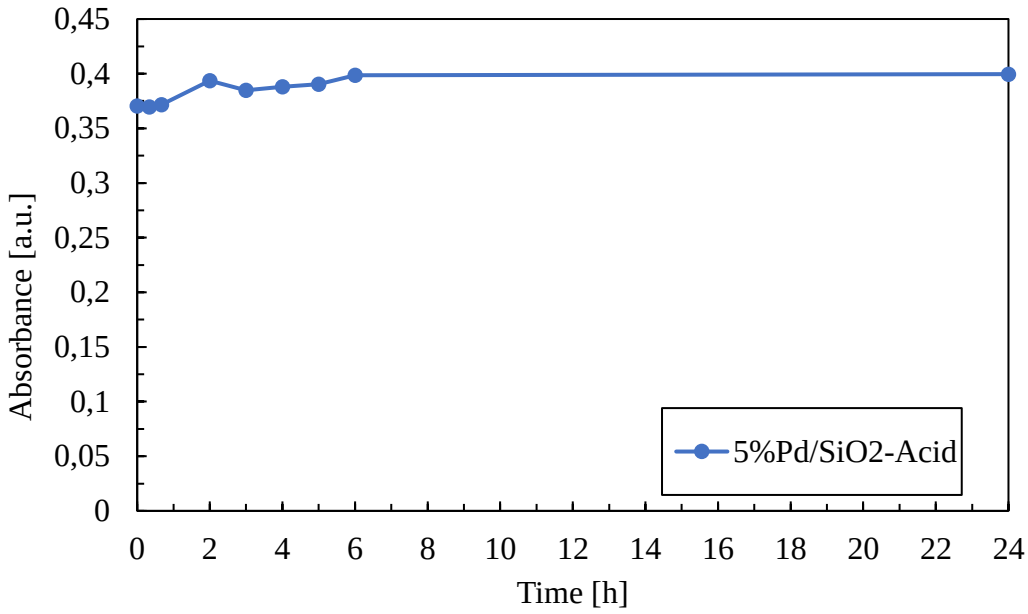

Figure A2-1: *Evolution of the absorbance over time for 5%Pd/SiO_2-Acid*
Reaction conditions: 100 mg of catalyst; 30mL of aqueous solution MO (1.54E-4 M); 40°C; 1bar; 400rpm; non-light.